SWECO

Deltares

Kattegat and Hesselø South Site MetOcean Conditions Assessments

Part B: Analyses and Design Parameters for Kattegat

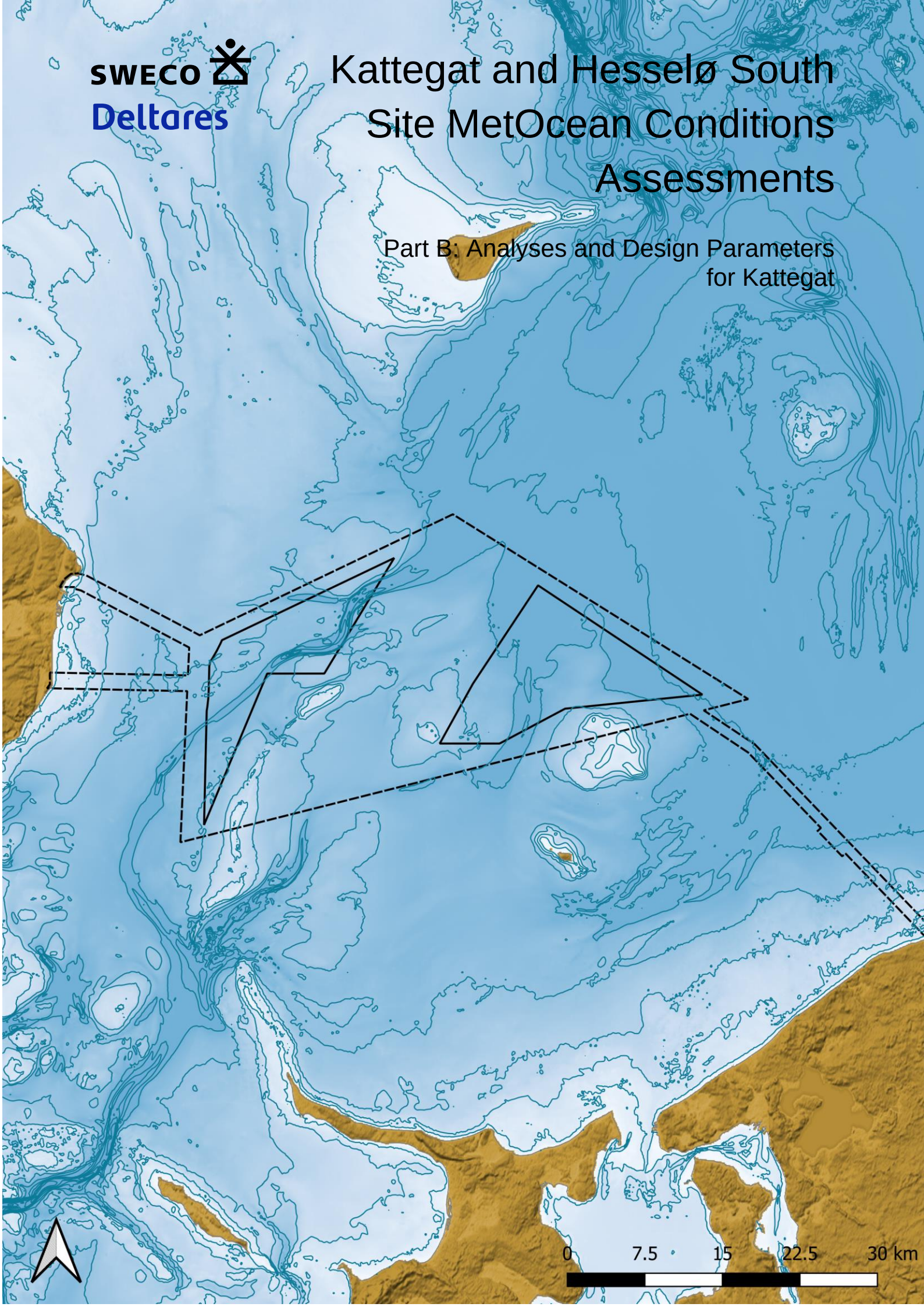

Change list

Ver	Date	Description of the change	Author	Reviewed	Approved by
0	2024-07-12	New Document	Magnus Maribo	Per Kofoed Rasmussen	Anders Helkjær
1	2024-08-28	Update with HD data	Magnus Maribo	Per Kofoed Rasmussen	Anders Helkjær
2	2024-10-13	Updated with Clients comments	Magnus Maribo	Per Kofoed Rasmussen	Anders Helkjær
3	2025-01-22	Updated with Certifiers comments	Magnus Maribo	Per Kofoed Rasmussen	Anders Helkjær

Project Name	Site MetOcean Conditions Assessment
Project Manager	Anders Helkjær, anders.helkjaer@sweco.dk, +4527233341
Client	Energinet Eltransmission A/S
Author	Magnus Maribo Vinter
Controlled by	Per Kofoed Rasmussen
Approved by	Anders Helkjær
Date	2025-01-22
Ver	3
Document number	41011328B
Document reference	41011328B_KG_PartB_Analyses_and_Design_Parameters

Table of contents

List of Figures

List of Tables

Nomenclature

Variable	Abbreviation	Unit
Atmosphere		
Wind speed @ 10 m height	U_{10mag}	m/s
Wind direction @ 10 m height	U_{10dir}	°N (clockwise from)
Wind speed @ 150 m height	U_{150mag}	m/s
Wind direction @ 150 m height	U_{150dir}	°N (clockwise from)
Air pressure @ mean sea level	P	Pa
Air temperature @ 2 m height	T_{2m}	°C
Relative humidity @ 2 m height	RH	-
Surface solar radiation	SSR	J/m2
Ocean		
Total Water level	WL	mMSL
Current speed	CS	m/s
Current direction	CD	°N (clockwise to)
Seawater	T_{sw}	°C
Water Salinity	Sal	PSU (practical salinity unit)
Waves		
Significant wave height	H_{m0}	m
Maximum wave height	H_{max}	m
Maximum wave crest height	C_{max}	m
Peak wave period	T_p	s
Wave energy period	T_{mm10}	s
Mean wave period	T_{m01}	s
Zero-crossing wave period	T_{m02}	s
Wave period associated with the maximum wave height	T_{Hmax}	s
Peak wave direction	PWD	°N (clockwise from)
Mean wave direction	MWD	°N (clockwise from)
Direction standard deviation	DSpr	°

Definitions	
Coordinate System	WGS84 EPSG 4326 (unless specified differently)
Direction	Clockwise from North
Wind	°N coming from

Current	°N going to
Waves	°N coming from
Time	Times are relative to UTC
Vertical Datum	MSL (unless specified differently)

Abbreviations	
2D	2-dimensional
3D	3-dimensional
DMI	Danish Meteorological Institute
DNV	Det Norske Veritas
ECMWF	European Centre for Medium-Range Weather Forecasts
ERA5	ECMWF Re-analysis v5
ESS	Extreme Sea State
EVA	Extreme Value Analysis
FEED	Front-End Engineering Design
IEC	International Electrotechnical Commission
ISO	International Organization for Standardization
KG	Kattegat
mMSL	Metres above Mean Sea Level
MSL	Mean Sea Level
NSS	Normal Sea State
OWF	Offshore Wind Farm
POT	Peak Over Threshold
SSS	Severe Sea State
UTC	Coordinated Universal Time
WGS84	World Geodetic System 1984

1 Summary

This report presents the results of MetOcean site conditions assessment study focusing on analysis of design parameters for the Kattegat OWF.

The report analyses a hindcast modelling period covering 45 years, from January 1st 1979, to December 31st 2023. This hindcast data is used to estimate operational and extreme hydrographic conditions for the FEED design of the OWF. The selected period includes several extreme storm events with varying direction, duration, and extreme peak values of wind, water level, waves, and currents. Additionally, the report analyses other atmospheric and oceanographic conditions such as air temperature, pressure, humidity, solar radiation, lightning strikes, seawater temperature, salinity, and marine growth. Three reference locations within the OWF area are chosen to capture the variation across the site.

Data is categorized by spatial, temporal, and spectral dimensions and is delivered in two packages: one for detailed analysis at reference locations and another for a fine-gridded overview across the entire data delivery area. The data is presented in various formats, such as time series, wind roses, scatter plots, and histograms. The document presents data for one point but with appendices with additional data for all points.

Below are the most important extreme parameters summarized. The report contains also parameters for operational conditions.

It is noted that all Extreme Value Analysis results presented in the relevant sections of this report (ie. sections 6.2, 7.2 and 9.3) are unscaled, in other words raw results from the EVA without scaling with regards to directionality. Scaled results according to DNV-RPC205 where consistency between directional extremes and Omni for all return periods are ensured can be found in the appendices, see section 6.3 and 7.3 for details on the scaling.

Table 1-1 Extreme design conditions for 50-year return period wave conditions at KG-1 (unscaled).

	MWD [°N-from]																
Parameter	0.0	22.5	45.0	67.5	90.0	112.5	135.0	157.5	180.0	202.5	225.0	247.5	270.0	292.5	315.0	337.5	Omni
H_{m0} [m]	4.0	3.3	3.1	3.5	3.3	2.9	2.6	2.7	3.2	3.9	4.7	4.0	4.1	4.2	4.0	3.9	4.7
T_p [s]	7.4	6.8	6.8	7.1	6.9	6.5	6.0	6.0	6.6	7.3	7.8	7.3	7.1	7.3	7.4	7.5	7.8
H_{max} [m]	7.7	6.5	6.1	6.7	6.5	5.7	5.1	5.2	6.3	7.6	9.2	7.9	7.9	8.2	7.8	7.5	9.2
$T_{Hmax,ass,low}$ [s]	7.1	6.5	6.3	6.6	6.5	6.1	5.7	5.8	6.4	7.0	7.7	7.1	7.2	7.3	7.1	7.0	7.7
$T_{Hmax,ass,high}$ [s]	9.1	8.3	8.1	8.5	8.3	7.8	7.4	7.5	8.2	9.0	9.9	9.2	9.2	9.4	9.1	9.0	9.9
C_{max} [m]	4.5	3.8	3.5	3.9	3.8	3.3	2.9	3	3.7	4.4	5.5	4.6	4.7	4.9	4.6	4.4	5.5

Table 1-2 Extreme design conditions for 50-year return period current conditions at KG-1 (unscaled).

Parameter	CD [°N-going]																
	0.0	22.5	45.0	67.5	90.0	112.5	135.0	157.5	180.0	202.5	225.0	247.5	270.0	292.5	315.0	337.5	Omni
CS_{stot} [m/s]	1.3	1.6	1.6	1.1	1.1	1.2	1.8	1.5	1.5	1.2	1.3	1.7	1.5	0.8	0.9	1.1	1.8
CS_{mtot} [m/s]	0.6	0.6	0.5	0.6	0.6	0.6	0.6	0.6	0.7	0.7	0.9	0.8	0.8	0.7	0.6	0.5	0.9
CS_{btot} [m/s]	0.4	0.5	0.4	0.4	0.4	0.3	0.3	0.5	0.5	0.6	0.6	0.6	0.6	0.4	0.4	0.3	0.6

Table 1-3 Extreme design conditions for 50-year return period water level conditions at KG-1.

Parameter	Omni
WL [mMSL]	1.6
WL_r [mMSL]	1.5
WL_{low} [mMSL]	-1.0
$WL_{r,low}$ [mMSL]	-1.1

2 Introduction

The Danish Energy Agency has tasked Energinet with undertaking site MetOcean conditions assessments for the development of the offshore wind farm areas Kattegat and Hesselø South. The offshore wind farms are to be in Kattegat east of the Danish peninsula Djursland. An overview is shown on Figure 2-1.

The site MetOcean conditions assessments will form part of the larger site conditions assessment work and will be a part of the technical basis for the public tender on the development of offshore wind farms within the areas. The site MetOcean conditions assessment is considered suitable for the Front-End Engineering and Design (FEED) of offshore WTG and other support structures for the offshore wind farms.

Figure 2-1 Overview of the windfarm areas Kattegat and Hesselø South and naming of the reference locations per OWF. The dashed line indicates the full data delivery area, and the full line indicate the OWFs.

The full study consists of several deliverables in which this report, Part B, is one of several:

- Part A: Measurements and Hindcast Data Basis (report).
- Part B: Analyses and Design Parameters for Kattegat (this report).
- Part C: Analyses and Design Parameters for Hesselø South (report)
- Long-term hindcast data (digital time series).
- Measurement data (digital time series).
- Reverification of Hindcast Data (report).

The study refers to the following standards and guidelines (hierarchy):

1) IEC 61400-3-1:2019
2) DNV-ST-0437:2024-05
3) DNV-RP-C205:2021-09
4) ISO 19901-1:2015

3 Data basis

The data basis for the analysis is based on Part A: Measurements and Hindcast Data Basis [1]. Along the report is hindcast data for the selected reference locations within the OWFs. For more information of this matter please consult Part A.

The digital data deliveries are split into different parts due to their native dimensions. Their native dimensions are given based on spatial, temporal, and spectral discretization. Within the spatial dimension is latitude, longitude, and depth, within the temporal dimension is time and within the spectral dimension is frequency and direction.

The wind and wave data are grouped into a single file due to their similarity in dimensions. The rest of the atmospheric data is grouped into a single file describing the OWF area. The wave spectrum is grouped into a single file due to its unique spectral dimensions. Likewise, the water level and current data is grouped into a single file due to their variation across the depth.

The data is delivered in two different packages. One for the reference locations used for detailed analysis and one fine gridded across the full data delivery area. The reference locations are named based on this key:

{area}_{reference location name}_{latitude}_{longitude}_{type}_{timespan}.nc

The individual reference locations in the data delivery area are named based on this key:

{area}_{latitude}_{longitude}_{type}_{timespan}.nc

The main body of this report presents results at reference location KG-1, while results at all reference locations are given in the appendices which are attached to this report. The appendices contain all tables and figures presented below.

3.1 Reference Locations

For the KG offshore wind farm three reference locations have been chosen. The reference locations are to capture the variation across the area. The reference locations are chosen based on variations in H_{m0}, T_p and CS with most attention towards their maximum value and the 95th percentile in the time domain. The three chosen reference are listed in Table 3-1 and shown in the overview map in Figure 3-1.

Table 3-1 List of the reference locations for the area for KG with name, location, and depth.

Reference location	Latitude WGS84 [°N]	Longitude WGS84 [°E]	Seabed level [mMSL]
KG-1	56.3702	11.3305	-32.99
KG-2	56.3008	11.1500	-23.39
KG-3	56.4496	11.4395	-18.66

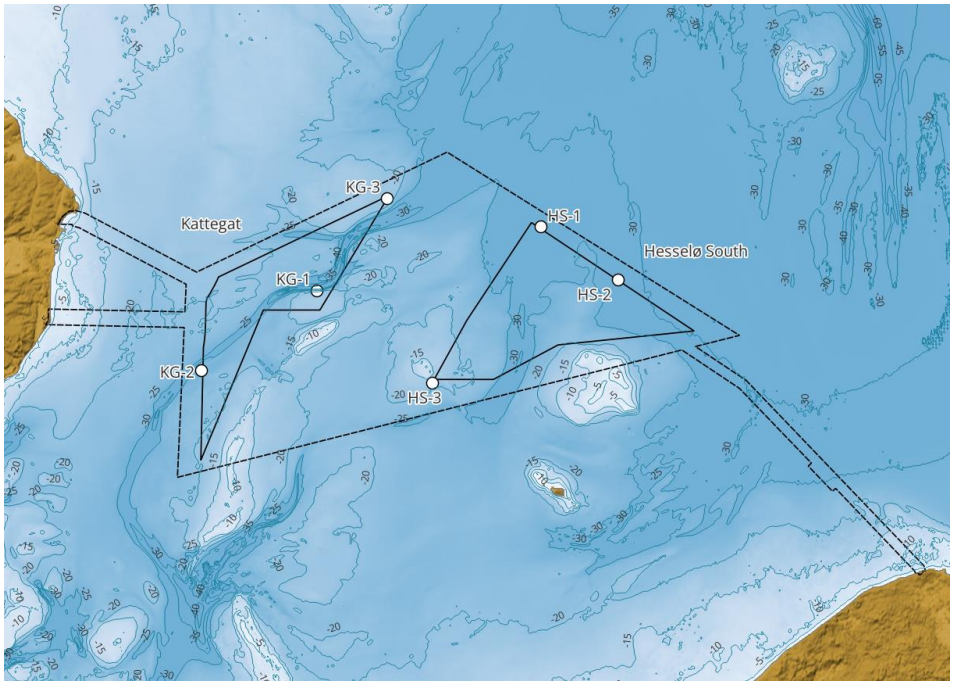

Figure 3-1 Overview of the reference locations within each OWF. The dashed line indicates the full data delivery area, and the full line indicate the OWFs. Contour lines are seabed levels in metres below MSL.

3.2 Historical extreme events

The hindcast modelling is elaborated and presented in Part A: Measurements and Hindcast Data Basis [1]. The data is based on a hydrodynamic simulation of relevant hydrographic variables covering the period 1 January 1979 – 1 January 2024, ie. a period with a total duration of 45 years.

The extreme hydrographic conditions as elaborated and presented in this Part B report, see Chapter 5, 6 and 7, have been estimated by carrying out EVA analyses of the relevant data in the 45-year period.

The selected 45-year simulation period includes several extreme storm events, with varying direction, duration and extreme peak values of wind, water level, waves and currents.

A hindcast period of 45-year duration will normally be considered sufficiently long for the elaboration of extreme design values, especially for the actual

project with a requirement of estimations of values with return periods up to maximum 50 years only, i.e. the required return period for estimation of extreme values is only a few years longer than the duration of the hindcast simulation.

However, a review of historical records of storm events might potentially reveal that the selected 45-year hindcast period, forming the basis for the EVA analyses, is not fully statistically representative for long-term conditions. This is assessed in this section.

3.2.1 Storm frequency in Denmark

The Danish Meteorological Institute (DMI) currently assesses storms and storm patterns in Denmark, dividing storms into 4 categories:

- Class 1 – Average wind speeds in the range, 20.8-24.5 m/s
- Class 2 – Average wind speeds in the range, 24.5-26.5 m/s
- Class 3 – Average wind speeds in the range, 26.6-28.5 m/s
- Class 4 – Average wind speeds of 28.5 m/s or above

Some storms are national (covering > 30% of coastal areas), while others are regional storms affecting only parts (10-30% of Danish coastal areas). A storm may not be classified as a storm by DMI, if it only affects less than 10% of the coastal areas. Figure 3-2 shows the timing of all Class 2, 3 and 4 storms occurred in Denmark in the period, 1891 – 2021 (130 years), as observed by DMI. The actual hindcast simulation period, 1979-2023, is also shown in Figure 3-2.

In [2] DMI presents a list of all storms observed in Denmark in the period, 1891 – 2024, including Class 1 events also and the main wind direction for each storm. Table 3-2 presents the number of storms observed within each storm Class in the entire period, 1891-2023, however distinguished between the period, 1891-1978 (88 years) and 1979-2023 (45 years).

It is noted that the required design return period is up to a 50-year return period event, therefore a 133-year record of storms is considered sufficient for this analysis. Furthermore, the older the events the larger the uncertainty on the event, particularly when evaluating extreme current and wave conditions. In [2] it is informed that the classification of storms has become more accurate the last 20 years.

Going through the record of Class 2, 3 and 4 storm events illustrated in Figure 3-2 and Table 3-2 covering the period 1891-2021, it appears that most of these storms are associated with winds from westerly directions, especially for Class 3 and 4 storms with only one Class 3 and none Class 4 storms from easterly directions within the entire 130-year period. This is also illustrated by Figure 4-7 showing a scatter plot of simulated wind directions versus wind speeds for the 45-year hindcast period, with apparent relatively small wind speeds from easterly directions, see also below section 3.2.50.

It shall be noted that while the illustration in Figure 3-2 is based on wind observations only, the occurrence of extreme waves, currents and water levels in Danish waters are normally well-correlated to extreme wind speeds. With respect to extreme water levels, current and waves it shall, however, also be noted that the actual path of the low pressure, wind direction, and storm duration do also play a significant role for the development of extreme

conditions.

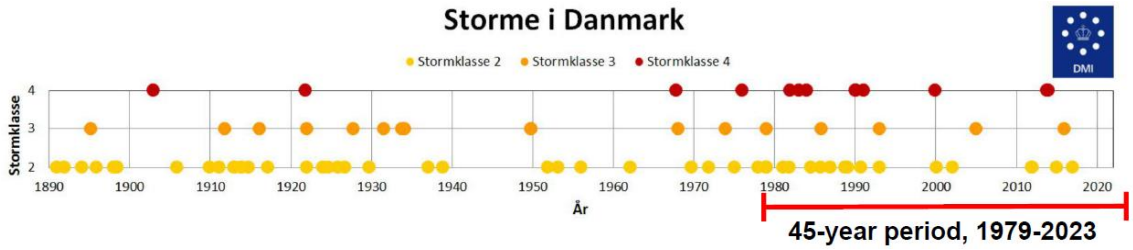

Figure 3-2 Observed Class 2, 3 and 4 storms in Denmark, 1891 – 2021 (130 years), from [3].

Table 3-2 Number of storms observed by DMI between 1891 and 2024 [2].
* By DMI listed as a snow storm without wind direction, the majority likely to be easterly.

Storm Class	Number of storms observed				
	1891-1978 (88 years)			1979-2023 (45 years)	
	w/o direction	Easterly	Westerly	Easterly	Westerly
1 (>20.8 m/s)	17*	7	46	2	39
2 (>24.5 m/s)	2*	3	27	1	19
3 (>26.5 m/s)	-	1	11	0	4
4 (>28.5 m/s)	-	0	4	0	9

3.2.2 Assessment of the 45-year hindcast period

From Figure 3-2 and Table 3-2 it is clear that within the 45-year hindcast period, storms of Class 2 and 3 are in general represented well within the period, while it appears that Class 4 are over-represented within the hindcast period, compared to the full 130-year period considered in [3]. This may be a result of the random, stochastic nature of extreme storm events. However, this might potentially also be a result of climate change, but it is beyond the scope of this report to evaluate this further.

The 45-year hindcast period includes two of the most prominent Class 4 hurricanes ever recorded in the North Sea and Denmark, namely the storms on 24 November 1981 and 3 December 1999. However, while the inner Danish waters were affected by extreme wind speeds during these two storms, the associated storm surges mainly hit the west coast of Denmark and not the Kattegat region. Extreme water levels in the Kattegat region were generated during the storms on 1 November 2006 and 5-6 December 2013 (Bodil), during which two storms, also within the 45-year hindcast period, the highest water levels ever observed in the Kattegat region have been recorded, see [4].

On 20 October 2023 an easterly storm generated storm surge levels in the western Baltic Sea region of a size not observed since 1904, ie. 120 years ago.

In [4] the Danish Coastal Directorate (KDI) has for a large number of water level stations in Denmark presented a ranked list of the highest 40 high waters observed in the data recording period. A number of these stations have data

records going back to the 1880-es, ie. with an observation period longer than 130 years, similar to the DMI storm observation period. Six stations in Kattegat and the adjacent parts of the belts all have records of a duration > 130 years: Aarhus, Hornbæk, Fredericia, Slipshavn, Korsør and København Going through these lists, it appears that the hindcast period, 1979-2023 is well-represented in the top 5 of all these, with the no. 1 event for all 6 stations within the hindcast period, and both Aarhus and Hornbæk have 4 events in Top 5 within the hindcast period, 1979-2023.

Generally, the strongest and most extreme currents in Kattegat and inner Danish waters occur in events with a high water level difference between Kattegat and the western part of the Baltic Sea. With respect to south-going currents these are associated with extreme high water in Kattegat, hence also included in the hindcast period.

For the 133-year period, 1891 – 2023, DMI has observed a total number of 13 Class 4 storms in Denmark, while 9 of these fall within the 45-year hindcast period, see Table 3-2, in which the number of storms in each Class is presented, distinguishing between the period 1891-1978 and the hindcast period, 1979-2023.

The general assessment of the chosen 45-year hindcast period is therefore that the Class 4 storms appear to be over-represented compared to long-term conditions, and the most extreme water levels with return periods in the order of 100 years are also observed within the hindcast period.

Therefore, the use of the chosen 45-year period is considered conservative for derivation of MetOcean variables with a 50-year return period.

3.2.3 Very extreme historical events

The above assessments of historical events are based on data records going 133 years back, starting in 1891. Going further back in history, observations of very extreme events are mainly based on storm surges, due to their very significant impact on coasts, damage on buildings and loss of lives.

For the Kattegat region, the available observations of storm surges shows that the 45-year hindcast period includes the most extreme high water levels observed within a 130-year period, see above section 3.2.2.

For the western Baltic Sea region there are observations of storm surges, which significantly exceed records within the 133-year period. Notably, the easterly storm event on 13 November 1872 and also one on 10 January 1694 can be mentioned. However, central estimates of their statistical return period are in the order of 1,000 and 250 years respectively, and for estimation of values with a 50-year return period it is considered acceptable not to consider these very extreme historical events further.

3.2.4 Easterly storms

Easterly winds rarely exceed a wind speed of 24.5 m/s, to be classified as a Class 2 storm or above, which appears in Table 3-2. Of all Class 2 storms observed by DMI less than 10% are of easterly origin. Only one easterly Class 3 storm has been observed, while no easterly Class 4 storms have been observed in the entire period, 1891 - 2024.

Even the easterly storm on 20 October 2023, generating 100-year storm surges in the western part of the Baltic Sea (along southern and southeastern Danish coasts), is only classified as a Class 1 storm by DMI, with an average wind speed of 20.8 m/s or above, in DMI's list of Danish storms [2].

Kattegat is less prone to the occurrence of strong easterly winds than the Baltic Sea, due to the long free fetches in open waters towards east in the Baltic Sea. However, the DMI list of storms does not provide any information on specific area(s) affected by each storm on the list.

3.2.5 Extreme events 1979-2023

For the reference location, KG-1, cf. section 3.1, Figure 3-3 presents a scatter plot of the simultaneous simulated values of wind direction vs. wind speed, associated with the simulated values of H_{m0} underlying the EVA analysis of H_{m0} for this reference location. It is clear that easterly storms have relatively low wind speeds, and their importance for the wave climate is relatively limited, as they are also associated with relatively short fetches at KG-1.

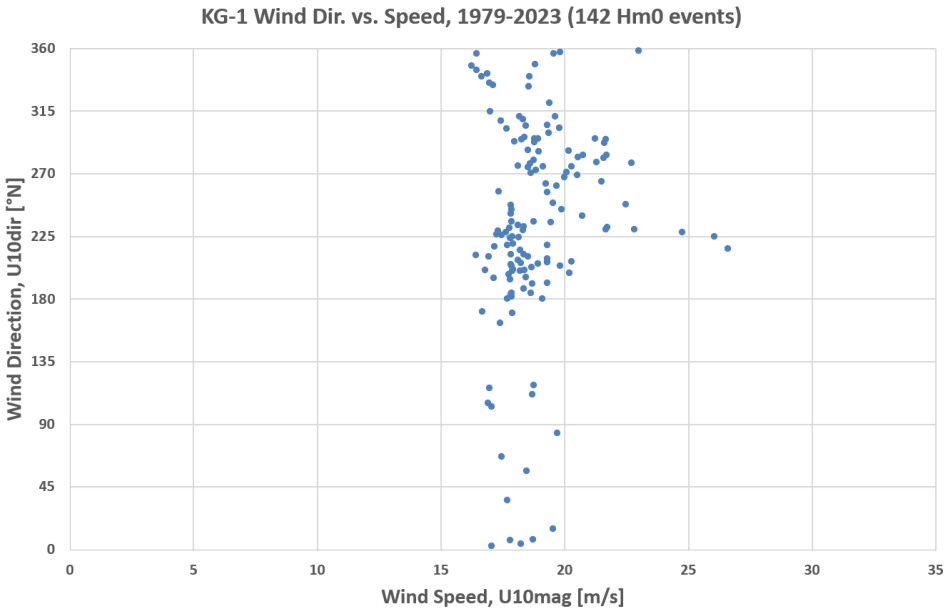

Figure 3-3 Scatter plot of simulated wind direction versus the wind speed, associated with the 142 highest H_{m0} events underlying the EVA of H_{m0} at KG-1.

3.2.6 Conclusion

The conclusion is that the 45-year hindcast period is assessed to have a sufficient number of storm events from westerly directions, to be used for reliable estimates of extreme values of hydrographic variables up to 50 years recurrency intervals for the KG offshore wind farms area.

For easterly directions the period 1979-2023 seems to have an underrepresentation of easterly storms, in terms of wind speed, compared to 1891-1978, se Table 3-2. Thus there is an indication that 50 year extreme current, water level and wave conditions during easterly storms may be slightly underestimated when only considering the wind speed as the driving parameter.

However extreme current, water level and wave conditions are also dependent on low pressure, wind direction, and storm duration, as well as bathymetry and potential climate effects. Keeping these uncertainties in mind and considering that both model hindcast and measurement data used for model calibration contains an extreme water level event generated by an easterly storm (20-21 October 2023) with an estimated return period of 100 years, it is assessed to be reasonable to apply the 45 years hindcast modelling for reliable estimates of extreme values of hydrographic variables up to 50 years recurrency intervals for the KG offshore wind farms area.

4 Wind Conditions

This section presents a summary of the modelled wind data, followed by a presentation of normal wind conditions.

Note that wind data is included only to assess the misalignment relative to waves and for descriptions of sea states. Other wind conditions are addressed in a separate wind study assessing the wind conditions within the OWF area. This report only briefly describes the wind to give a general understanding of the site-specific conditions.

The wind data is adopted from [1] and consists of ERA5 [5] data during the period 1979 – 2024 (45 years). The ERA5 data is available at a 0.25° grid and used to run the wave model. The wind is interpolated from the ERA5 data from its native resolution (0.25° and 1 hour) to the mesh and output time step of the wave model of this study (~300 m and 1 hour). The wind dataset is combined with the wave dataset due to their common dimensions. Table 3.1 summarises the metadata.

Table 4-1 Metadata of the wind dataset

Name	Value
Start Date [UTC]:	1979-01-01 00:00:00
End Date [UTC]:	2023-12-31 23:00:00
Time Step [s]	3600

The data is calibrated with local measurements, details are available in [1]. The data set is considered representative of a 1-hour averaging period for both 10mMSL and 150mMSL height. The 150mMSL height is referred to as hub height.

The wind analyses cover the entire period and are presented in windspeed bins of 1.0 m/s and directional bins of 22.5° at both 10mMSL and 150mMSL height.

Table 4-2 presents the variables of the dataset, including the bin sizes applied in the analyses of the normal conditions.

Table 4-2 Wind variables of the data set

Variable name	Abbrev.	Unit	Bin size
Wind speed at 10 mMSL	U_{10mag}	m/s	1.0
Wind speed at 150 mMSL	U_{150mag}	m/s	1.0
Wind direction at 10 mMSL	U_{10dir}	°N-from	22.5
Wind direction at 150 mMSL	U_{150dir}	°N-from	22.5

4.1 Normal wind conditions

The normal wind conditions are presented both reference at 10mMSL and hub height at 150mMSL at the three reference locations in terms of:

- Time series

- Windrose
- Scatter plot
- Statistics – monthly and directional
- Histogram

4.1.1 Wind speed at reference height

The sections present the wind speed at reference height at 10mMSL.

4.1.1.1 Timeseries

Figure 4-1 shows a time series of wind speed at reference height at KG-1 during the 45-year hindcast period. The mean wind speed is 7.7 m/s, and the maximum wind speed is 26.2 m/s.

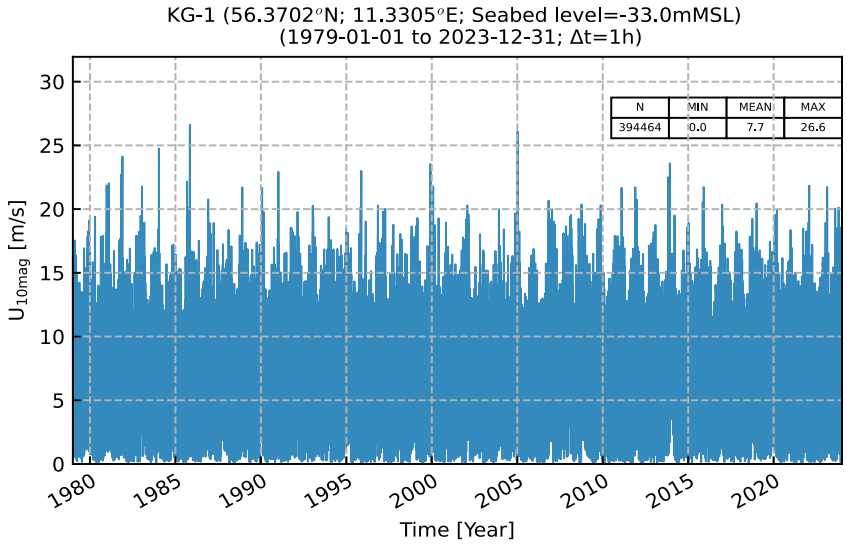

Figure 4-1 Time series of U_{10mag} at KG-1.

4.1.1.2 Windrose

Figure 4-2 shows a wind rose at KG-1, showing the dominant wind coming from the west. Figure 4-2 shows the scatter plot of the wind speed and the wind direction at KG-1. This aligns with the wind rose that the most frequent and dominant direction is west.

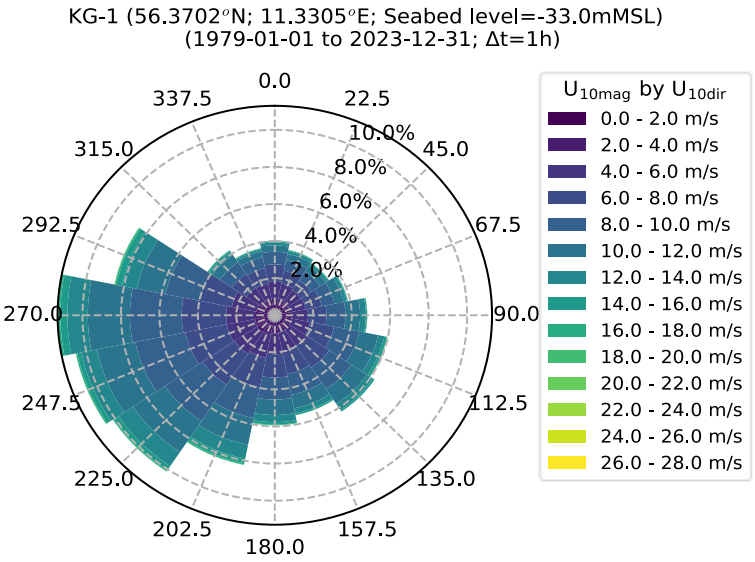

Figure 4-2 Rose plot of U_{10mag}, sorted by U_{10dir}, at KG-1.

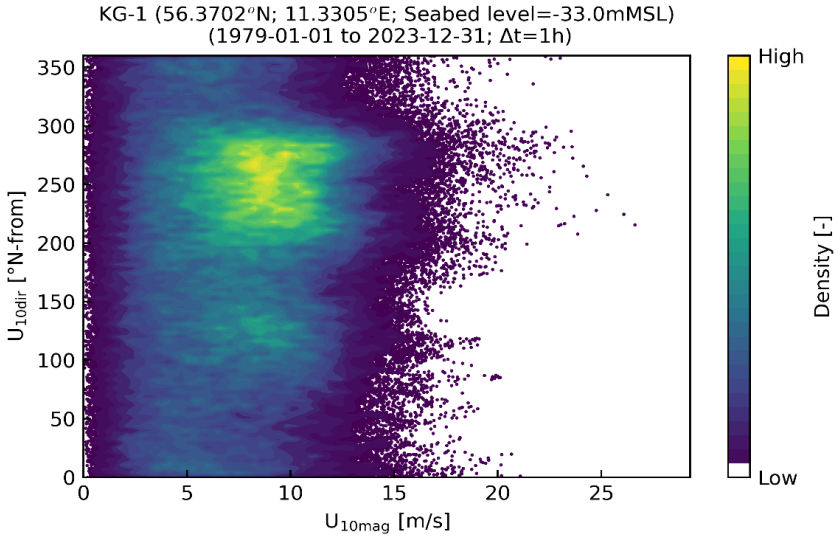

Figure 4-3 Scatter of U_{10mag} and U_{10dir} at KG-1.

Table 4-3 Table of U_{10mag} and U_{10dir} in percentage, at KG-1.

U_{10mag} [m/s]	U_{10dir} [°N-from]																
	0.0	22.5	45.0	67.5	90.0	112.5	135.0	157.5	180.0	202.5	225.0	247.5	270.0	292.5	315.0	337.5	Omni
0.0 - 2.0	0.21	0.22	0.21	0.21	0.21	0.21	0.23	0.24	0.23	0.24	0.23	0.24	0.23	0.23	0.21	0.23	3.6
2.0 - 4.0	0.67	0.68	0.61	0.60	0.64	0.67	0.72	0.73	0.75	0.82	0.87	0.81	0.80	0.76	0.66	0.63	11.4
4.0 - 6.0	0.97	0.85	0.80	0.84	0.87	0.99	1.03	1.03	1.11	1.28	1.40	1.50	1.50	1.29	0.92	0.89	17.3
6.0 - 8.0	0.90	0.71	0.65	0.83	0.96	1.27	1.41	1.24	1.26	1.63	2.01	2.19	2.31	1.72	0.90	0.83	20.8
8.0 - 10.0	0.68	0.58	0.57	0.67	0.98	1.34	1.39	1.14	1.19	1.69	2.36	2.65	2.69	1.79	0.75	0.60	21.1
10.0 - 12.0	0.35	0.34	0.35	0.48	0.77	0.99	0.97	0.74	0.83	1.47	2.00	2.03	2.19	1.52	0.47	0.31	15.8
12.0 - 14.0	0.15	0.15	0.14	0.18	0.30	0.34	0.38	0.28	0.38	0.76	0.91	0.82	1.06	0.79	0.20	0.11	6.9
14.0 - 16.0	0.07	0.05	0.05	0.05	0.06	0.13	0.10	0.09	0.14	0.26	0.28	0.22	0.37	0.30	0.09	0.06	2.3
16.0 - 18.0	0.02	0.01	0.01	0.01	0.01	0.03	0.01	0.01	0.04	0.08	0.06	0.07	0.11	0.07	0.02	0.01	0.6
18.0 - 20.0	0.01	0.00	0.00	0.00	0.00	0.00	0.00	0.00	0.01	0.02	0.01	0.01	0.02	0.02	0.01	0.00	0.1
20.0 - 22.0	0.00	0.00	0.00	0.00	0.00	0.00	0.00	0.00	0.00	0.00	0.00	0.00	0.01	0.01	0.00	0.00	0.0
22.0 - 24.0	0.00	0.00	0.00	0.00	0.00	0.00	0.00	0.00	0.00	0.00	0.00	0.00	0.00	0.00	0.00	0.00	0.0
24.0 - 26.0	0.00	0.00	0.00	0.00	0.00	0.00	0.00	0.00	0.00	0.00	0.00	0.00	0.00	0.00	0.00	0.00	0.0
26.0 - 28.0	0.00	0.00	0.00	0.00	0.00	0.00	0.00	0.00	0.00	0.00	0.00	0.00	0.00	0.00	0.00	0.00	0.0
All	4.0	3.6	3.4	3.9	4.8	6.0	6.2	5.5	5.9	8.2	10.1	10.6	11.3	8.5	4.2	3.7	####

4.1.1.3 Histogram

The histogram Figure 4-4 provides a visual representation of the binned wind speeds at the refence height at 10mMSL. The 30% quantile is 5.76 m/s, the 50% quantile is 7.72 m/s, and the 70% quantile is 9.58 m/s.

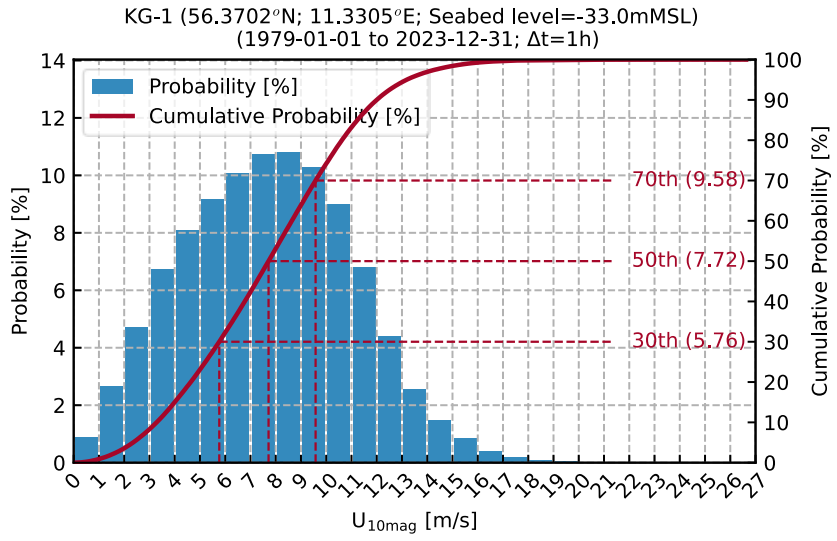

Figure 4-4 Probability plot of U_{10mag} at KG-1.

The seasonal variation across U_{10mag} is shown in Table 4-4. At KG-1 the largest winds are expected during winter.

Table 4-4 Probability table of U_{10mag}, at KG-1.

Season	U_{10mag} [m/s]		
Month	30%-tile	50%-tile	70%-tile
Jan	7.2	9.2	10.9
Feb	6.8	8.6	10.4
Mar	6.0	7.9	9.7
Apr	4.9	6.7	8.4
May	4.6	6.3	8.0
Jun	4.6	6.3	8.1
Jul	4.5	6.3	8.1
Aug	5.0	6.7	8.5
Sep	6.0	7.9	9.6
Oct	7.0	8.8	10.4
Nov	7.3	9.1	10.7
Dec	7.2	9.1	10.8

4.1.2 Wind speed at hub height

The sections present the wind speed at hub height at 150mMSL.

4.1.2.1 Timeseries

Figure 4-5 shows a time series of wind speed at hub height at KG-1 during the 45-year hindcast period. The mean wind speed is 9.2 m/s, and the maximum wind speed is 34.3 m/s.

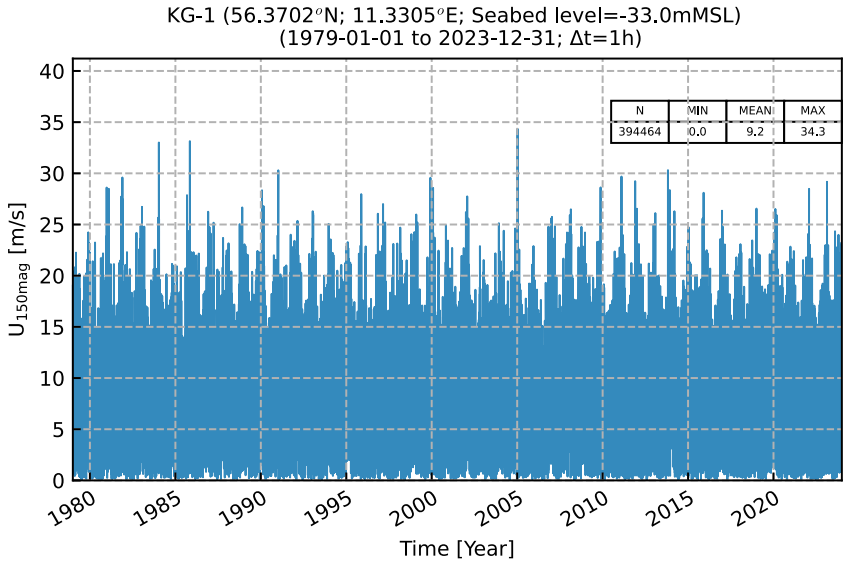

Figure 4-5 Time series of U_{150mag} at KG-1.

4.1.2.2 *Windrose*

Figure 4-6 shows a wind rose at KG-1, showing the dominant wind coming from the west. Figure 4-7 shows the scatter plot of the wind speed and the wind direction at KG-1. This aligns with the wind rose that the most frequent and dominant direction is west.

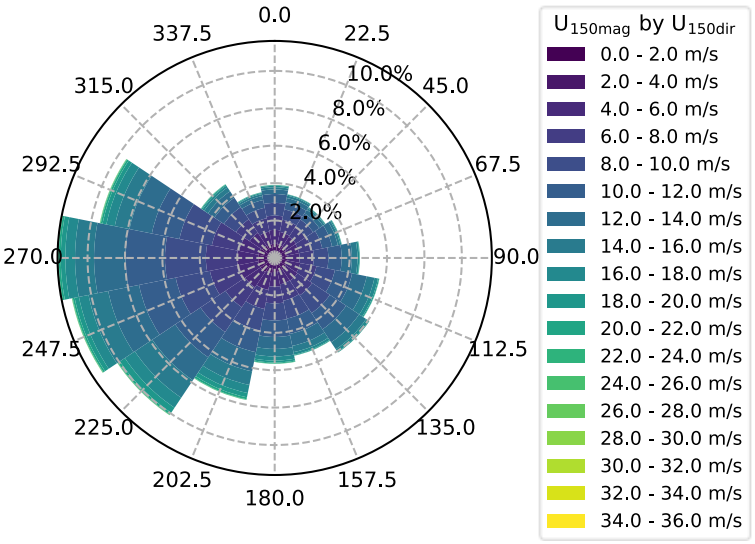

Figure 4-6 Rose plot of U_{150mag}, sorted by U_{150dir}, at KG-1.

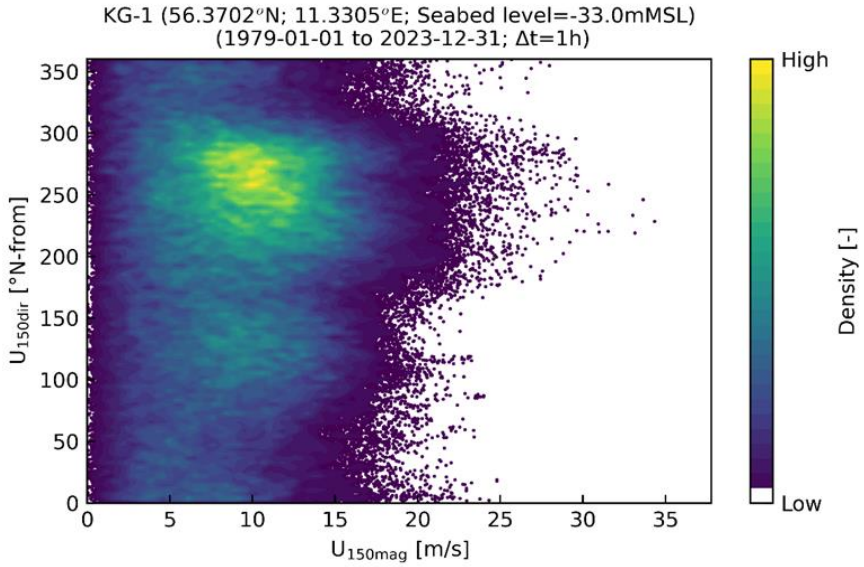

Figure 4-7 Scatter of U_{150mag} and U_{150dir} at KG-1.

Table 4-5 Table of U_{150mag} and U_{150dir} in percentage, at KG-1.

U_{150mag} [m/s]	U_{150dir} [°N-from]																
	0.0	22.5	45.0	67.5	90.0	112.5	135.0	157.5	180.0	202.5	225.0	247.5	270.0	292.5	315.0	337.5	Omni
0.0 - 2.0	0	0	0	0	0	0	0	0	0	0	0	0	0	0	0	0	3
2.0 - 4.0	1	1	1	0	0	0	1	1	1	1	1	1	1	1	1	1	9
4.0 - 6.0	1	1	1	1	1	1	1	1	1	1	1	1	1	1	1	1	13
6.0 - 8.0	1	1	1	1	1	1	1	1	1	1	1	1	2	1	1	1	16
8.0 - 10.0	1	1	0	1	1	1	1	1	1	1	2	2	2	2	1	1	17
10.0 - 12.0	0	0	0	1	1	1	1	1	1	1	2	2	2	2	1	0	16
12.0 - 14.0	0	0	0	0	1	1	1	1	1	1	1	2	2	1	0	0	12
14.0 - 16.0	0	0	0	0	0	0	0	0	0	1	1	1	1	1	0	0	8
16.0 - 18.0	0	0	0	0	0	0	0	0	0	0	1	1	1	0	0	0	4
18.0 - 20.0	0	0	0	0	0	0	0	0	0	0	0	0	0	0	0	0	2
20.0 - 22.0	0	0	0	0	0	0	0	0	0	0	0	0	0	0	0	0	1
22.0 - 24.0	0	0	0	0	0	0	0	0	0	0	0	0	0	0	0	0	0
24.0 - 26.0	0	0	0	0	0	0	0	0	0	0	0	0	0	0	0	0	0
26.0 - 28.0	0	0	0	0	0	0	0	0	0	0	0	0	0	0	0	0	0
28.0 - 30.0	0	0	0	0	0	0	0	0	0	0	0	0	0	0	0	0	0
30.0 - 32.0	0	0	0	0	0	0	0	0	0	0	0	0	0	0	0	0	0
32.0 - 34.0	0	0	0	0	0	0	0	0	0	0	0	0	0	0	0	0	0
34.0 - 36.0	0	0	0	0	0	0	0	0	0	0	0	0	0	0	0	0	0
All	4	3	3	4	5	6	6	5	6	8	10	11	12	10	5	4	100

4.1.2.3 Histogram

The histogram on Figure 4-8 provides a visual representation of the binned wind speeds at the hub height at 150mMSL. The 30% quantile is 6.61 m/s, the 50% quantile is 9.05 m/s, and the 70% quantile is 11.48 m/s.

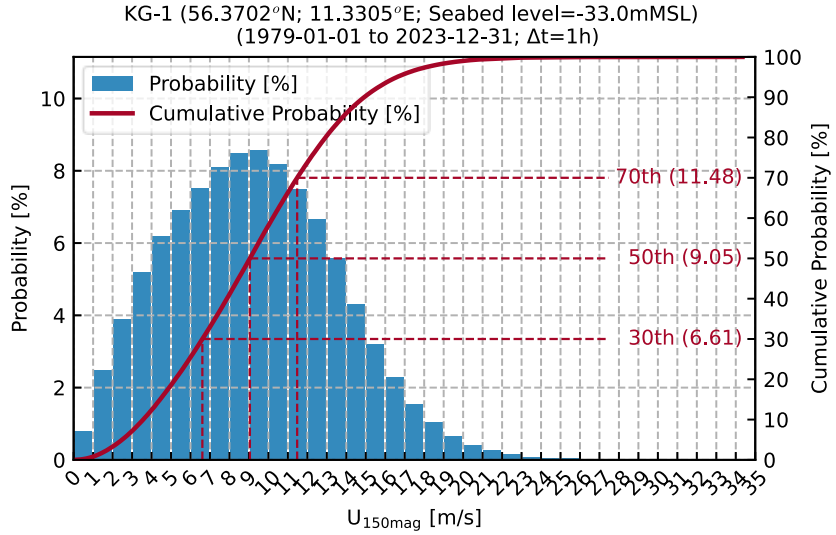

Figure 4-8 Probability plot of U_{150mag} at KG-1.

The seasonal variation across U_{150mag} is shown on Table 4-6. At KG-1 the largest wind speeds are expected during winter.

Table 4-6 Probability table of U_{150mag}, at KG-1.

Season	U_{150mag} [m/s]		
Month	30%-tile	50%-tile	70%-tile
Jan	8.3	10.9	13.5
Feb	7.8	10.4	13.1
Mar	7.3	9.8	12.2
Apr	5.9	8.3	10.6
May	5.4	7.6	9.8
Jun	5.3	7.4	9.6
Jul	5.2	7.3	9.4
Aug	5.7	7.7	9.8
Sep	6.7	9.0	11.1
Oct	7.8	10.2	12.3
Nov	8.0	10.4	12.7
Dec	8.0	10.7	13.2

5 Water levels

This section presents a summary of the water level data basis established in [1]**, followed by a presentation of normal and extreme water level conditions at the KG area.**

The Water Level consists of a tidal and a residual component. The total Water Level was separated by a decomposition done by harmonic analysis, into a tidal and a residual water level component [1]. Table 5-1 summarises the metadata of the dataset.

Table 5-1 Metadata of the water level dataset.

Name	Value
Start Date [UTC]:	1979-01-01 00:00:00
End Date [UTC]:	2023-12-31 23:00:00
Time Step [s]	3600

The water level data is relative to mean sea level (MSL).

Analyses are organized into 0.1 m bins, with Table 4.2 detailing the dataset's water level variables, including the applied bin sizes in the figures and tables. Each variable has a corresponding derived variable for the tidal (suffix "t") and residual (suffix "r") components.

Table 5-2 Wave variables of the water level dataset

Variable name	Abbrev.	Unit	Bin size
Water Level	WL	mMSL	0.1
Water Level - Tide	WL_t	mMSL	0.1
Water Level - Residual	WL_r	mMSL	0.1

In this chapter mainly the Water Level (WL) is presented, In the appendices the full statistics of the tide and residual components can be found.

5.1 Normal water level conditions

The normal water level conditions are presented in terms of:

- Time series
- Tidal levels
- Histograms
- Monthly statistics

5.1.1 Timeseries

Figure 5-1 shows a time series of the water level at KG-1 during the 45-year period. The decomposition of water levels is explained in part A [1]. The tidal levels are given in section 5.1.2.

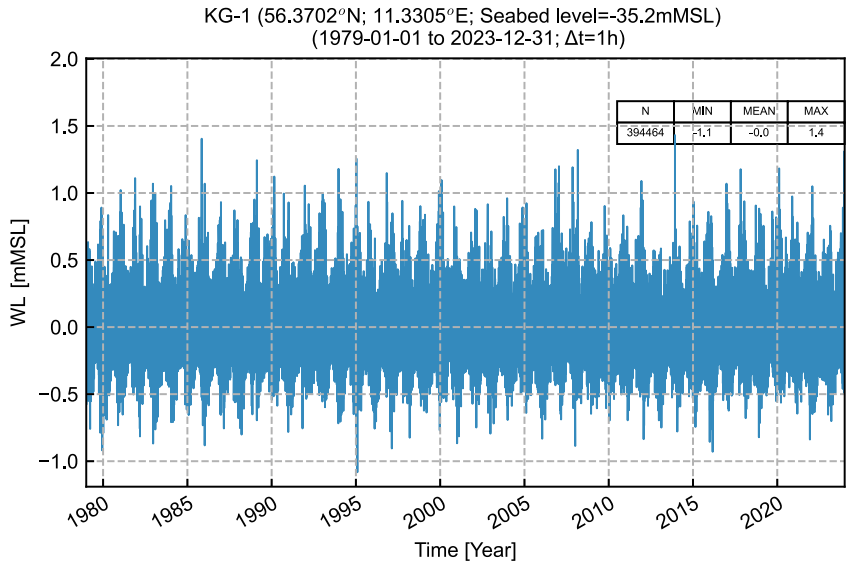

Figure 5-1 Time series of water level at KG-1.

5.1.2 Tidal levels

To quantify the tidal levels at KG the astronomical water levels (tidal levels) are provided below.

Figure 5-1 shows the time series of the total, astronomical tidal and residual water level KG-1, while Table 5-3 summarises the astronomical water levels.

The astronomical water levels are defined as (https://ntslf.org/tgi/definitions):

- HAT: Maximum predicted tidal WL.
- MHWS: Average of the two successive high waters reached during the 24 hours when the tidal range is at its greatest (spring tide).
- MHWN: Average of the two successive high waters reached during the 24 hours when the tidal range is at its lowest (neap tide).
- MLWN: Average of the two successive low waters reached during the24 hours when the tidal range is at its lowest (neap tide).
- MLWS: Average of the two successive low waters reached during the 24 hours when the tidal range is at its greatest (spring tide).
- LAT: Minimum predicted tidal WL.

Table 5-3 Tidal levels at KG.

Tidal level	Abbrev.	KG-1	KG-2	KG-3	Unit
Highest astronomical tide	HAT	0.31	0.32	0.3	mMSL
Mean high water springs	MHWS	0.2	0.21	0.2	mMSL
Mean high water neaps	MHWN	0.18	0.19	0.18	mMSL
Mean sea level	MSL	0	0	0	mMSL
Mean low water neaps	MLWN	-0.18	-0.18	-0.17	mMSL
Mean low water springs	MLWS	-0.2	-0.21	-0.19	mMSL
Lowest astronomical tide	LAT	-0.37	-0.38	-0.37	mMSL

5.1.3 Histogram

Figure 5-2 shows a histogram of total water level at KG-1.

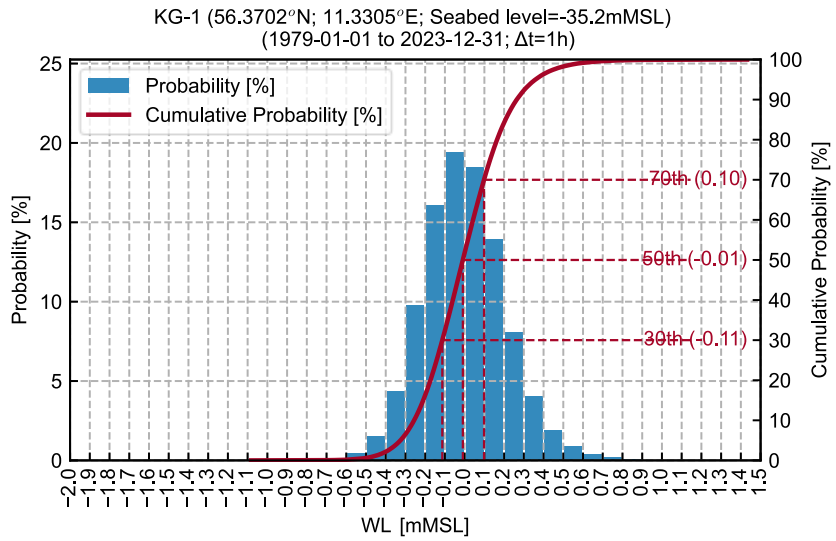

Figure 5-2 Histogram of the water level, WL, at KG-1.

5.1.4 Monthly statistics

Figure 5-3 shows the monthly statistics of the water level at KG-1. The variation in the monthly mean water level is small, about 0.1 m during the year. The highest (+1.5 mMSL) as well as the lowest (-1.0 mMSL) water levels occur during winter.

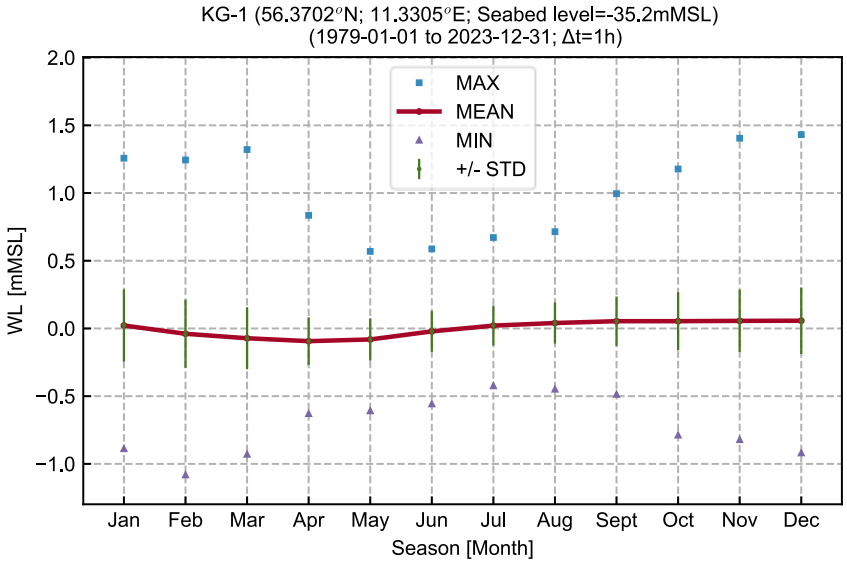

Figure 5-3 Monthly statistics of the water level, WL, at KG-1.

5.2 Extreme water level conditions

Extreme water level conditions are established using Extreme Value Analysis. The analysis is based on its performance and sensitivity to selection of distribution, threshold selection method, λ-value evaluation, and fitting estimator. A description of the methodology and the selection of settings is available in Appendix B.

For both the low- and high-water levels, the 3-parameter Weibull distribution was fitted by the least square method to 180 peak events (λ=4) separated by at least 72 hours. It is noted that the average relative error on the residual water level in the EVA does not stabilize until after 3 events per year, therefore 4 events have been preferred. It is noted, however, that the actual effect on the estimated quantiles is very low for the range of 1-4 events, thus using 1 or 4 events will not significantly impact resullts.

5.2.1 Extreme high-water levels

The extreme total high water level fit for the 45-year hindcast period is shown on Figure 5-4. Values for selected return periods are additionally shown in Table 5-4. The Weibull distribution fitted with the least squares method in shown along the upper 97.5% and lower 2.5% confidence interval. The fitted distribution aligns well to the hindcast data points, also at the tail, and all events are within the confidence levels. The 50-year total high-water level is 1.6 mMSL.

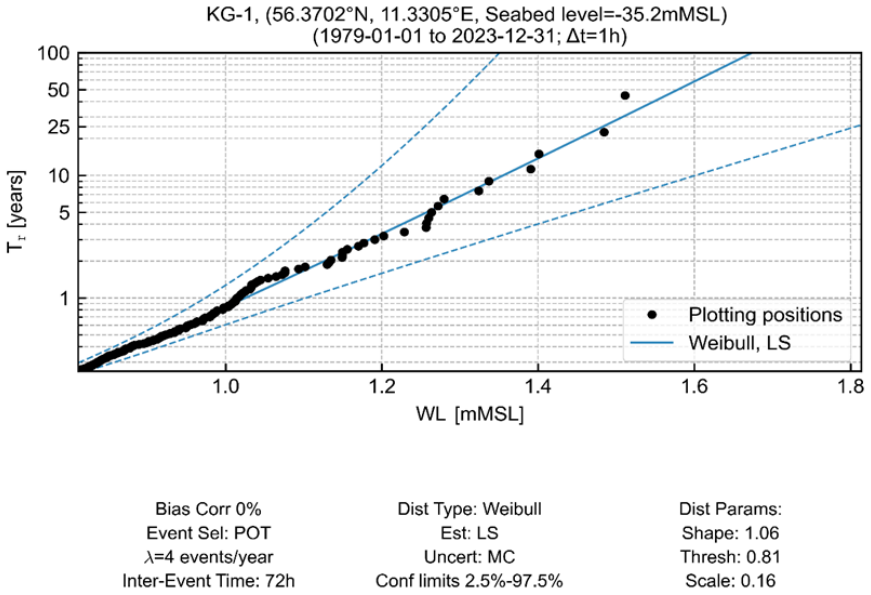

Figure 5-4 Marginal EVA of total high-water level, WL, at KG-1.

Table 5-4 Estimates of total water level, WL, at KG-1.

	WL [mMSL]					
	Quantile	T_r 1	T_r 5	T_r 10	T_r 25	T_r 50
Omni	2.5%-tile	1	1.1	1.2	1.2	1.3
	50%-tile	1	1.3	1.4	1.5	1.6
	97.5%-tile	1.1	1.4	1.6	1.8	2

5.2.2 Extreme residual high-water levels

The extreme residual high water level fit for the 45-year hindcast period is shown on Figure 5-5. Values for selected return periods are additionally shown in Table 5-5. The Weibull distribution fitted with the least squares method in shown along the upper 97.5% and lower 2.5% confidence interval. The fitted

distribution aligns well to the hindcast data points, also at the tail, and all events are within the confidence levels. The 50-year residual high-water level is 1.5 mMSL.

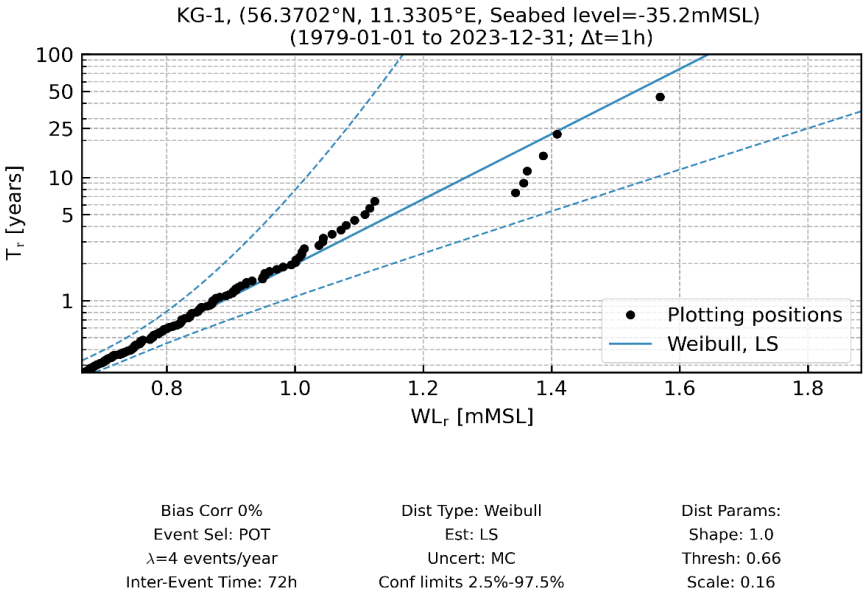

Figure 5-5 Marginal EVA of residual high-water level, WL_r, at KG-1.

Table 5-5 Estimates of residual high-water level, WL_r, at KG-1.

	WL_r [mMSL]					
	Quantile	T_r 1	T_r 5	T_r 10	T_r 25	T_r 50
Omni	2.5%-tile	0.8	1	1	1.1	1.2
	50%-tile	0.9	1.2	1.3	1.4	1.5
	97.5%-tile	1	1.4	1.6	1.8	1.9

5.2.3 Extreme low-water levels

The extreme low water level fit for the 45-year hindcast period is shown on Figure 5-6. Note that the low water levels are positive on the figure. Values for selected return periods are additionally shown in Table 5-6. The Weibull distribution fitted with the least squares method in shown along the upper 97.5% and lower 2.5% confidence interval. The fitted distribution aligns well to the hindcast data points, also at the tail, and all events are within the confidence levels. The 50-year total low-water level is -1.0 mMSL.

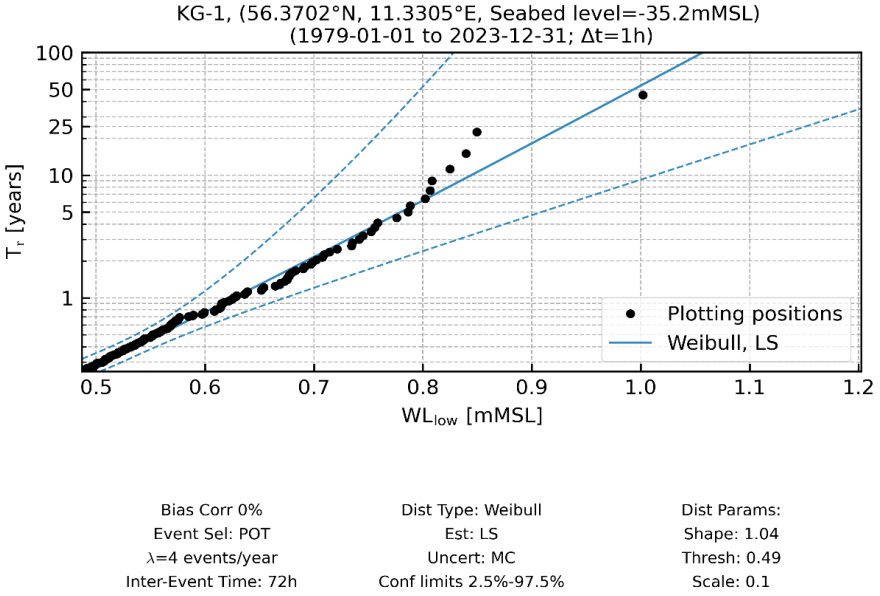

Figure 5-6 Marginal EVA of low-water level, WL_{low}, at KG-1. Note that the low water levels are positive on the figure.

Table 5-6 Estimates of low water level, WL_{low}, at KG-1.

	WL_{low} [mMSL]					
	Quantile	T_r 1	T_r 5	T_r 10	T_r 25	T_r 50
Omni	2.5%-tile	-0.6	-0.7	-0.7	-0.8	-0.8
	50%-tile	-0.6	-0.8	-0.8	-0.9	-1
	97.5%-tile	-0.7	-0.9	-1	-1.1	-1.2

5.2.4 Extreme residual low-water levels

The extreme residual low water level fit for the 45-year hindcast period is shown on Figure 5-7. Note that the low water levels are positive on the figure. Values for selected return periods are additionally shown in Table 5-6. The Weibull distribution fitted with the least squares method in shown along the upper 97.5% and lower 2.5% confidence interval. The fitted distribution aligns well to the hindcast data points, also at the tail, and all events are within the confidence levels. The 50-year residual low-water level is -1.1 mMSL.

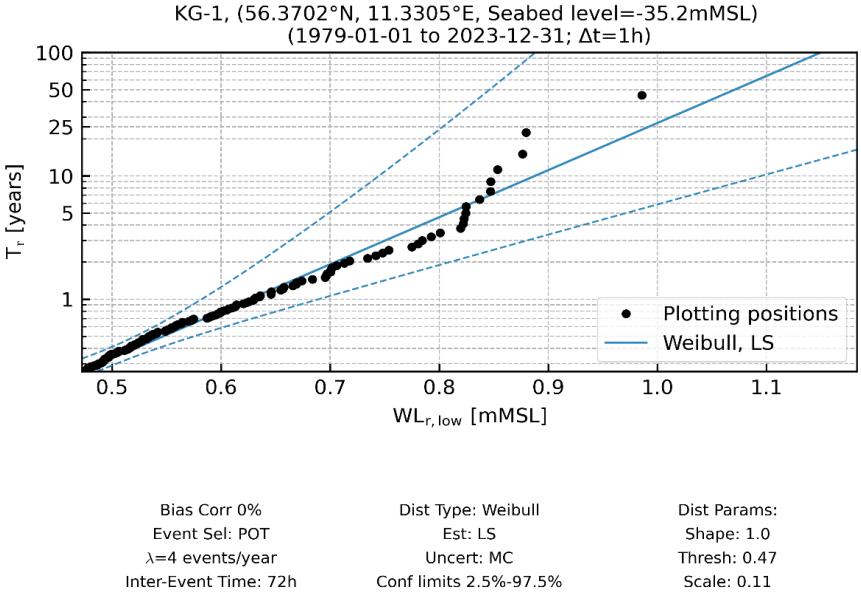

Figure 5-7 Marginal EVA of residual low-water level, $WL_{r,low}$, at KG-1. Note that the low water levels are positive on the figure.

Table 5-7 Estimates of residual low water level, $WL_{r,low}$, at KG-1.

	$WL_{r,low}$ [mMSL]					
	Quantile	T_r 1	T_r 5	T_r 10	T_r 25	T_r 50
Omni	2.5%-tile	-0.6	-0.7	-0.8	-0.8	-0.8
	50%-tile	-0.6	-0.8	-0.9	-1	-1.1
	97.5%-tile	-0.7	-1	-1.1	-1.2	-1.4

5.2.5 Maps of Extreme high-water levels

From Figure 5-8 to Figure 5-12 is shown the spatial variation of the high water levels across the data delivery area of KG for return periods of 1, 5, 10, 25 and 50 years based on individual extreme value analysis at each model grid point.

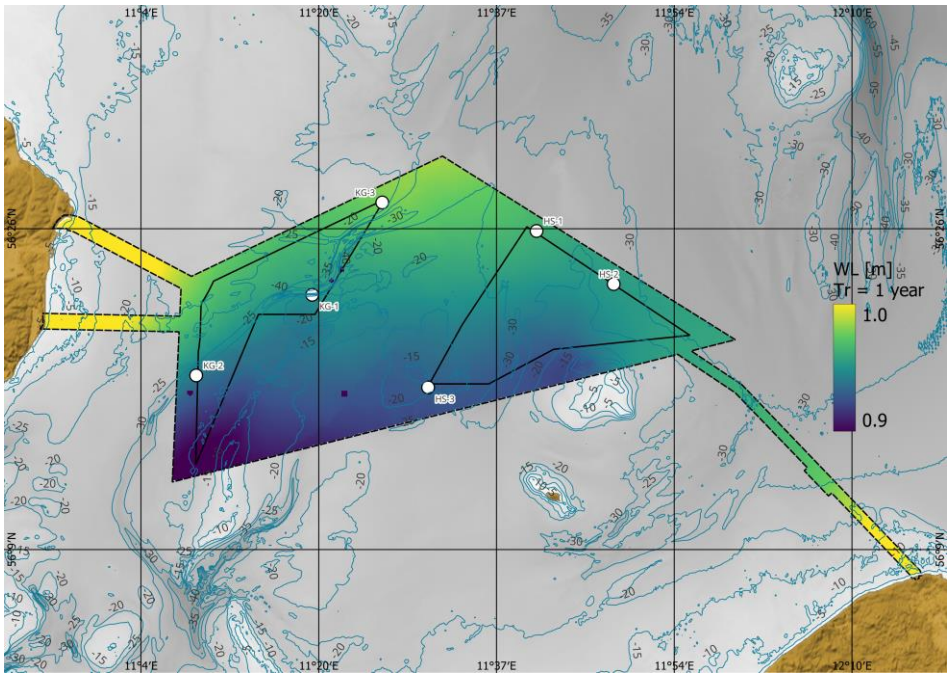

Figure 5-8 Spatial variation across the data delivery area of KG of total water level, WL, for return periods of 1 years. The colour map shows the water level, and the contours show water depths.

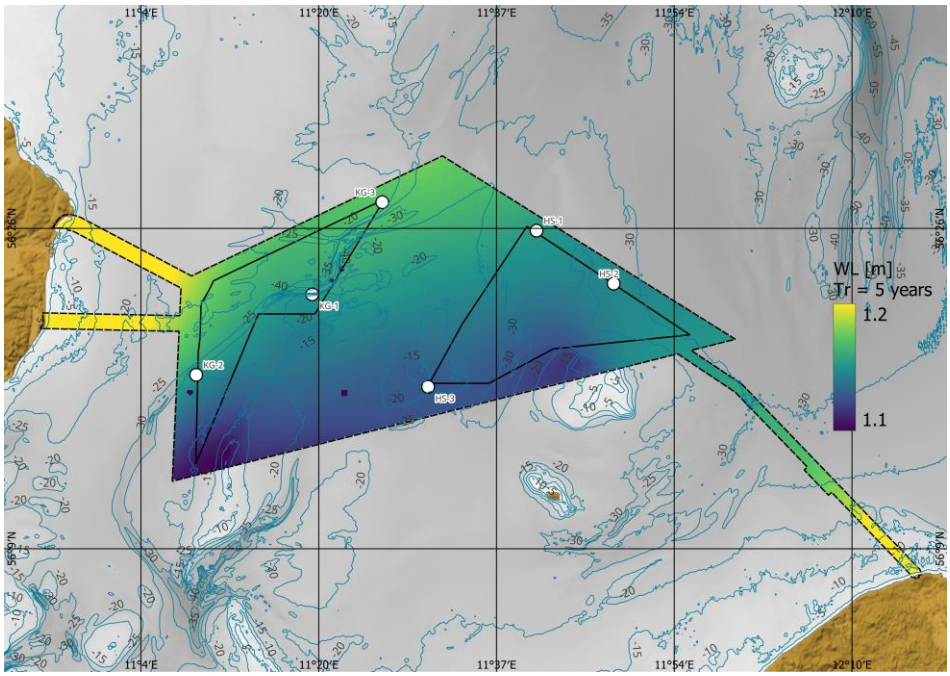

Figure 5-9 Spatial variation across the data delivery area of KG of total water level, WL,for return periods of 5 years. The colour map shows the water level, and the contours show water depths.

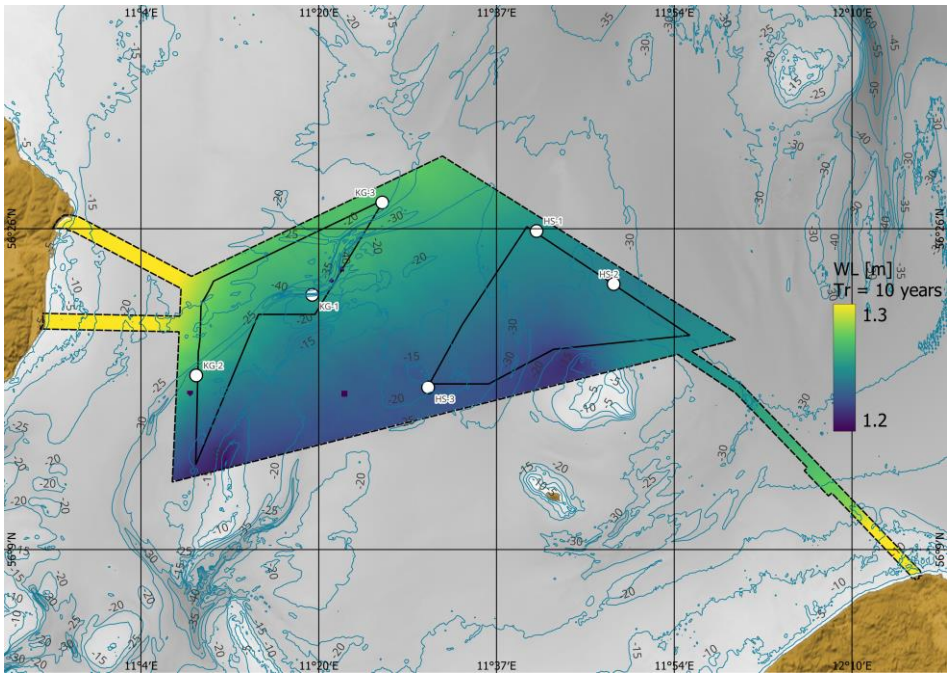

Figure 5-10 Spatial variation across the data delivery area of KG of total water level, WL,for return periods of 10 years. The colour map shows the water level, and the contours show water depths.

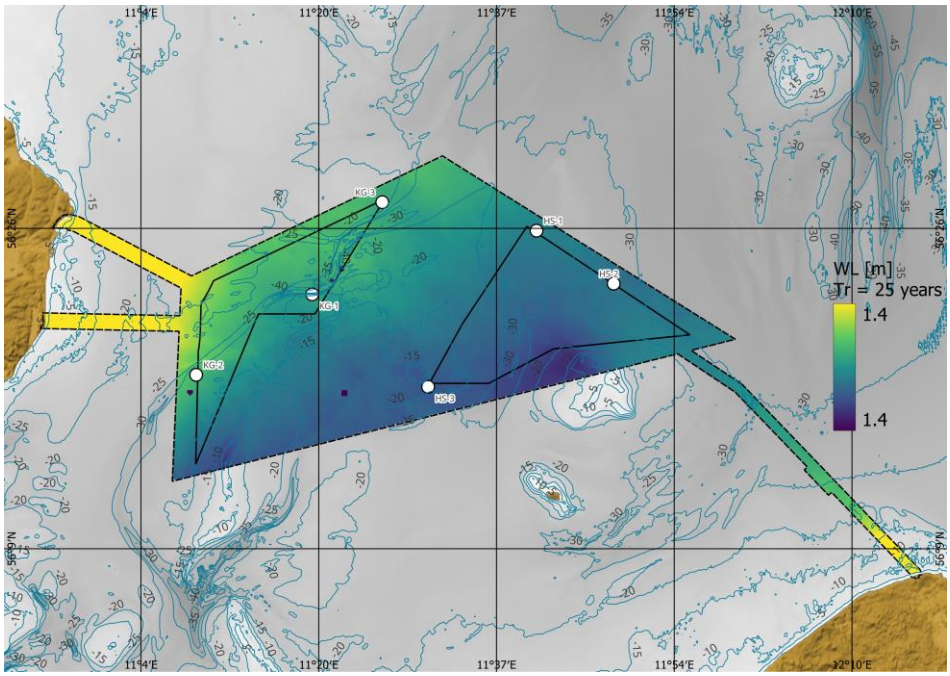

Figure 5-11 Spatial variation across the data delivery area of KG of total water level, WL,for return periods of 25 years. The colour map shows the water level, and the contours show water depths.

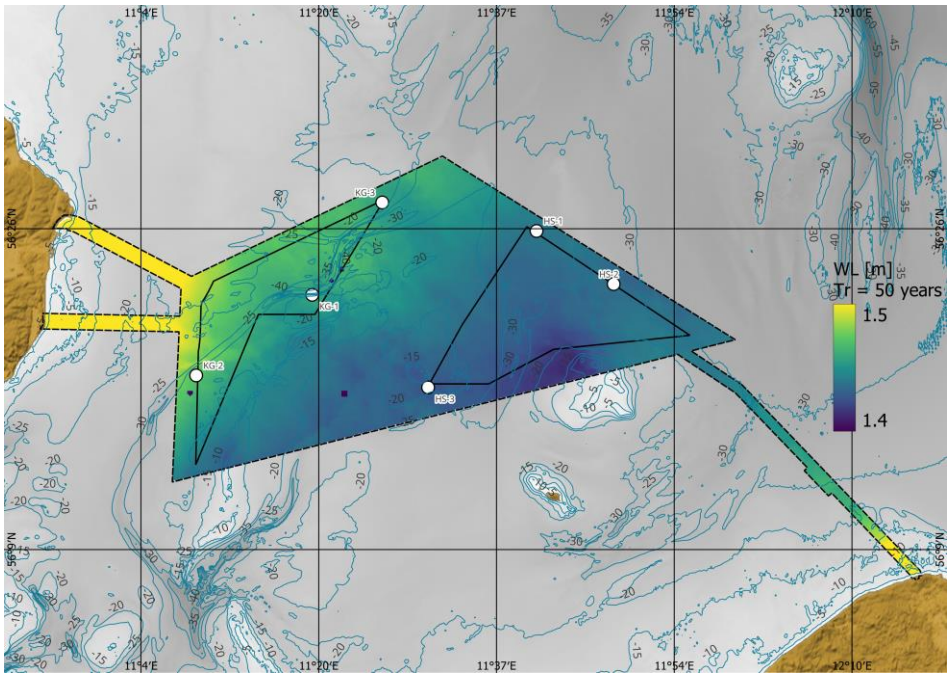

Figure 5-12 Spatial variation across the data delivery area of KG of total water level, WL,for return periods of 50 years. The colour map shows the water level, and the contours show water depths.

5.2.6 Maps of Extreme low-water levels

From Figure 5-13 to Figure 5-17 is the spatial variation of the low water levels across the data delivery area of KG for return periods of 1, 5, 10, 25 and 50 years based on individual extreme value analysis on each model grid point.

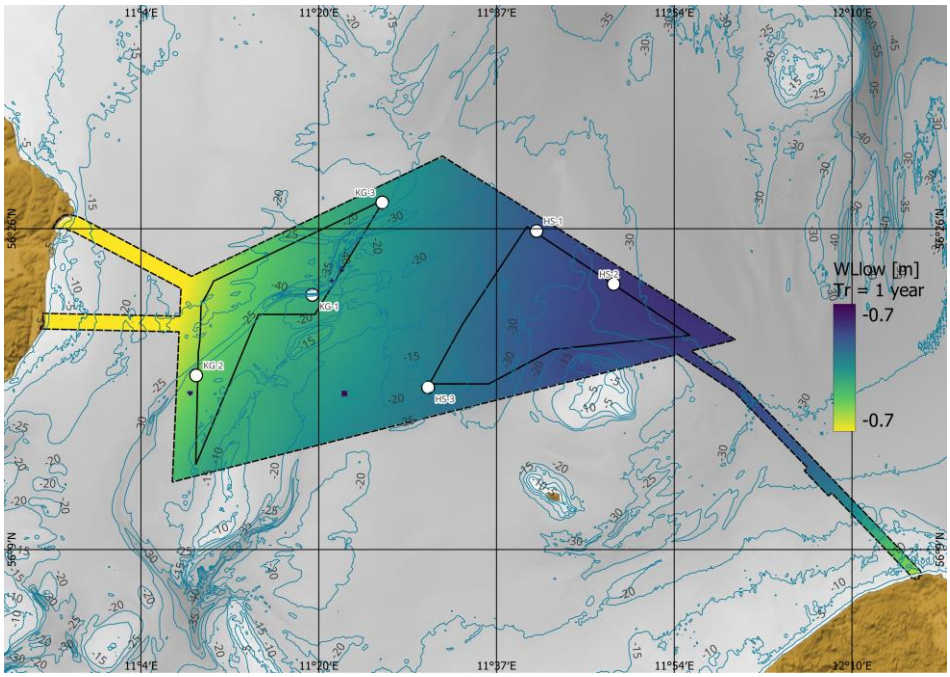

Figure 5-13 Spatial variation across the data delivery area of KG of total water level, WL_{low} for return periods of 1 years. The colour map shows the low water level, and the contours show water depths.

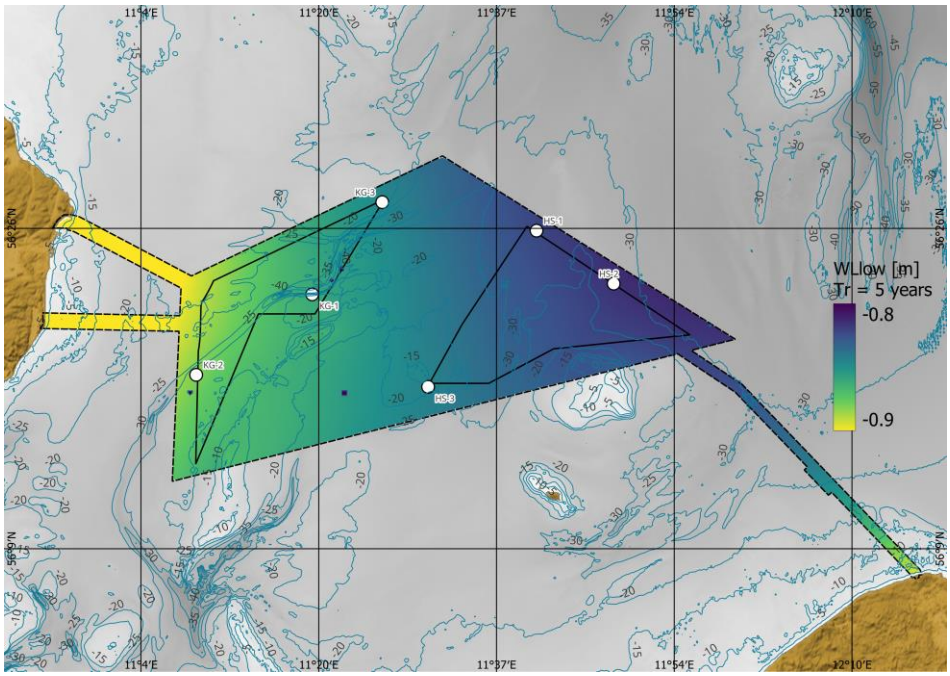

Figure 5-14 Spatial variation across the data delivery area of KG of total water level, WL_{low} for return periods of 5 years. The colour map shows the low water level, and the contours show water depths.

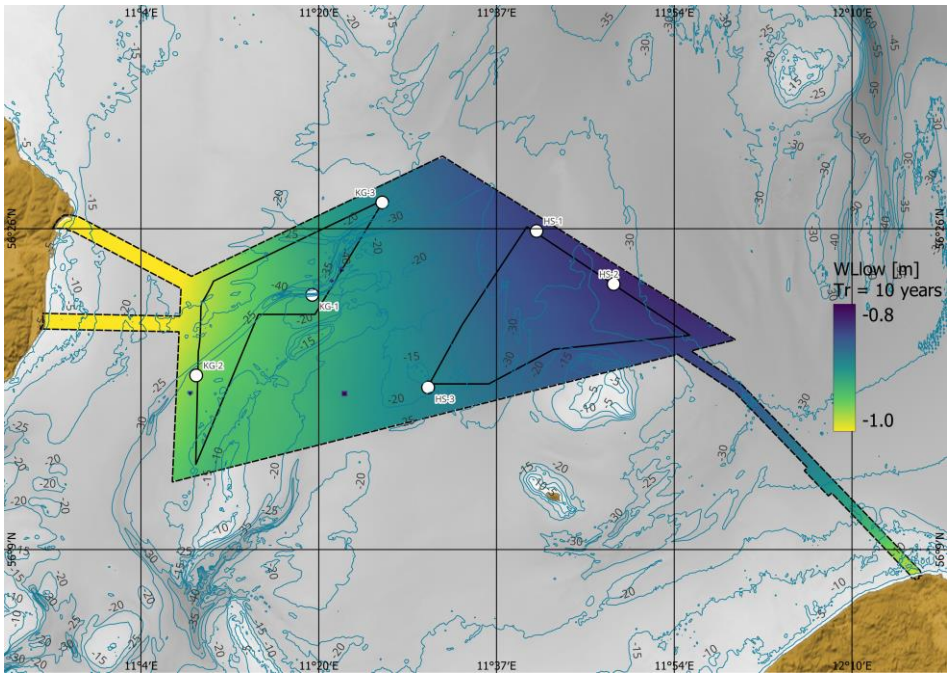

Figure 5-15 Spatial variation across the data delivery area of KG of total water level, WL_{low} for return periods of 10 years. The colour map shows the low water level, and the contours show water depths.

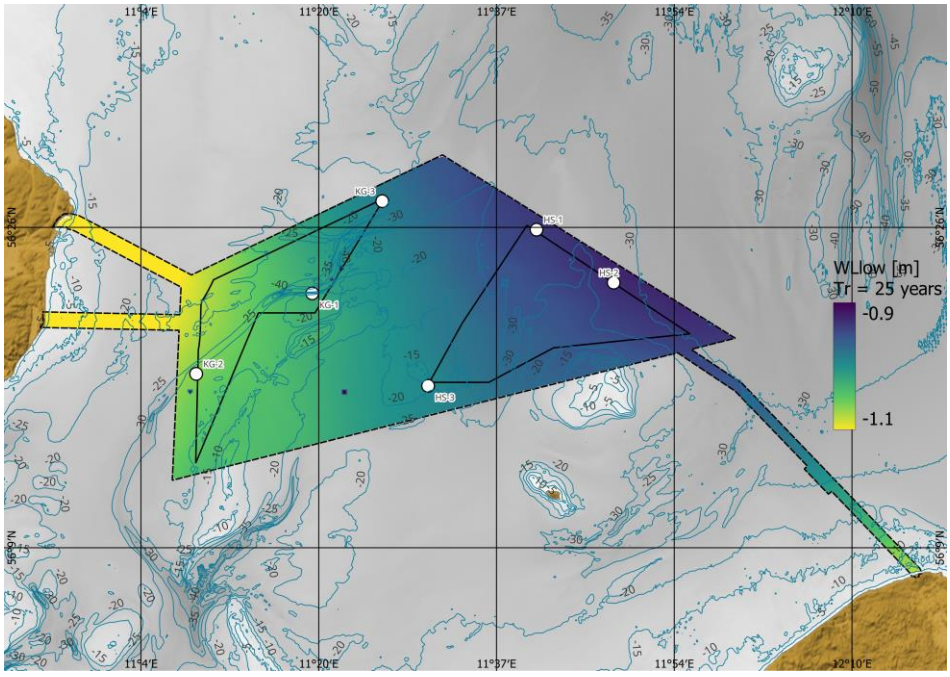

Figure 5-16 Spatial variation across the data delivery area of KG of total water level, WL_{low} for return periods of 25 years. The colour map shows the low water level, and the contours show water depths.

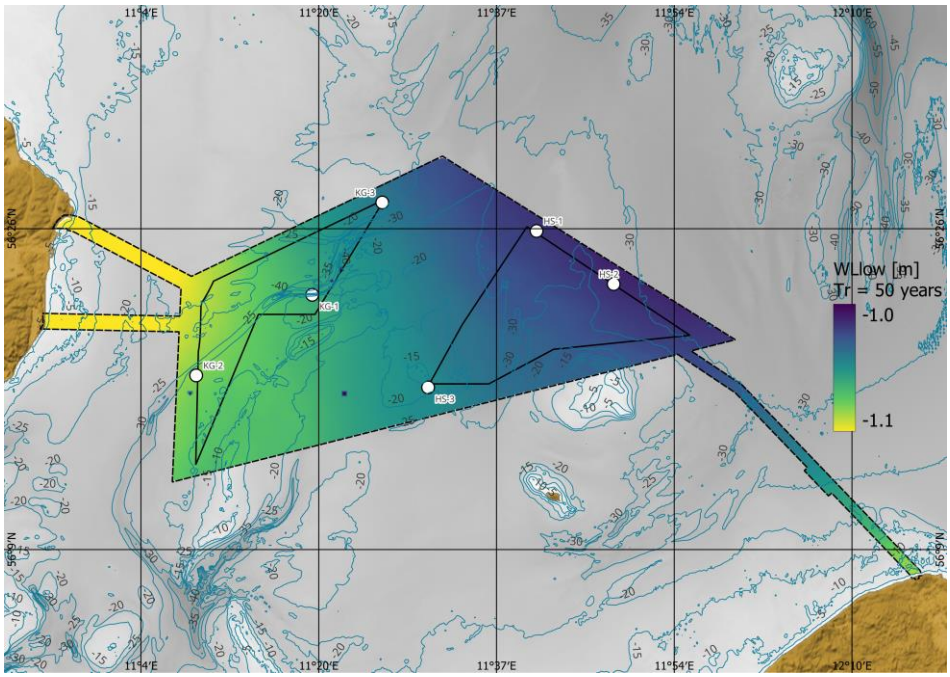

Figure 5-17 Spatial variation across the data delivery area of KG of total water level, WL_{low} for return periods of 50 years. The colour map shows the low water level, and the contours show water depths.

6 Current conditions

This section presents a summary of the current data basis established in [1], followed by a presentation of normal and extreme current conditions at the KG area.

The current consists of a tidal and a residual component. The total current was separated by a decomposition done by harmonic analysis, into a tidal and a residual current component [1]. Table 6-1 summarises the metadata of the dataset.

Table 6-1 Metadata of the wave dataset.

Name	Value
Start Date [UTC]:	1979-01-01 00:00:00
End Date [UTC]:	2023-12-31 23:00:00
Time Step [s]	3600

The current analyses are presented in bins of 0.1 m/s. Table 6-2 presents the current variables of the dataset, including the bin sizes applied in figures and tables throughout this report Each variable has a corresponding derived variable for the tidal (suffix "t") and residual (suffix "r") components. This chapter presents the total current only, tidal and residual components can be found in the appendices.

Note that peak current speeds may be higher than expected due to the 3D data extension method, and further study of current speeds is advised during detailed design.

The data is presented at 3 depths throughout the water column, near surface, mid depth, and near-bed.

Table 6-2 Total current variables of the hydrodynamic dataset

Variable name	Abbrev.	Unit	Bin size
Current speed – near surface	CS_{stot}	m/s	0.1
Current speed – mid depth	CS_{mtot}	m/s	0.1
Current speed – near bed	CS_{btot}	m/s	0.1
Current direction – near surface	CD_{stot}	°N-going	22.5
Current direction – mid depth	CD_{mtot}	°N-going	22.5
Current direction – near bed	CD_{btot}	°N-going	22.5

6.1 Normal current conditions

The normal current conditions are presented in terms of:

- Time series
- Current roses
- Scatter plots
- Histograms

- Monthly statistics
- Directional statistics

6.1.1 Timeseries

Figure 6-1, Figure 6-2 and Figure 6-3 shows the time series of the total current speed at 3 levels at KG-1 during the 45-year period. The lowest, mean, and highest current speed for each level is summarised in Table 6-3.

Table 6-3 Summary of current speed at 3 depths at KG-1.

Current speed [m/s]	MIN	MEAN	MAX
CS_{stot} [m/s]	0.0	0.3	1.8
CS_{mtot} [m/s]	0.0	0.2	0.9
CS_{btot} [m/s]	0.0	0.2	0.7

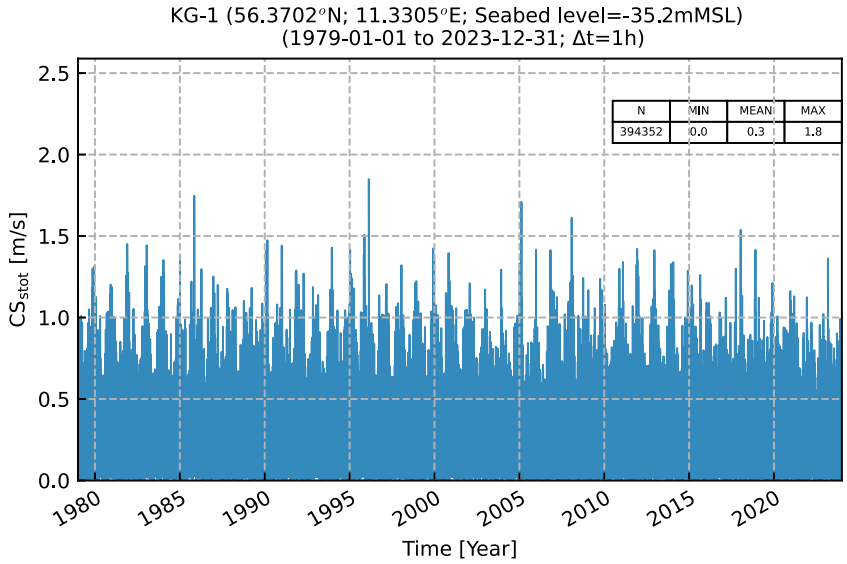

Figure 6-1 Time series of CS_{stot} at KG-1.

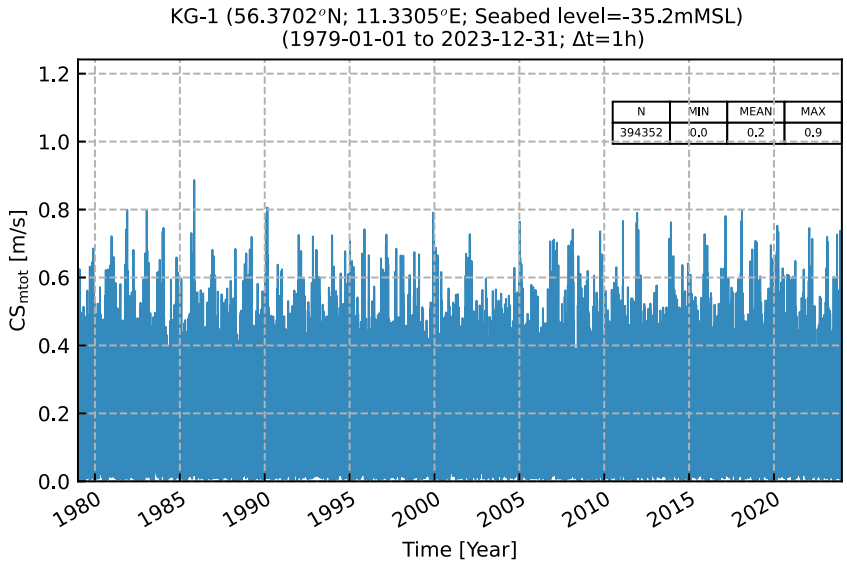

Figure 6-2 Time series of CS_{mtot} at KG-1.

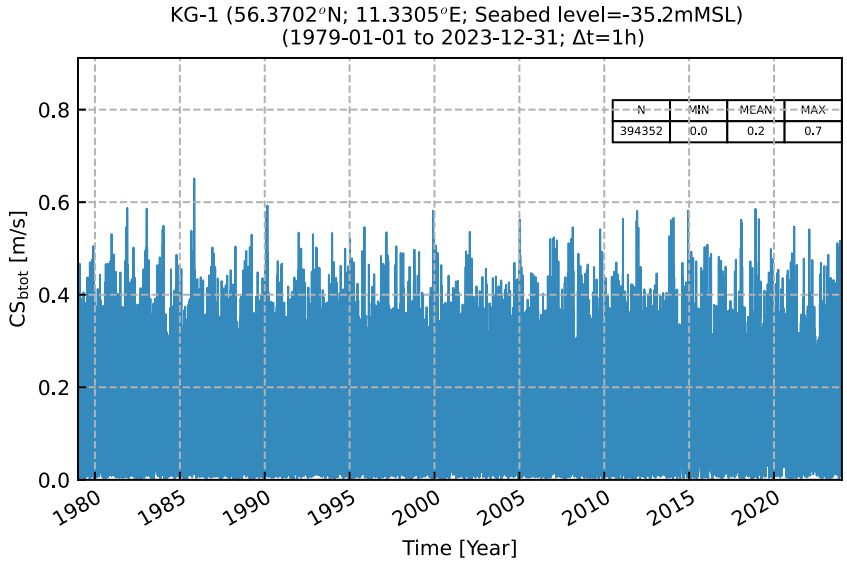

Figure 6-3 Time series of CS_{btot} at KG-1.

6.1.2 Current roses

Figure 6-4, Figure 6-5 and Figure 6-6 shows roses of current speed at near-surface, mid-depth, and near-seabed at KG-1. The near-surface and mid current shows currents predominantly going north-east and south-west. At near-seabed, the current is predominantly going to westerly directions, it is noted that the near-seabed current speeds are low, and at lower levels the effect of stratification and tide plays a larger role than higher in the water column where the effect of wind dominates, thus the current rose at near-seabed differs from the current rose at mid depth and surface.

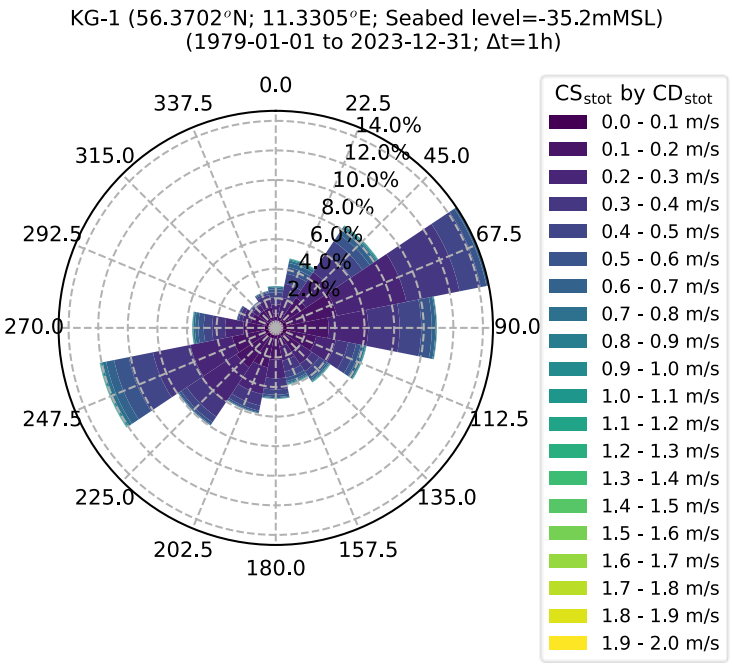

Figure 6-4 Rose plot of CS_{stot} at KG-1.

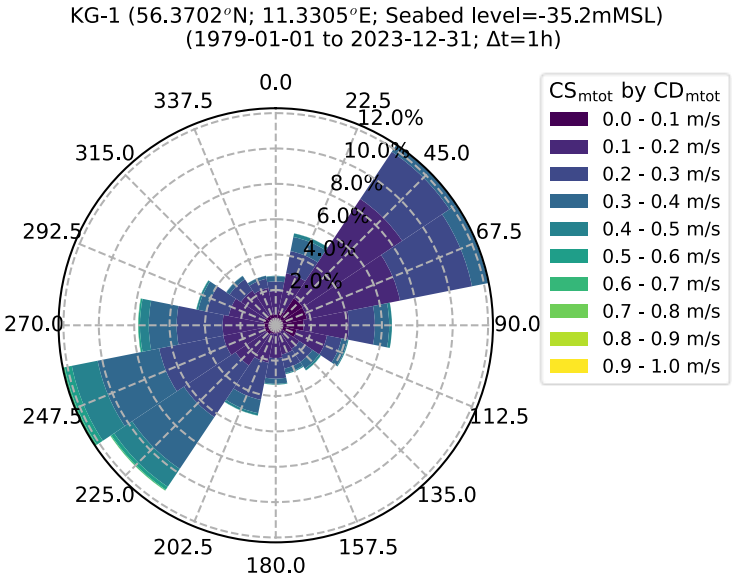

Figure 6-5 Rose plot of CS_{mtot} at KG-1.

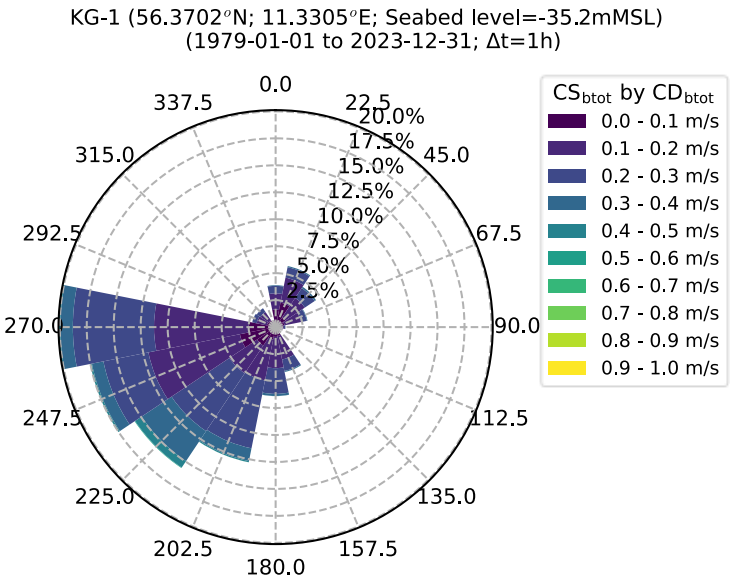

Figure 6-6 Rose plot of CS_{btot} at KG-1.

6.1.3 Histogram

Figure 6-7, Figure 6-8 and Figure 6-9 show the histogram current speed at KG-1, at near-surface, mid-depth, and near-seabed, respectively.

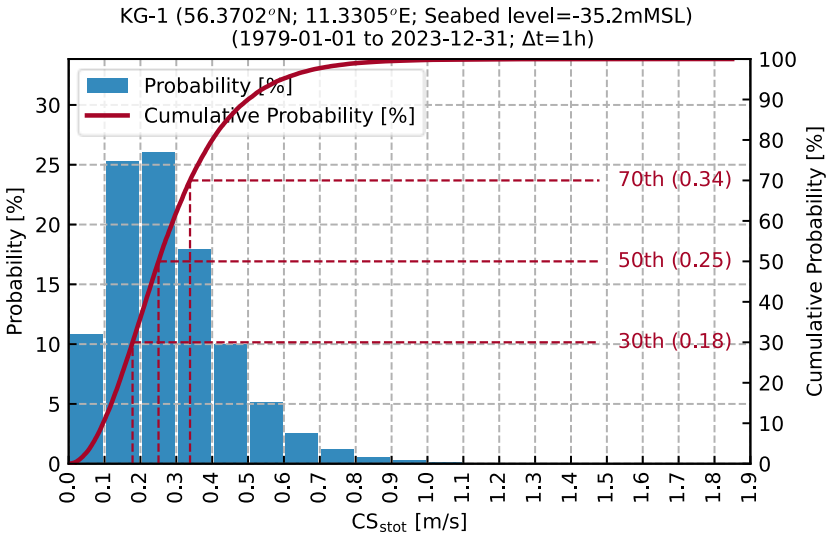

Figure 6-7 Probability plot of CS_{stot} at KG-1.

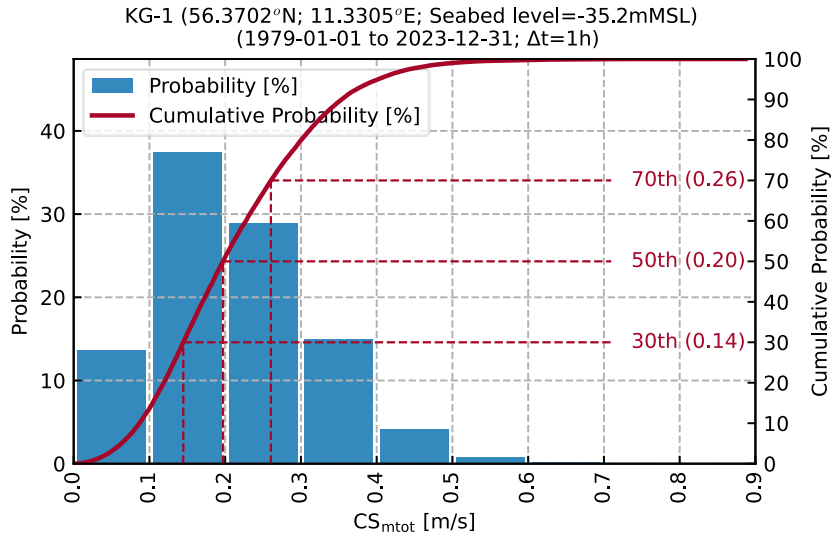

Figure 6-8 Probability plot of CS_{mtot} at KG-1.

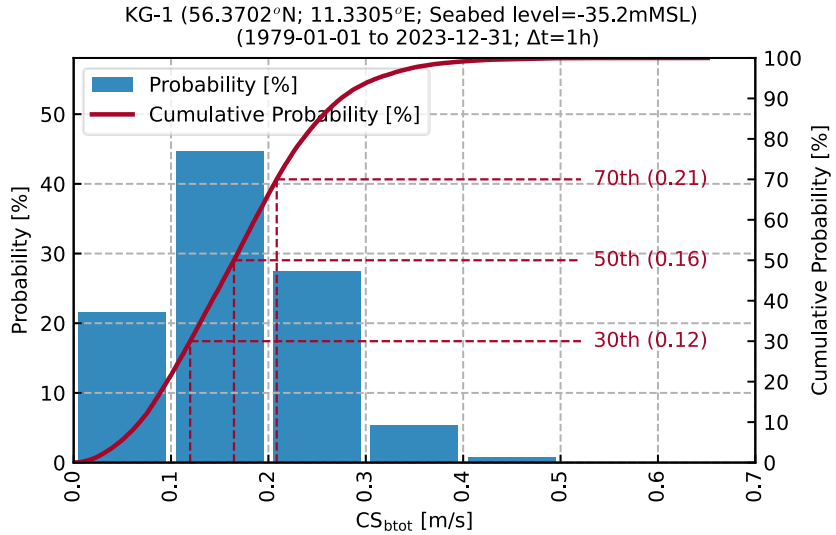

Figure 6-9 Probability plot of CS_{btot} at KG-1.

6.1.4 Monthly statistics

Figure 6-10, Figure 6-11 and Figure 6-12 show the monthly statistics of current speed at KG-1, at near-surface, mid-depth, and near-seabed, respectively.

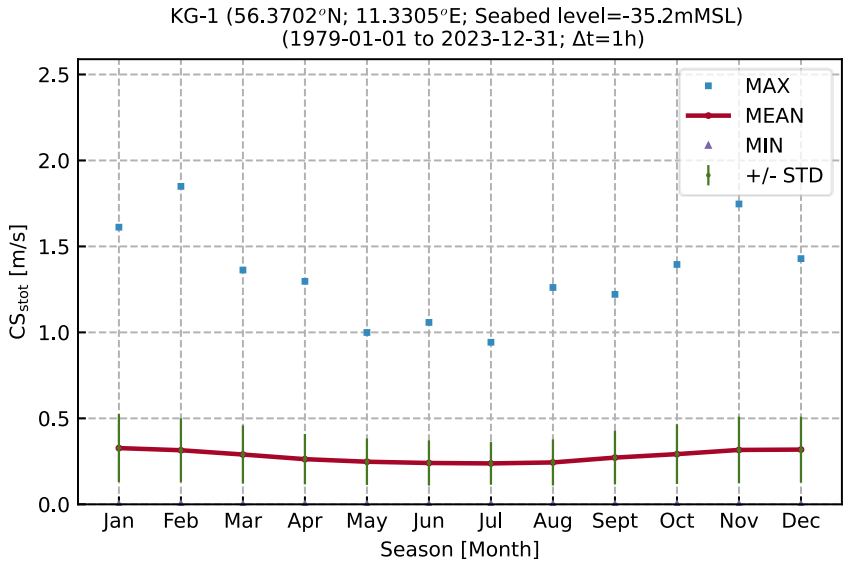

Figure 6-10 Monthly statistics of CS_{stot} at KG-1.

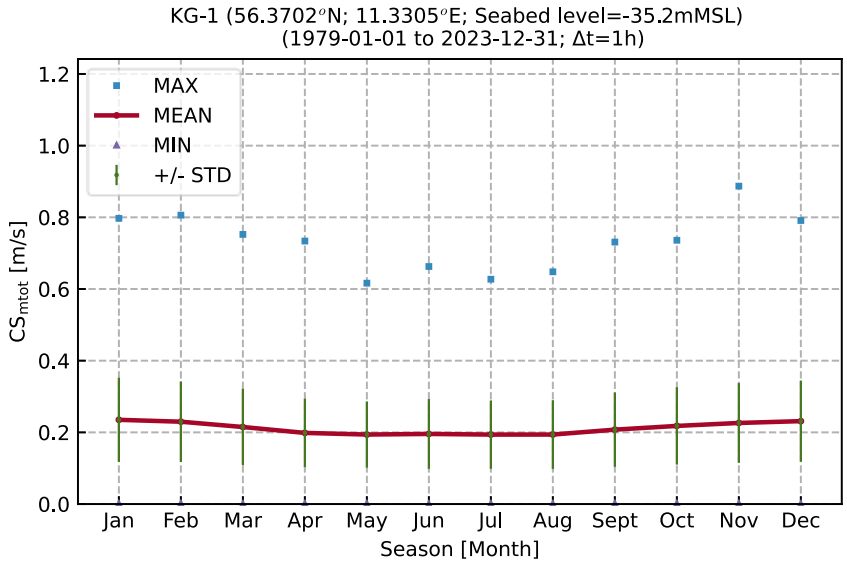

Figure 6-11 Monthly statistics of CS_{mtot} at KG-1.

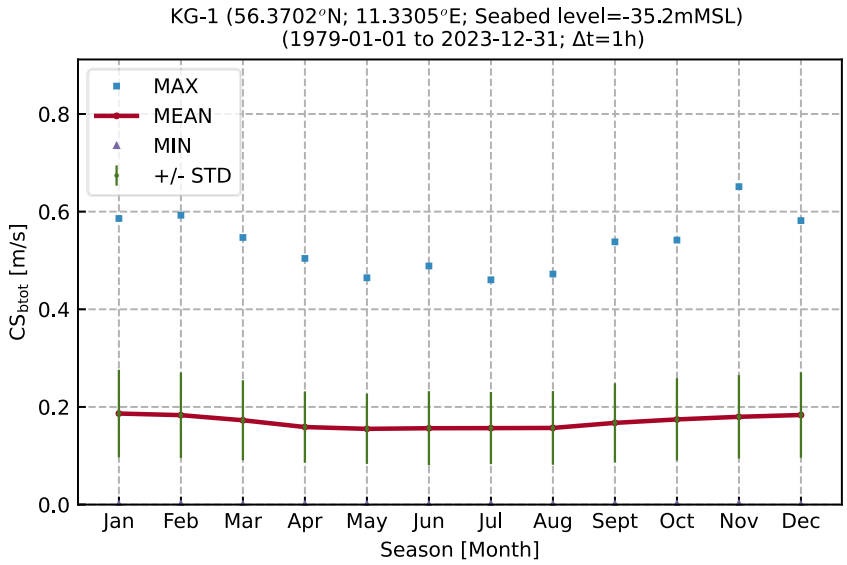

Figure 6-12 Monthly statistics of CS_{btot} at KG-1.

6.1.5 Directional statistics

Figure 6-13, Figure 6-14 and Figure 6-15 show the directional statistics of current speed at KG-1, at near-surface, mid-depth, and near-seabed, respectively.

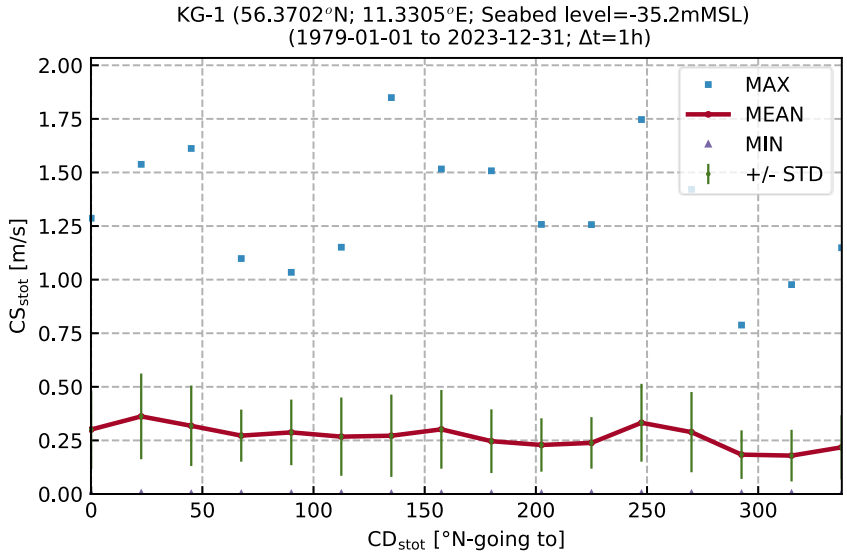

Figure 6-13 Directional statistics of CS_{stot}, sorted by CD_{stot}, at KG-1.

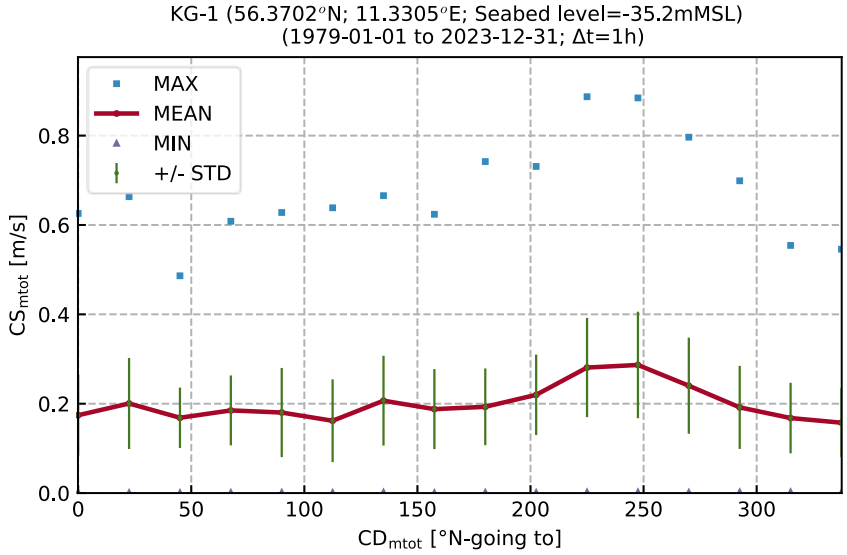

Figure 6-14 Directional statistics of CS_{mtot}, sorted by CD_{mtot}, at KG-1.

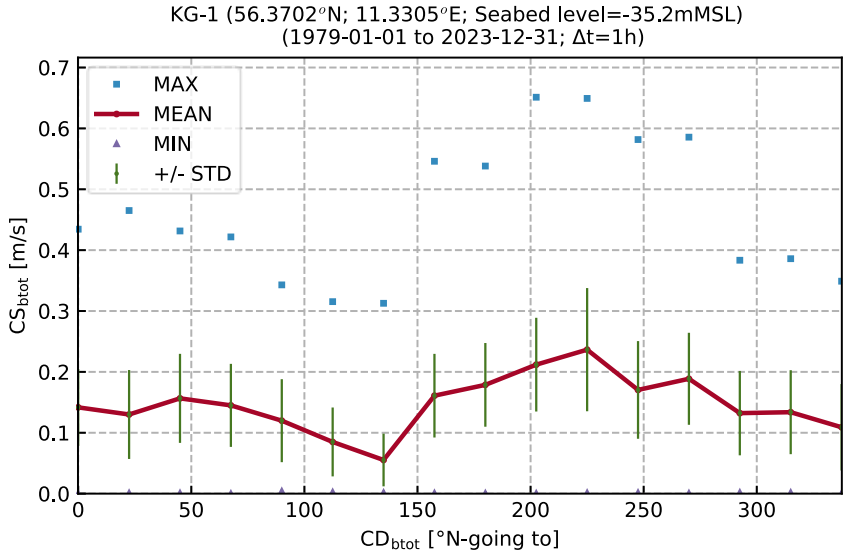

Figure 6-15 Directional statistics of CS_{btot}, sorted by CD_{btot}, at KG-1.

6.1.6 Vertical profiles of current speed, temperature, and salinity

The hydrodynamic dataset also includes oceanographic variables, covering a 10-year period from 2014 to 2023. These variables are detailed in Table 6-4 and are available at all model levels throughout the water column. These levels are used for profiling.

Table 6-4 Oceanographic variables of the hydrodynamic dataset

Variable name	Abbrev.	Unit	Bin size
Current speed	CS	m/s	0.1
Seawater temperature	T_{sw}	ºC	1
Salinity	Sal	PSU	2

In Figure 6-16 is the seasonal division of the vertical profile presented across 3-month groups. Summer is Jun, Jul, Aug. Fall is Sep, Oct, Nov. Winter is Dec, Jan, Feb. Spring is Mar, Apr, May. Figure 6-17 includes each individual month.

The current speeds are largest in the winter and smallest in the summer. The upper body of the water is hottest in the summer and coldest in the winter. The lower water bodies are coldest in spring and hottest in fall. The thermocline is not distinct during winter, spring and fall. In the summer period the thermocline is relatively pronounced and ranges from approximately -5 mMSL to -20 m MSL. The halocline is pronounced in all seasons and ranges from approximately -4 mMSL to -20 mMSL.

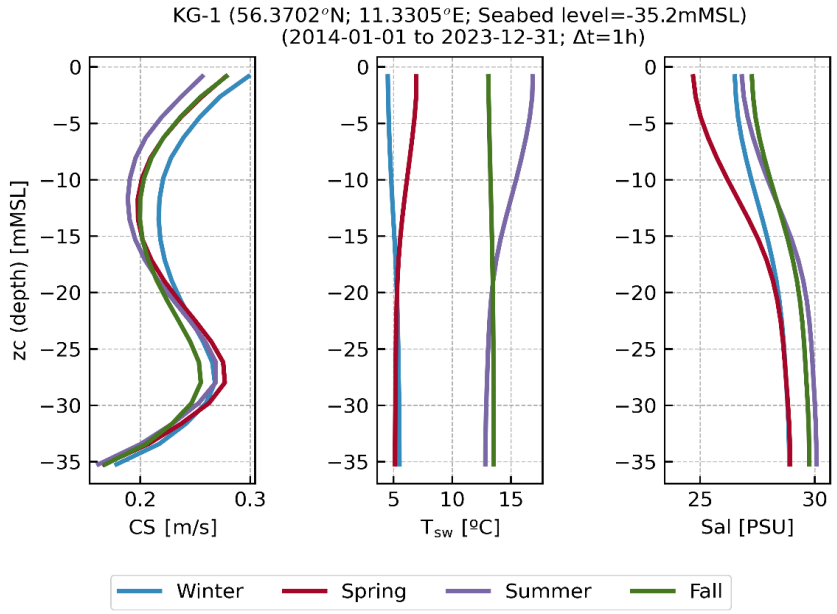

Figure 6-16 Profiles of current speed, Sea water temperature and salinity for each season winter, spring, summer, and fall.

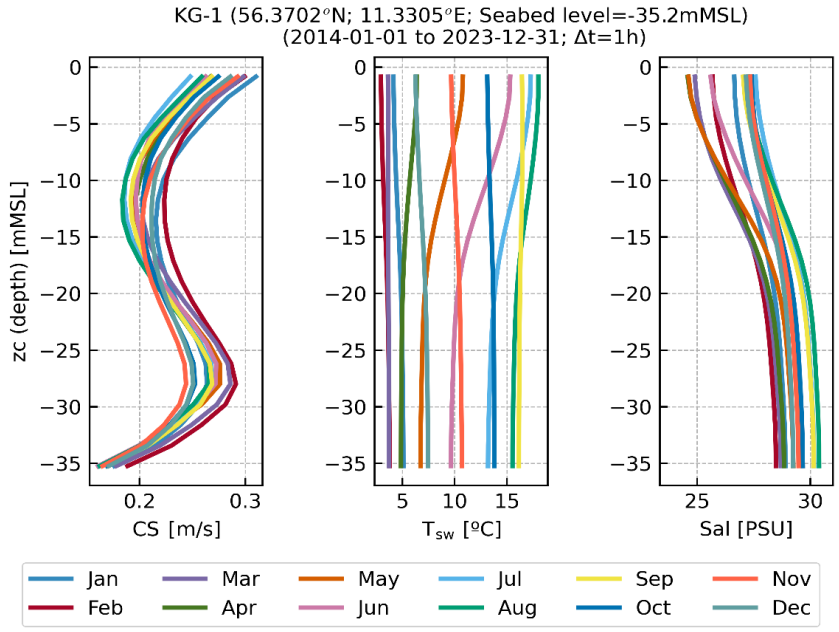

Figure 6-17 Profiles of current speed, Sea water temperature and salinity for each month.

6.1.7 Maps of C_S

Figure 6-18 to Figure 6-29 present maps across the data delivery area of the normalised moment of the current speed, C_S, calculated as follows.

$$\overline{C_S} = \left[\frac{1}{N}\sum_{i=1}^{N} {C_{S_i}}^m\right]^{\frac{1}{m}}$$

where m = (1,2,4,5) is the power coefficient, and N is the total number of hindcast data points. m = 1 is the mean C_s and m = 2 is the root-mean-square current speed.

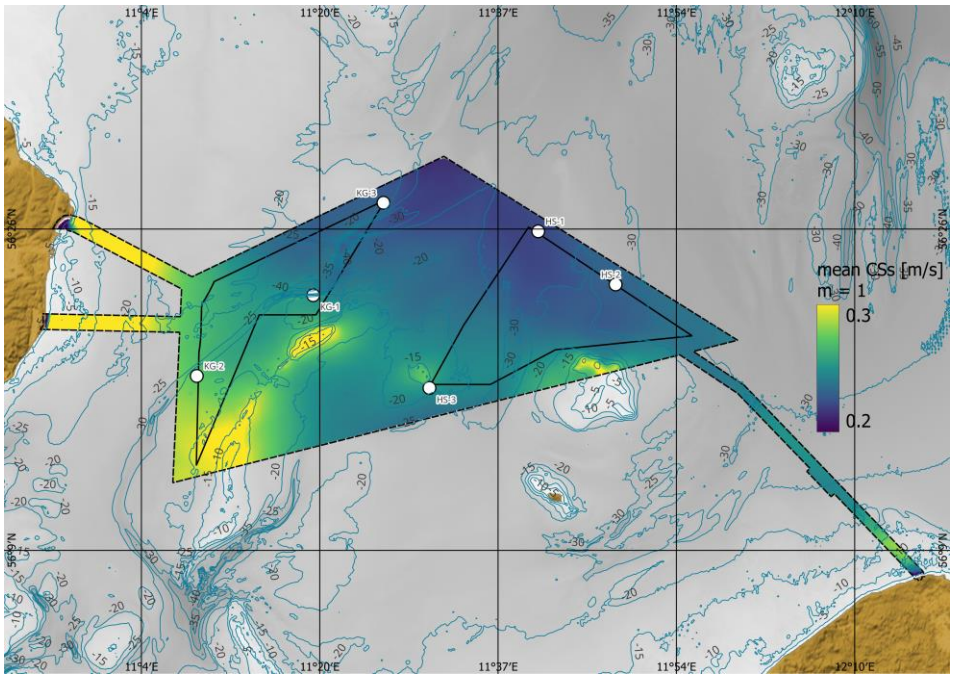

Figure 6-18 Spatial variation of moments of C_{ss} across the data delivery area, m=1

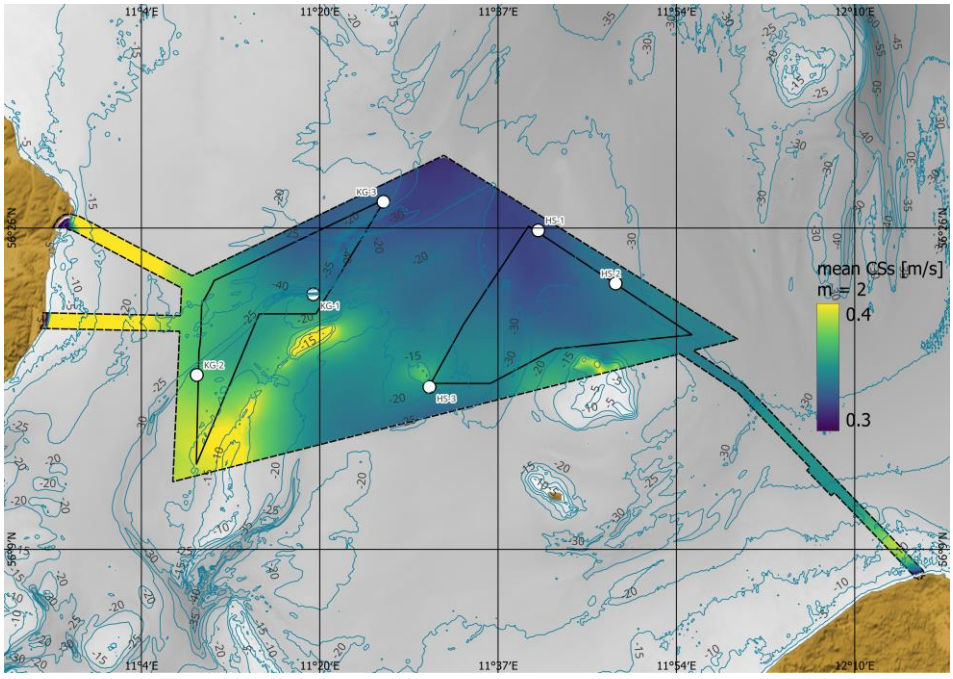

Figure 6-19 Spatial variation of moments of C_{ss} across the data delivery area, m=2

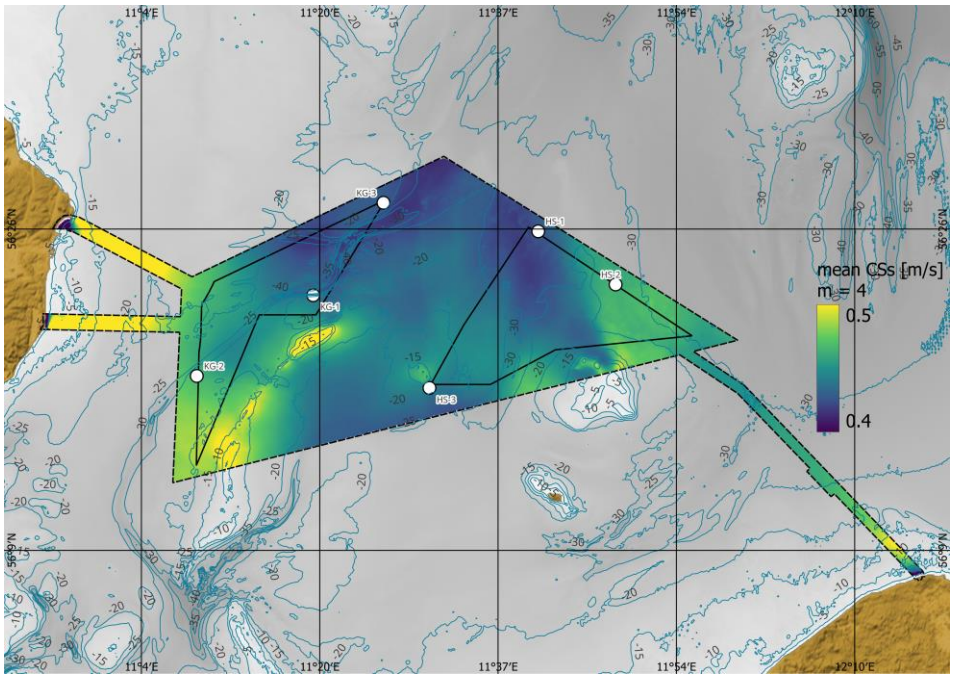

Figure 6-20 Spatial variation of moments of C_{ss} across the data delivery area, m=4

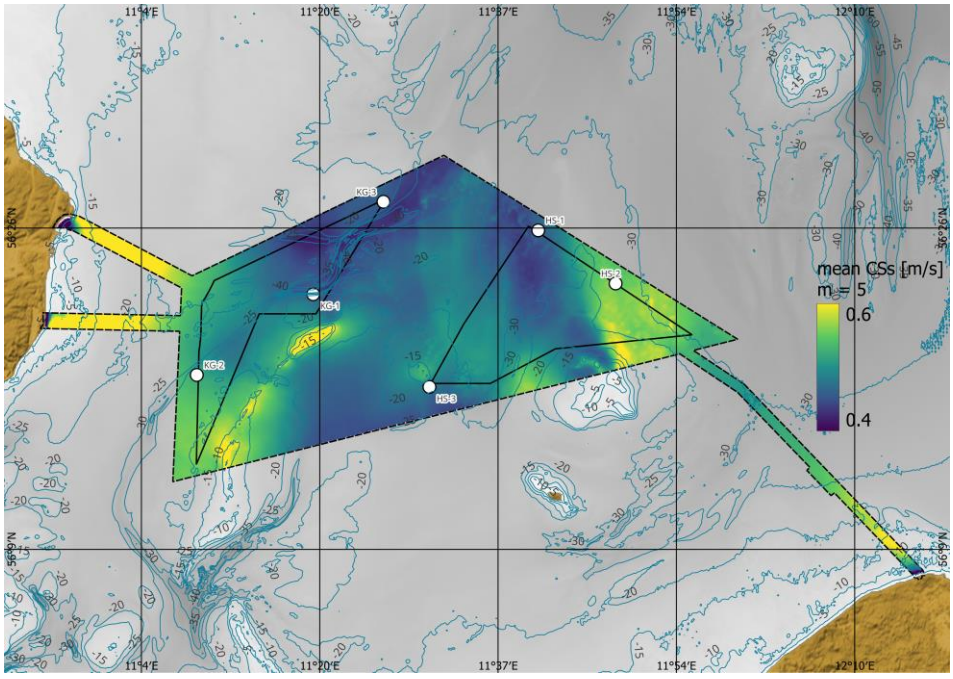

Figure 6-21 Spatial variation of moments of C_{ss} across the data delivery area, m=5

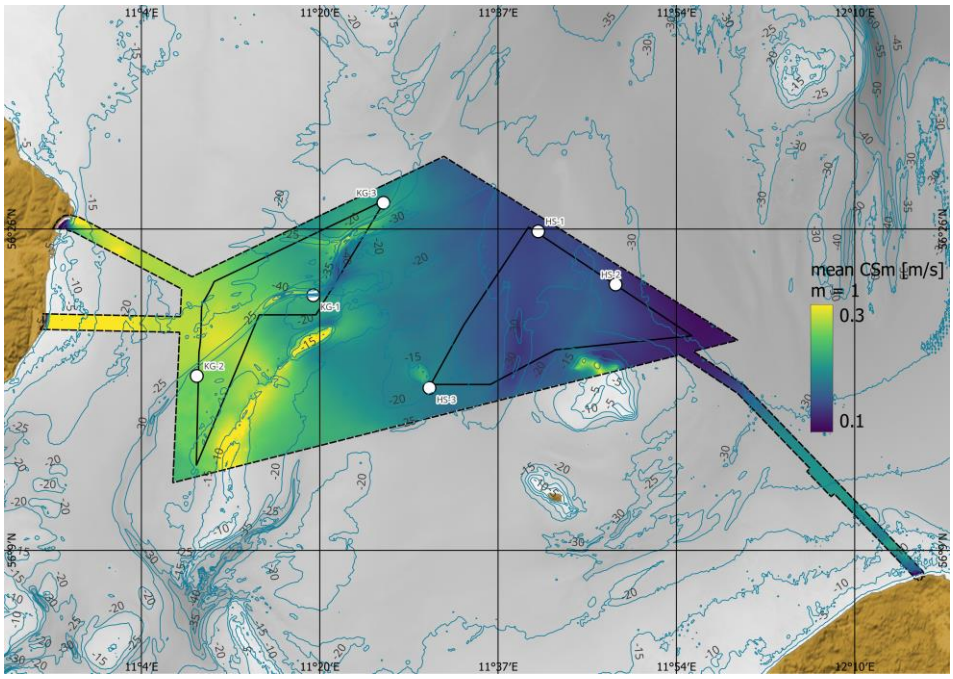

Figure 6-22 Spatial variation of moments of C_{sm} across the data delivery area, m=1.

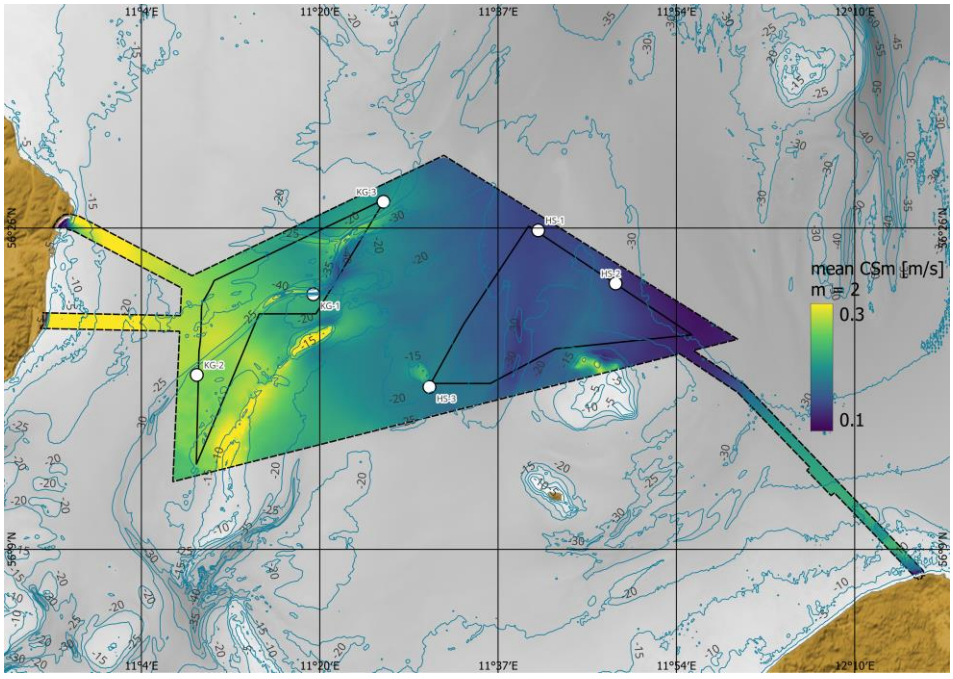

Figure 6-23 Spatial variation of moments of C_{sm} across the data delivery area, m=2.

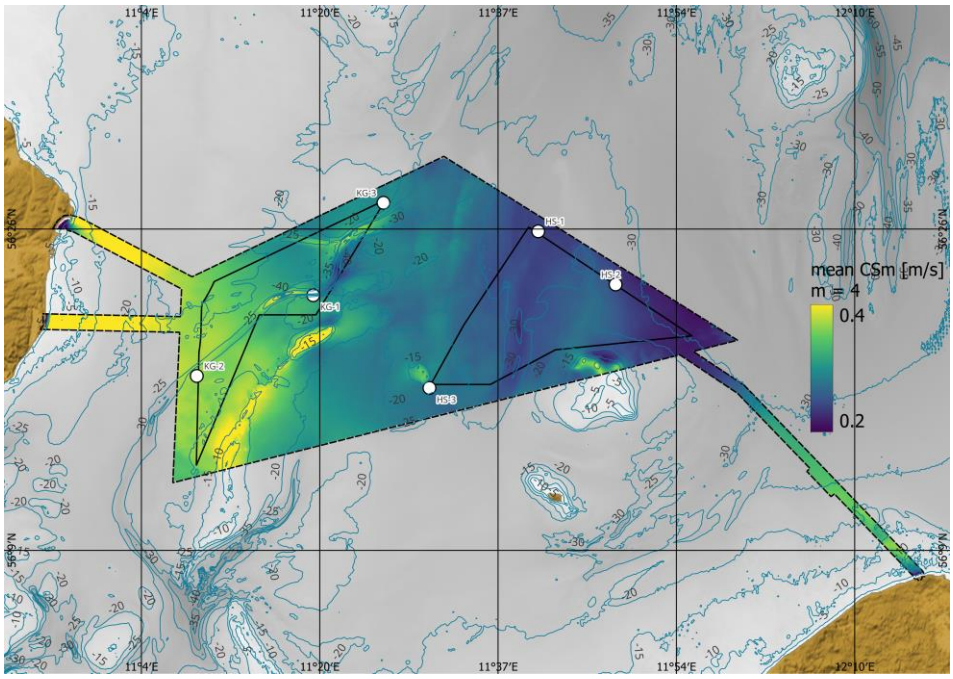

Figure 6-24 Spatial variation of moments of C_{sm} across the data delivery area, m=4.

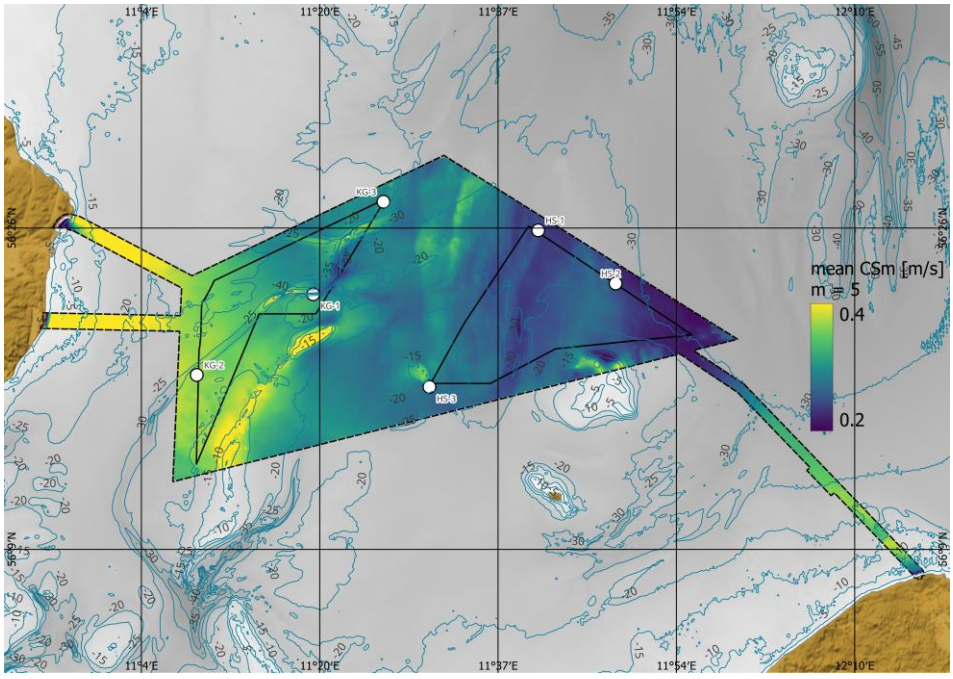

Figure 6-25 Spatial variation of moments of C_{sm} across the data delivery area, m=5.

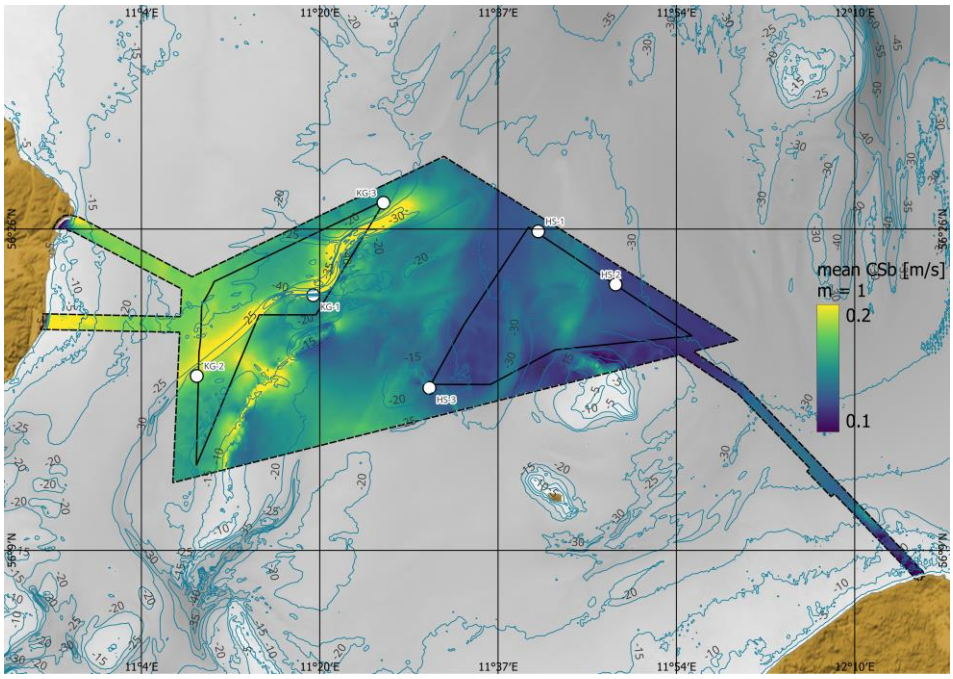

Figure 6-26 Spatial variation of moments of C_{sb} across the data delivery area, m=1.

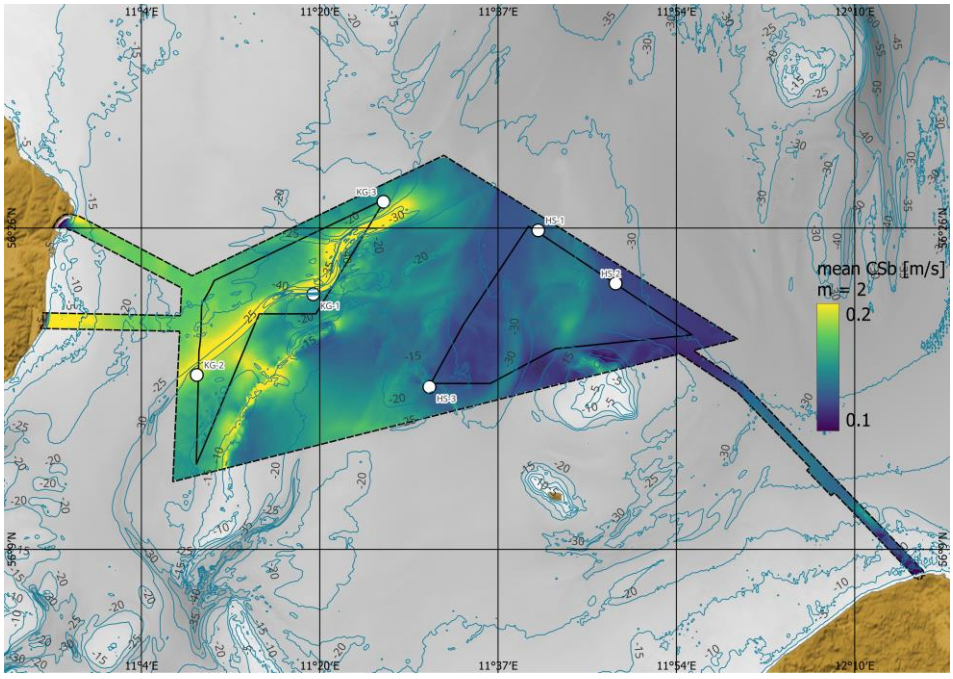

Figure 6-27 Spatial variation of moments of C_{sb} across the data delivery area, m=2.

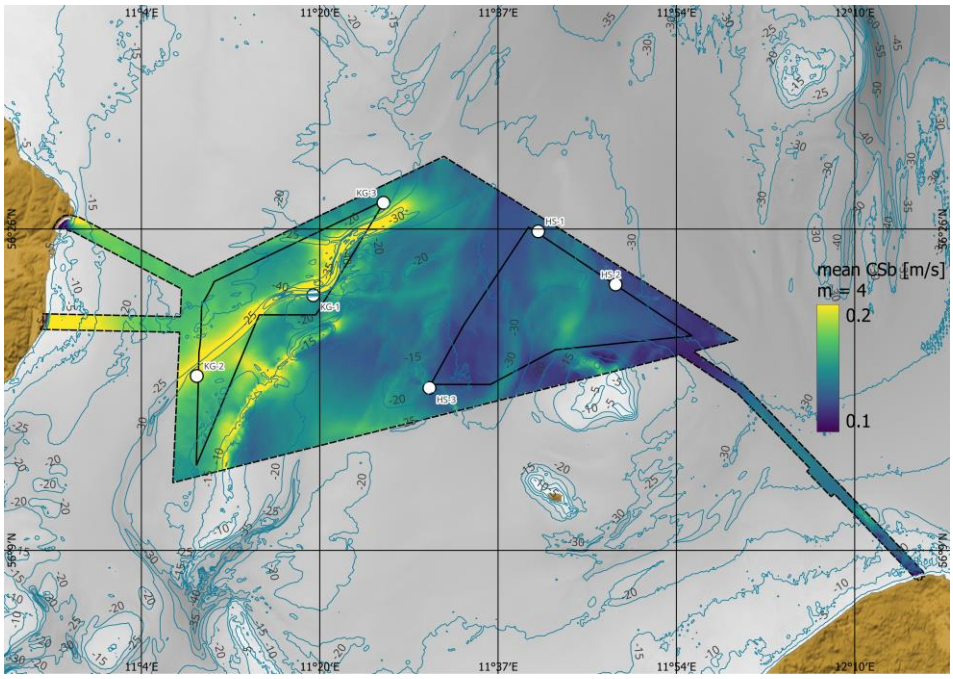

Figure 6-28 Spatial variation of moments of C_{sb} across the data delivery area, m=4.

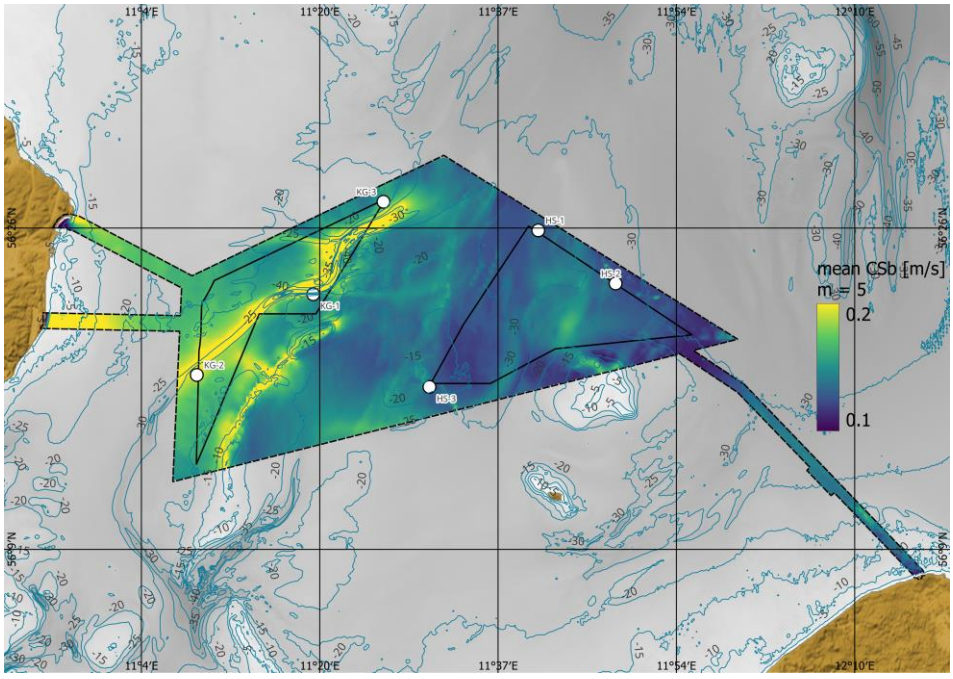

Figure 6-29 Spatial variation of moments of C_{sb} across the data delivery area, m=5.

6.2 Extreme current conditions unscaled

Extreme current conditions are established using Extreme Value analysis. The analysis is based on its performance and sensitivity to selection of distribution, threshold selection method, λ-value evaluation, and fitting estimator. A description of the methodology and the selection of settings is available in Appendix B.

For current speed, the 3-parameter Weibull distribution was fitted by the least square method to 45 peak events (λ=1) separated by at least 72 hours.

It is noted that all Extreme Value Analysis results presented in this section are unscaled, in other words raw results from the EVA without scaling with regards to directionality. Scaled results according to DNV-RPC205 where consistency between directional extremes and Omni for all return periods are ensured can be found in the appendices, see section 6.3 for details on the scaling.

6.2.1 Extreme total current speed at near surface

Figure 6-30 show the omni-directional EVA on current speed near surface. Figure 6-31 and Figure 6-32 shows the directional EVA on current speed near surface. Table 6-5 include the omni-directional EVA as well as the directional the directional extreme total near-surface current speed at KG-1.

The fitted distribution aligns well to the hindcast data points, also at the tail, and all events are within the confidence levels.

The 50-year total omni-directional near-surface current speed is 1.8 m/s.

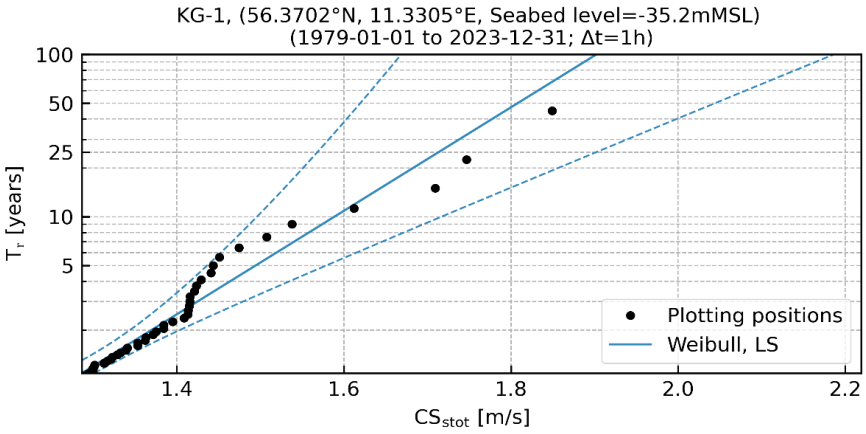

Figure 6-30 Marginal Omni-directional EVA estimates of CS_{stot} at KG-1.

Table 6-5 Marginal directional EVA estimates of CS_{stot} at KG-1.

Sector	CS_{stot} [m/s]					
CD_{stot} [°N-going to]	Quantile	T_r 1	T_r 5	T_r 10	T_r 25	T_r 50
0.0	Central estimate	0.8	1	1.1	1.2	1.3
22.5		1	1.2	1.3	1.4	1.6
45.0		1.1	1.3	1.4	1.5	1.6
67.5		0.8	0.9	1	1	1.1
90.0		0.8	0.9	1	1	1.1
112.5		0.8	1	1	1.1	1.2
135.0		1	1.3	1.5	1.7	1.8
157.5		0.9	1.2	1.3	1.4	1.5
180.0		0.8	1.1	1.2	1.4	1.5
202.5		0.6	0.9	1	1.1	1.2
225.0		0.7	1	1	1.2	1.3
247.5		1	1.3	1.4	1.6	1.7
270.0		0.9	1.2	1.2	1.4	1.5
292.5		0.5	0.7	0.7	0.8	0.8
315.0		0.5	0.7	0.7	0.8	0.9
337.5		0.6	0.8	0.9	1	1.1
Omni		1.3	1.5	1.6	1.7	1.8

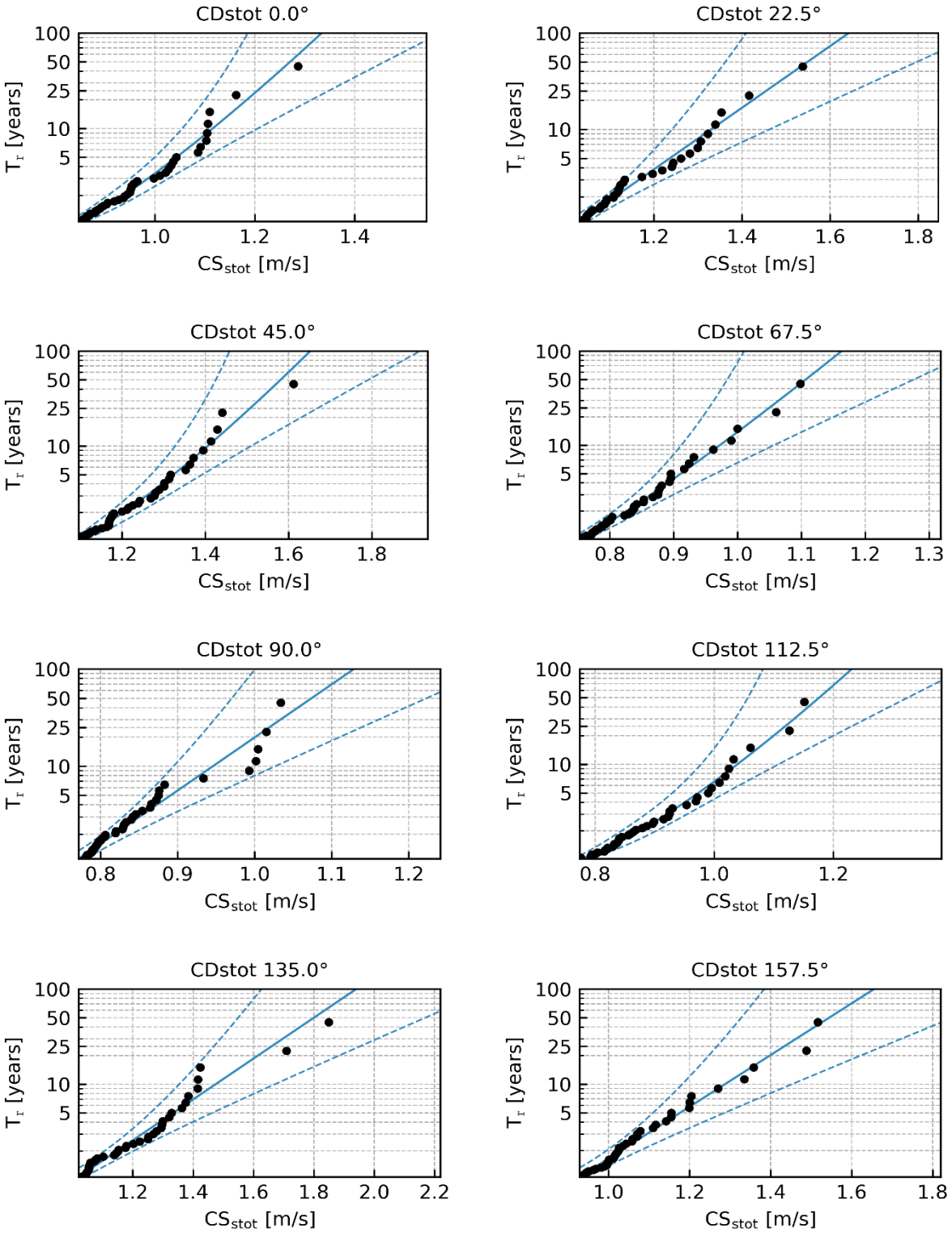

Figure 6-31 Marginal directional EVA estimates of CS_{stot} for CD_{stot} [°N-going to] sectors every 22.5° for KG-1. Weibull LS, λ = 1. Confidence limits 2.5% -97.5%.

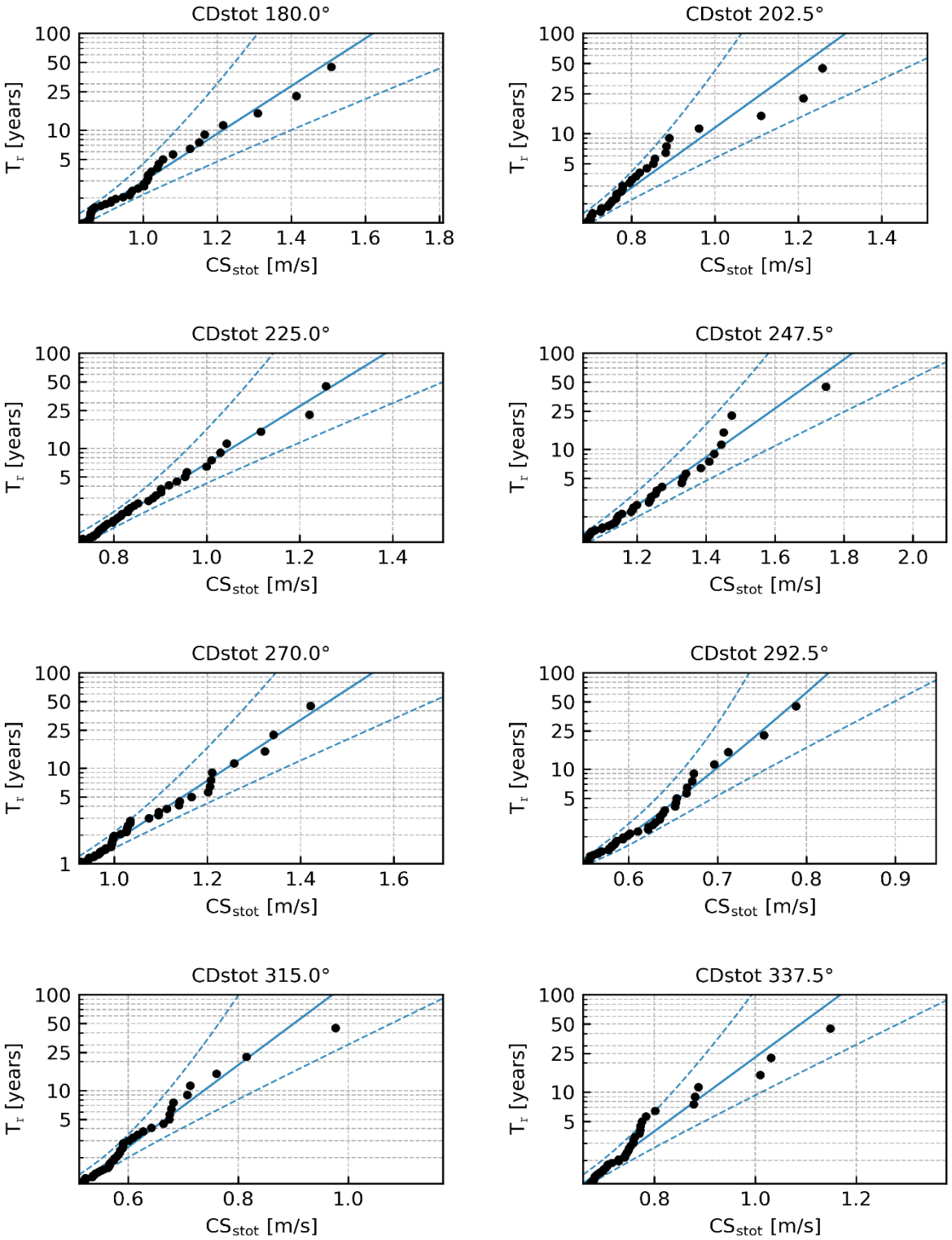

Figure 6-32 Marginal directional EVA estimates of CS_{stot} for CD_{stot} [°N-going to] sectors every 22.5° for KG-1. Weibull LS, λ = 1. Confidence limits 2.5% -97.5%.

6.2.2 Extreme total current speed at mid-depth

Figure 6-33 show the omni-directional EVA on current speed mid-depth. Figure 6-34 and Figure 6-35 shows the directional EVA on current speed mid-depth. Table 6-6 include the omni-directional EVA as well as the directional the directional extreme mid-depth current speed at KG-1

The fitted distribution aligns well to the hindcast data points, also at the tail, and all events are within the confidence levels.

The 50-year total omni-directional mid-depth current speed is 0.9 m/s.

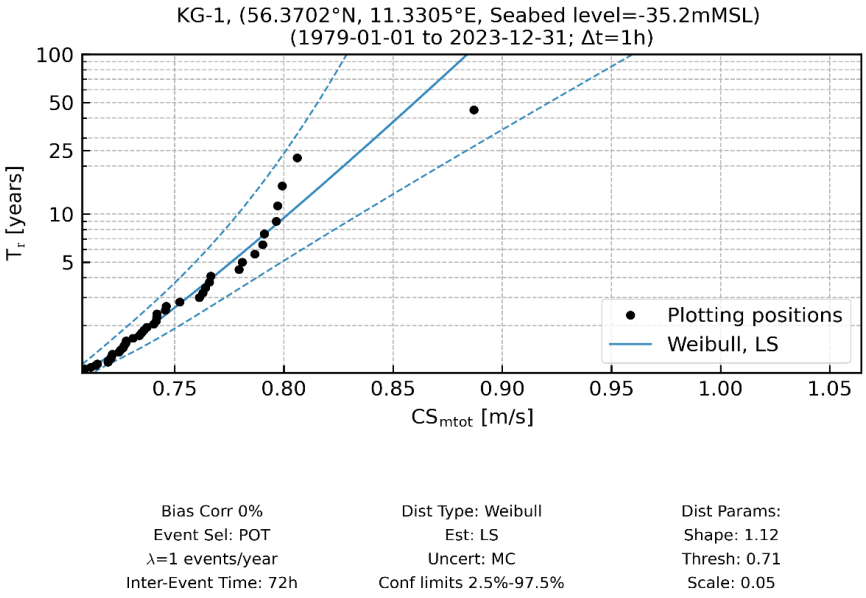

Figure 6-33 Marginal omni-directional EVA estimates of CS_{mtot} at KG-1.

Table 6-6 Marginal directional EVA estimates of CS_{mtot} at KG-1.

Sector	CS_{mtot} [m/s]					
CD_{mtot} [°N-going to]	Quantile	T_r 1	T_r 5	T_r 10	T_r 25	T_r 50
0.0	Central estimate	0.4	0.5	0.5	0.6	0.6
22.5		0.5	0.5	0.6	0.6	0.6
45.0		0.4	0.4	0.4	0.5	0.5
67.5		0.4	0.5	0.5	0.6	0.6
90.0		0.4	0.5	0.5	0.6	0.6
112.5		0.4	0.5	0.6	0.6	0.6
135.0		0.4	0.5	0.6	0.6	0.6
157.5		0.4	0.5	0.5	0.6	0.6
180.0		0.4	0.5	0.6	0.6	0.7
202.5		0.5	0.6	0.6	0.7	0.7
225.0		0.6	0.7	0.8	0.8	0.9
247.5		0.7	0.8	0.8	0.8	0.8
270.0		0.6	0.7	0.7	0.8	0.8
292.5		0.4	0.6	0.6	0.7	0.7
315.0		0.4	0.4	0.5	0.5	0.6
337.5		0.4	0.4	0.5	0.5	0.5
Omni		0.7	0.8	0.8	0.8	0.9

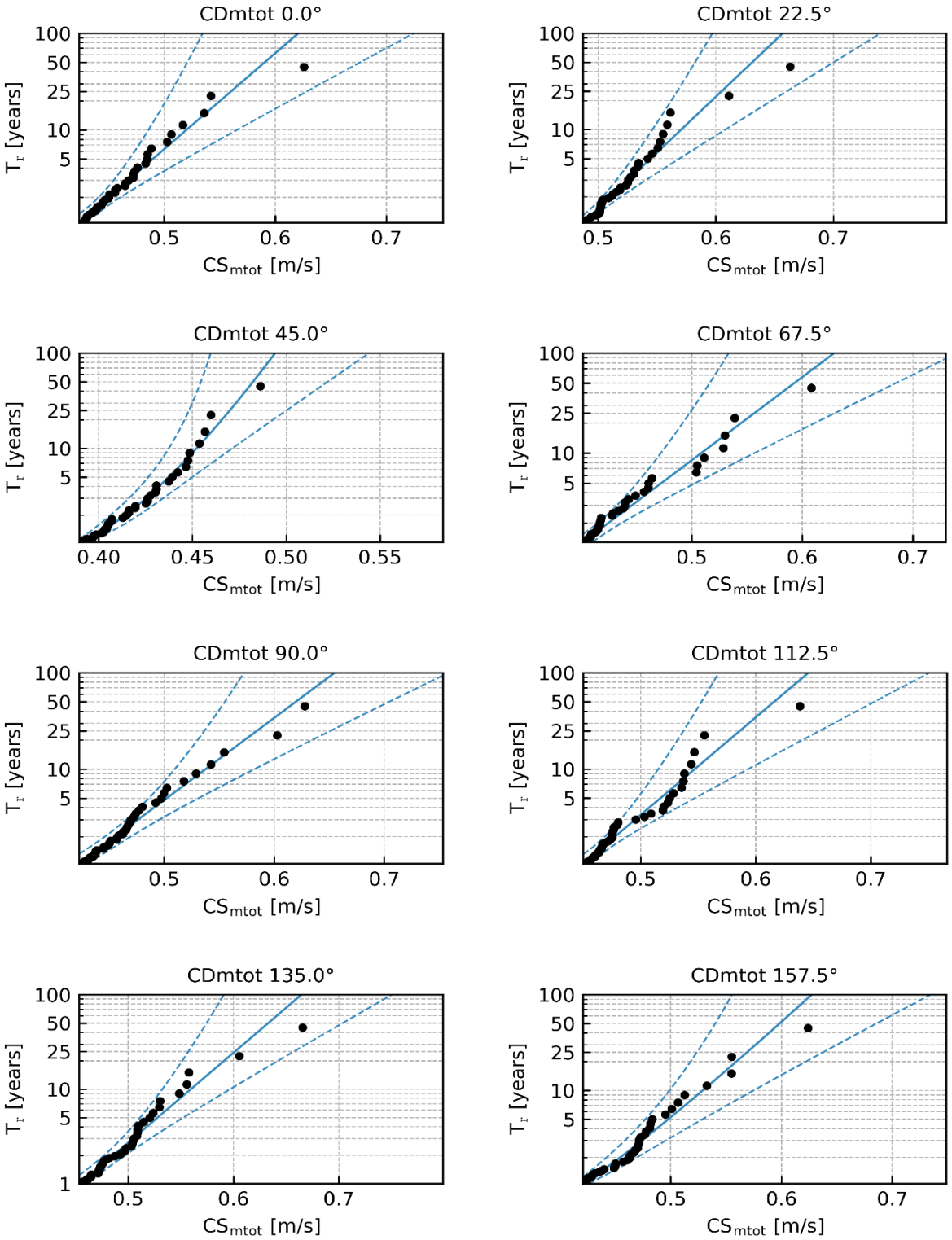

Figure 6-34 Marginal directional EVA estimates of CS_{mtot} for CD_{mtot} [°N-going to] sectors every 22.5° for KG-1. Weibull LS, λ = 1. Confidence limits 2.5% -97.5%.

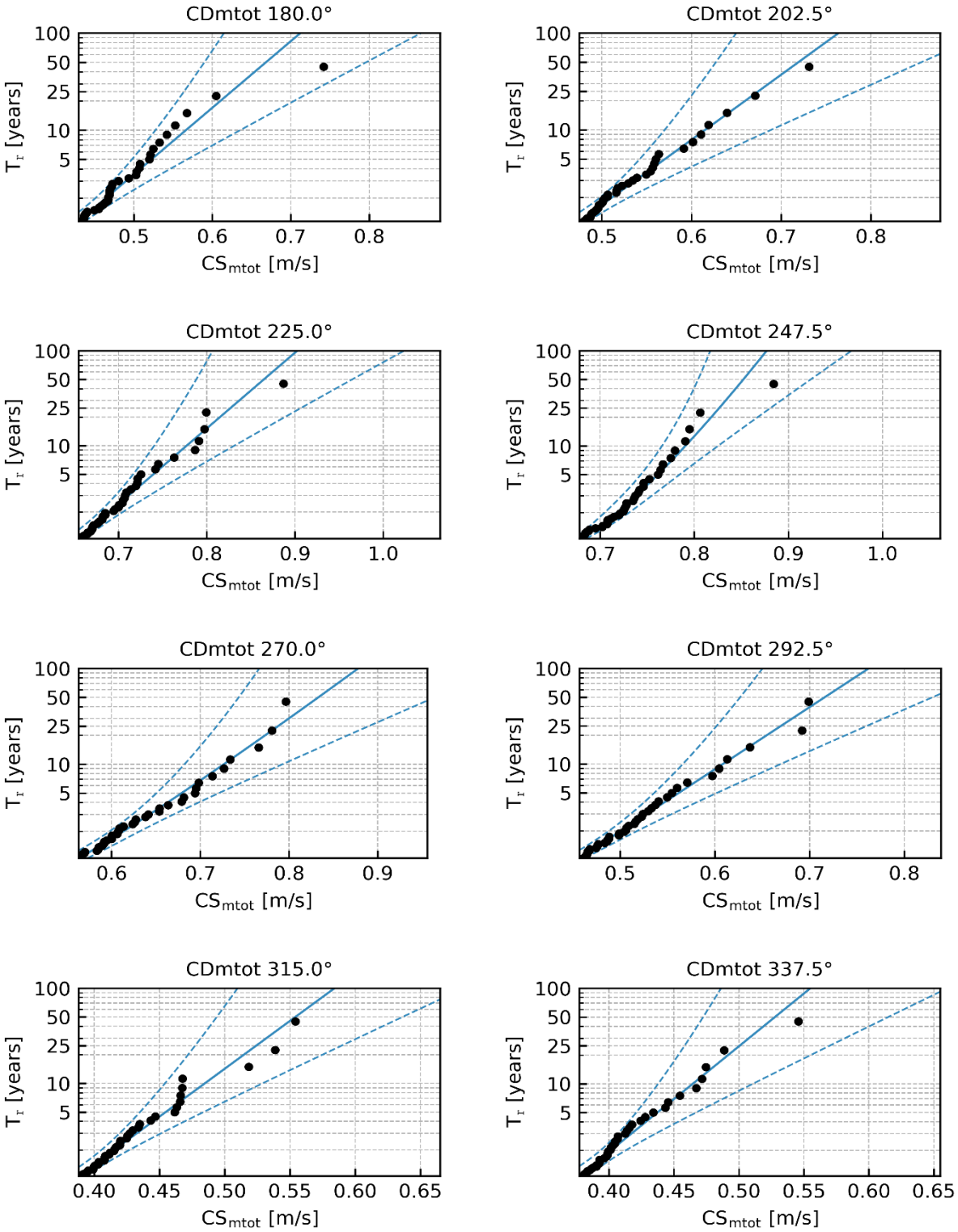

Figure 6-35 Marginal directional EVA estimates of CS_{mtot} for CD_{mtot} [°N-going to] sectors every 22.5° for KG-1. Weibull LS, λ = 1. Confidence limits 2.5% -97.5%.

6.2.3 Extreme total current speed at near bed

Figure 6-36 show the omni-directional EVA on current speed at near bed. Figure 6-37 and Figure 6-38 shows the directional EVA on current speed at near bed. Table 6-7 include the omni-directional EVA as well as the directional the directional extreme total near bed current speed at KG-1

The fitted distribution aligns well to the hindcast data points, also at the tail, and all events are within the confidence levels.

The 50-year total omni-directional near-surface current speed is 0.6 m/s.

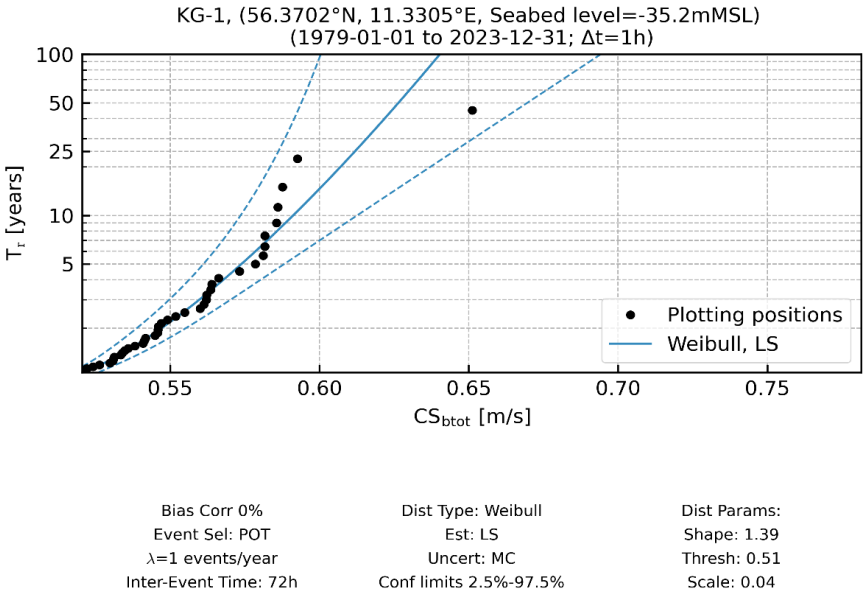

Figure 6-36 Marginal omni-directional EVA estimates of CS_{btot} at KG-1.

Table 6-7 Marginal directional EVA estimates of CS_{btot} at KG-1.

Sector	CS_{btot} [m/s]					
CD_{btot} [°N-going to]	Quantile	T_r 1	T_r 5	T_r 10	T_r 25	T_r 50
0.0	Central estimate	0.4	0.4	0.4	0.4	0.4
22.5		0.3	0.4	0.4	0.4	0.5
45.0		0.3	0.4	0.4	0.4	0.4
67.5		0.3	0.4	0.4	0.4	0.4
90.0		0.2	0.3	0.3	0.3	0.4
112.5		0.1	0.2	0.3	0.3	0.3
135.0		0.1	0.2	0.2	0.2	0.3
157.5		0.3	0.4	0.4	0.5	0.5
180.0		0.4	0.4	0.5	0.5	0.5
202.5		0.4	0.5	0.6	0.6	0.6
225.0		0.5	0.6	0.6	0.6	0.6
247.5		0.4	0.5	0.5	0.6	0.6
270.0		0.4	0.5	0.6	0.6	0.6
292.5		0.3	0.3	0.4	0.4	0.4
315.0		0.3	0.3	0.3	0.4	0.4
337.5		0.2	0.3	0.3	0.3	0.3
Omni		0.5	0.6	0.6	0.6	0.6

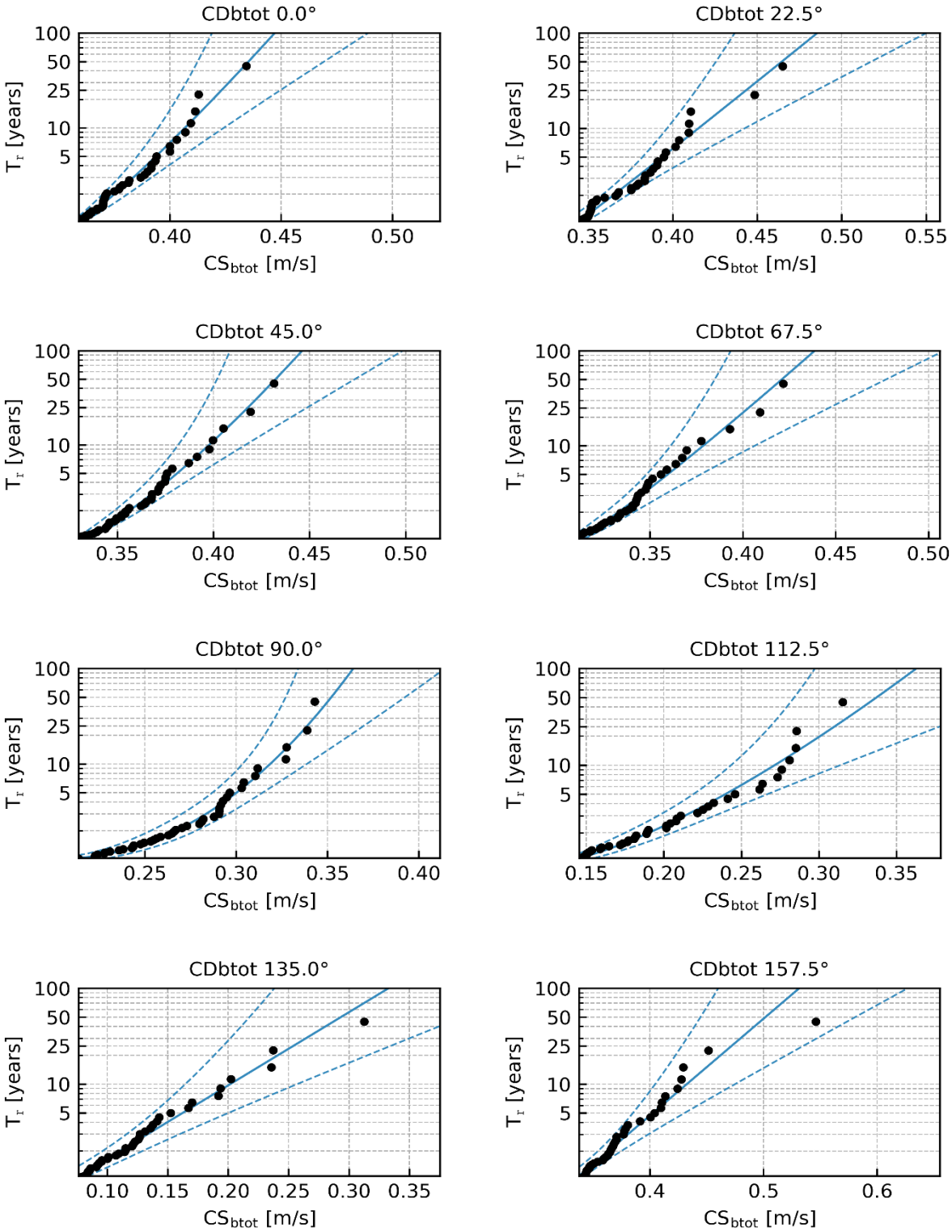

Figure 6-37 Marginal directional EVA estimates of CS_{btot} for CD_{btot} [°N-going to] sectors every 22.5° for KG-1. Weibull LS, λ = 1. Confidence limits 2.5% -97.5%.

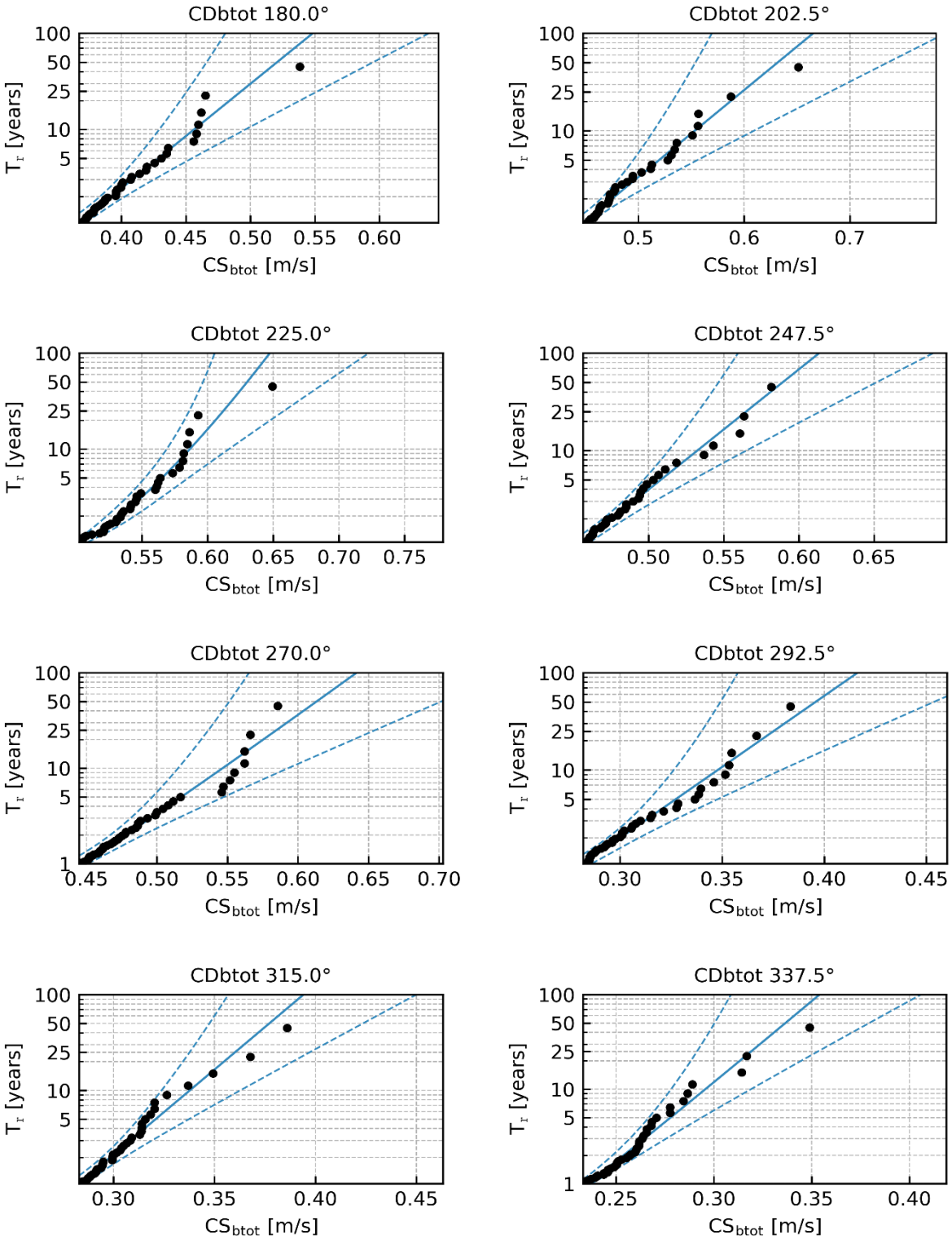

Figure 6-38 Marginal directional EVA estimates of CS_{btot} for CD_{btot} [°N-going to] sectors every 22.5° for KG-1. Weibull LS, λ = 1. Confidence limits 2.5% -97.5%.

6.2.4 Maps of extreme current speed at 3 levels

From Figure 6-39 to Figure 6-53 is the spatial variation of the omni-directional total current speed across the data delivery area of KG at 3 levels; near-surface, mid-depth and near-seabed, for return periods of 1, 5, 10, 25 and 50 years based on individual extreme value analysis on each model grid point.

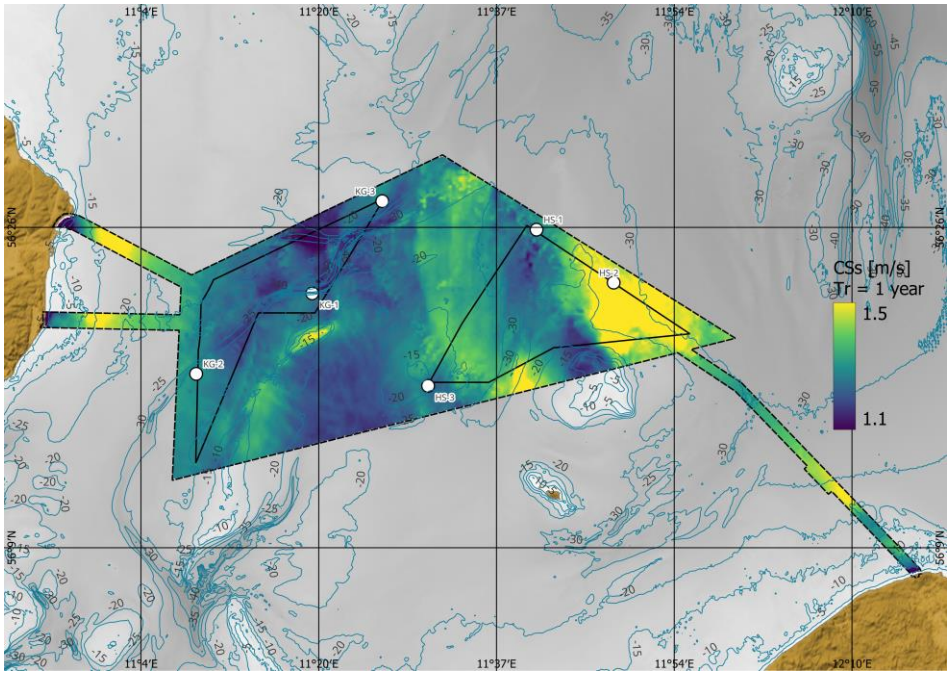

Figure 6-39 Spatial variation across the data delivery area of KG of CS_{stot} for return periods of 1 years. The colour map shows the current speed, and the contours show water depths.

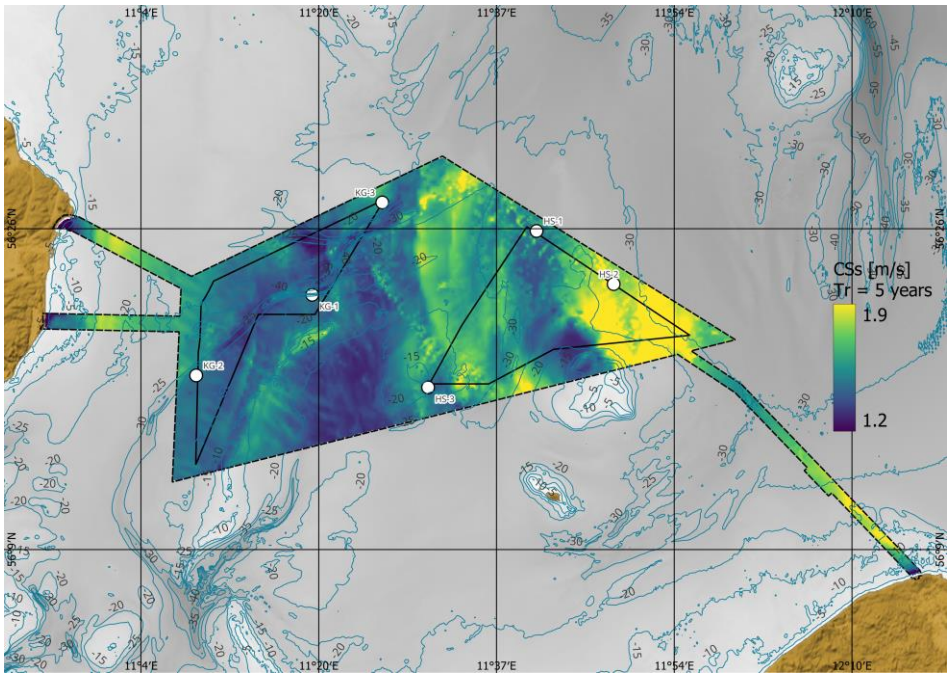

Figure 6-40 Spatial variation across the data delivery area of KG of CS_{stot} for return periods of 5 years. The colour map shows the current speed, and the contours show water depths.

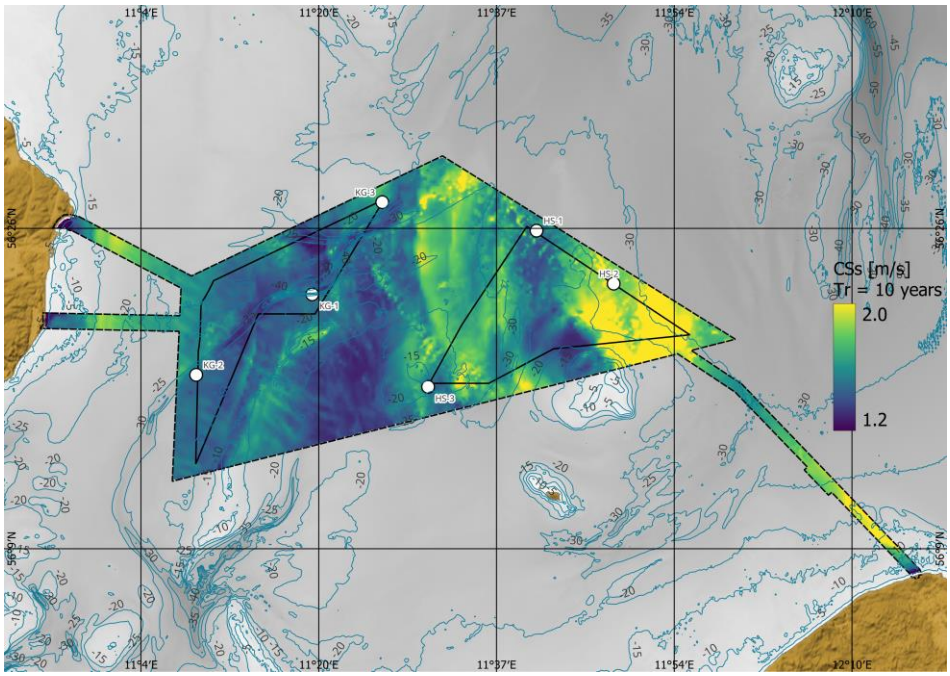

Figure 6-41 Spatial variation across the data delivery area of KG of CS_{stot} for return periods of 10 years. The colour map shows the current speed, and the contours show water depths.

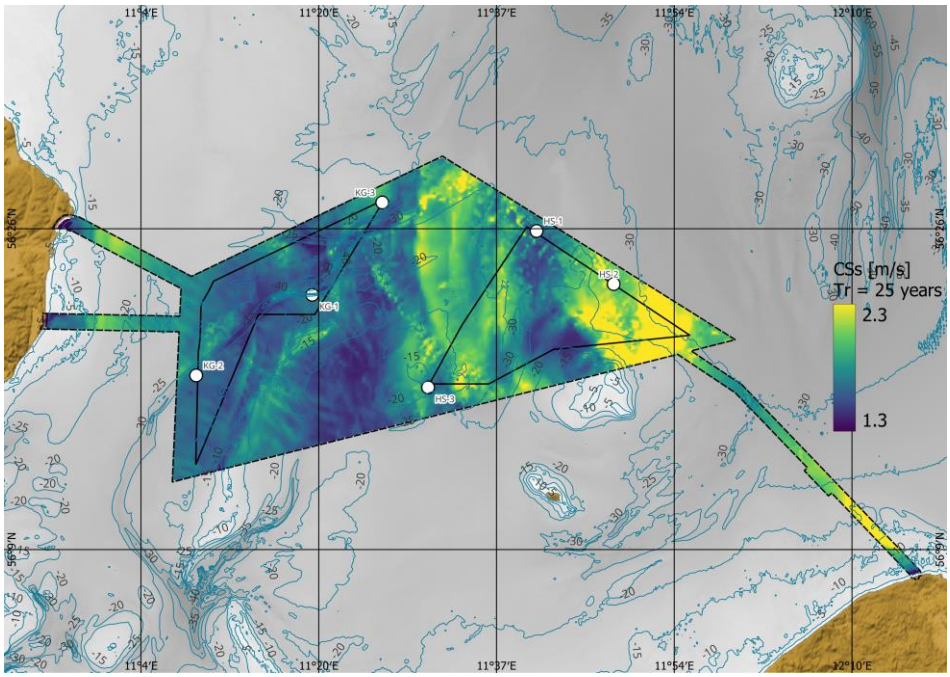

Figure 6-42 Spatial variation across the data delivery area of KG of CS_{stot} for return periods of 25 years. The colour map shows the current speed, and the contours show water depths.

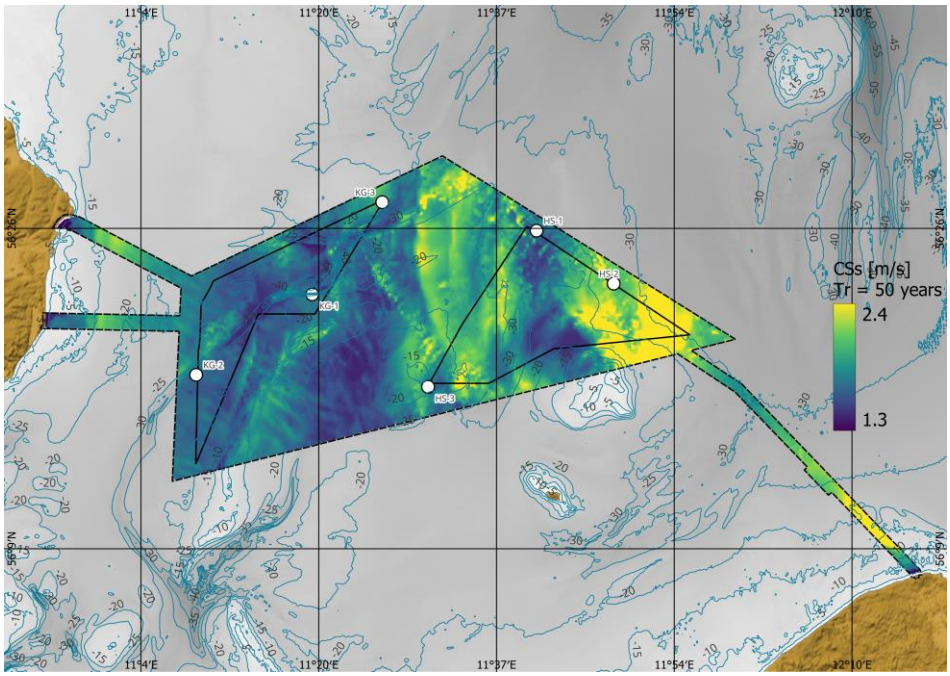

Figure 6-43 Spatial variation across the data delivery area of KG of CS_{stot} for return periods of 50 years. The colour map shows the current speed, and the contours show water depths.

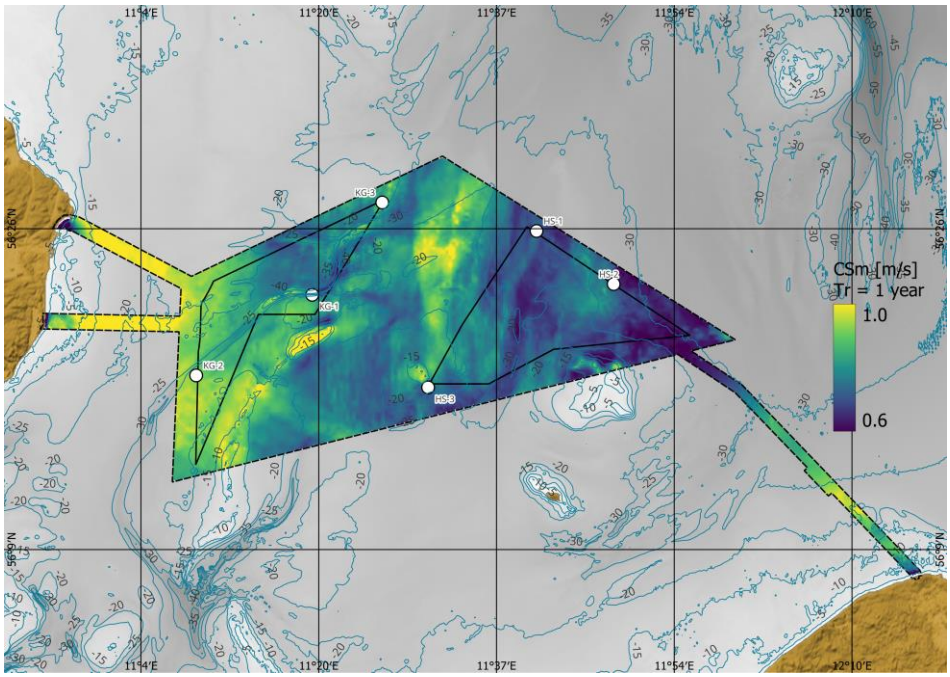

Figure 6-44 Spatial variation across the data delivery area of KG of CS_{mtot} for return periods of 1 years. The colour map shows the current speed, and the contours show water depths.

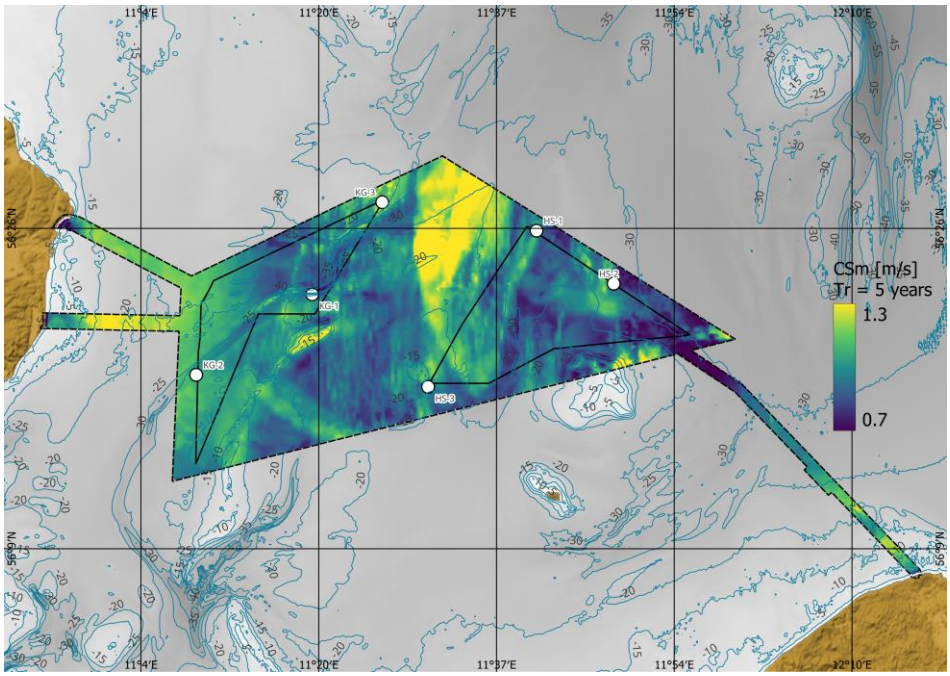

Figure 6-45 Spatial variation across the data delivery area of KG of CS_{mtot} for return periods of 5 years. The colour map shows the current speed, and the contours show water depths.

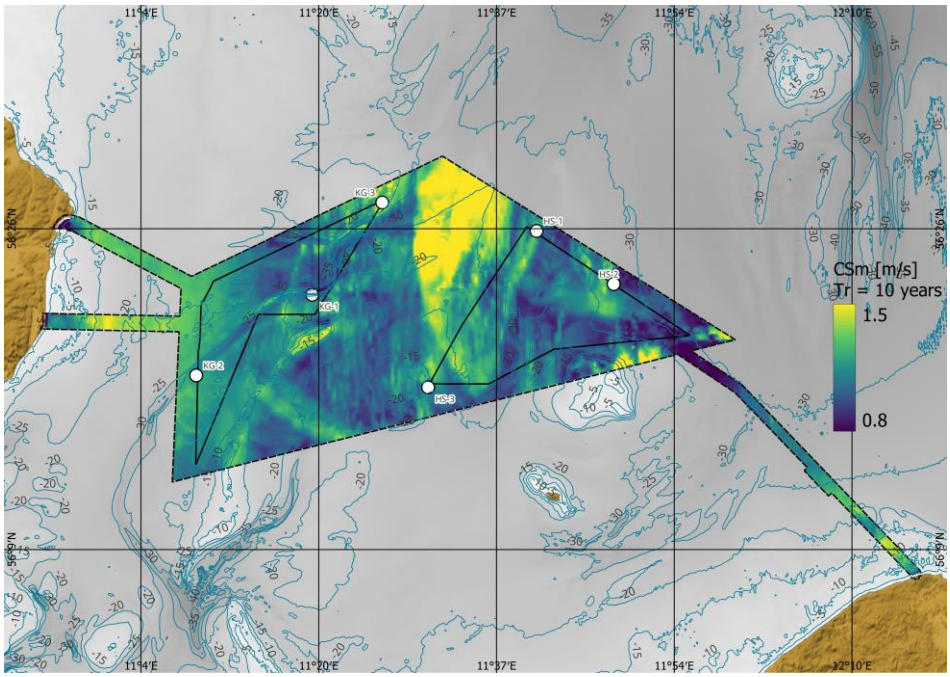

Figure 6-46 Spatial variation across the data delivery area of KG of CS_{mtot} for return periods of 10 years. The colour map shows the current speed, and the contours show water depths.

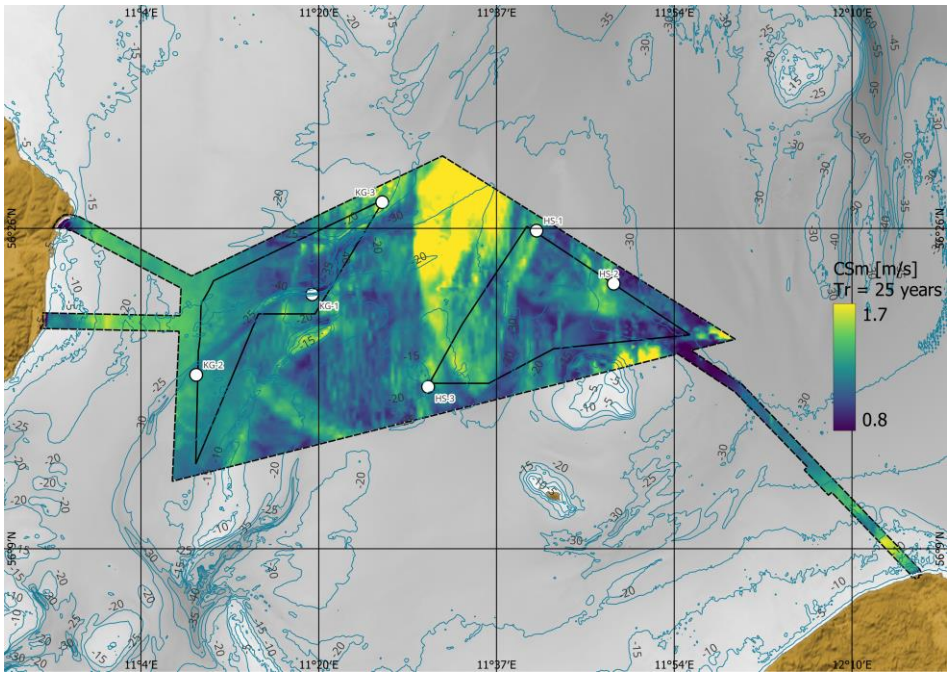

Figure 6-47 Spatial variation across the data delivery area of KG of CS_{mtot} for return periods of 25 years. The colour map shows the current speed, and the contours show water depths.

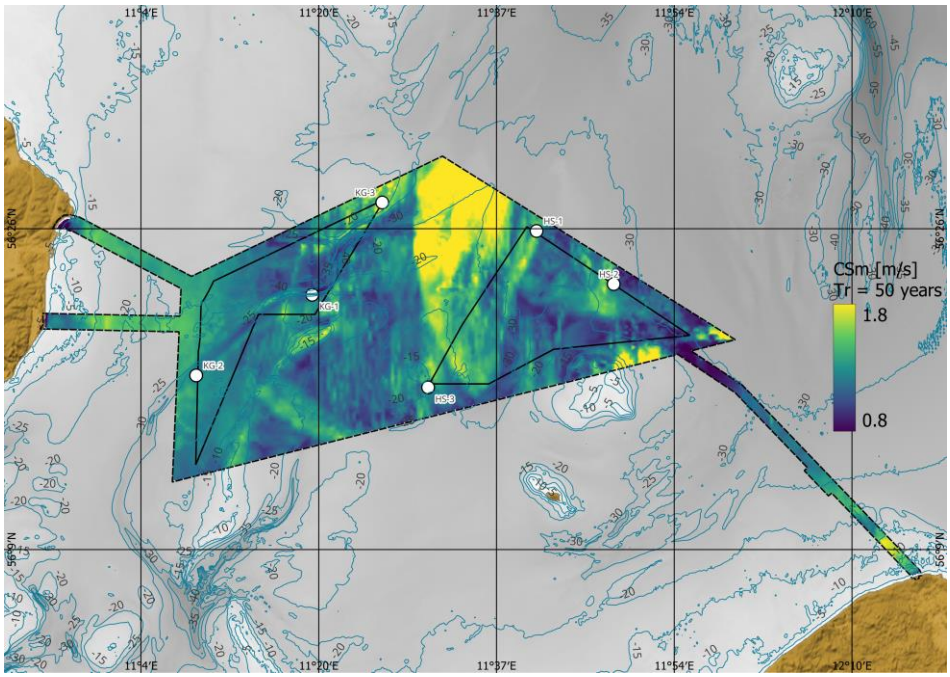

Figure 6-48 Spatial variation across the data delivery area of KG of CS_{mtot} for return periods of 50 years. The colour map shows the current speed, and the contours show water depths.

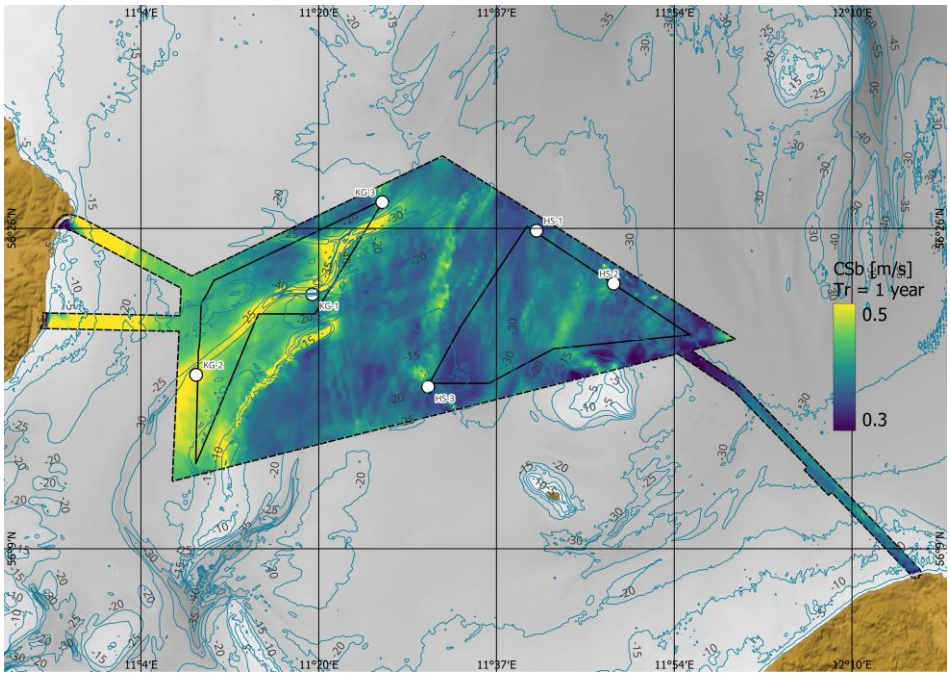

Figure 6-49 Spatial variation across the data delivery area of KG of CS_{btot} for return periods of 1 years. The colour map shows the current speed, and the contours show water depths.

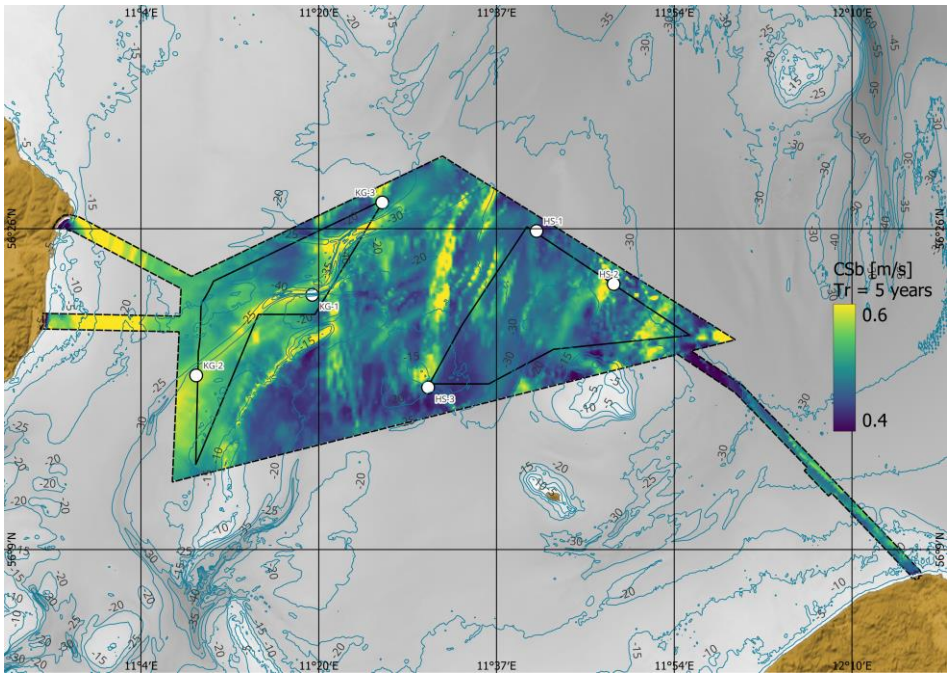

Figure 6-50 Spatial variation across the data delivery area of KG of CS_{btot} for return periods of 5 years. The colour map shows the current speed, and the contours show water depths.

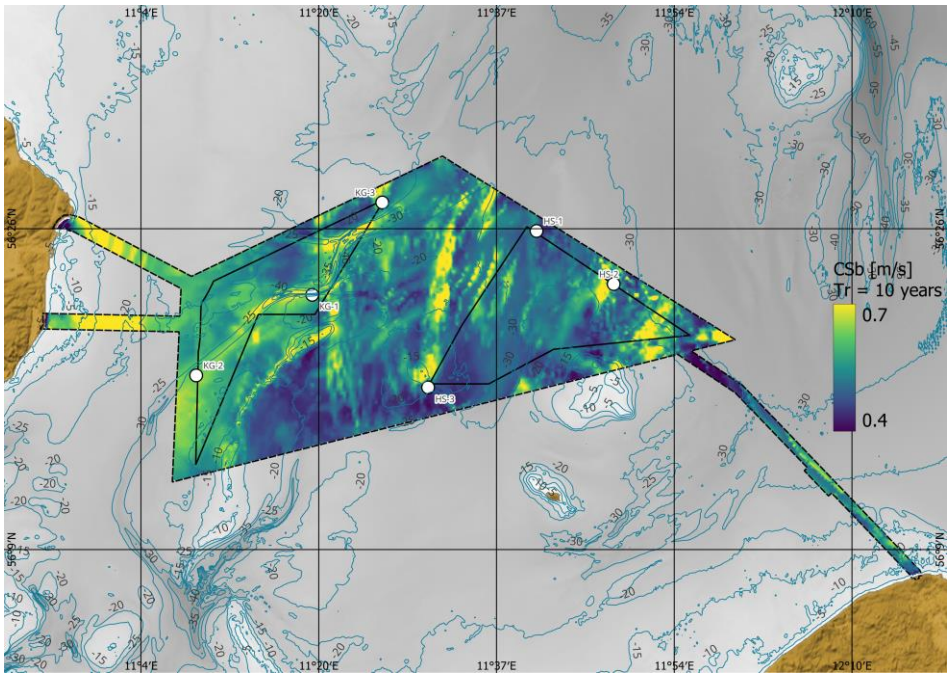

Figure 6-51 Spatial variation across the data delivery area of KG of CS_{btot} for return periods of 10 years. The colour map shows the current speed, and the contours show water depths.

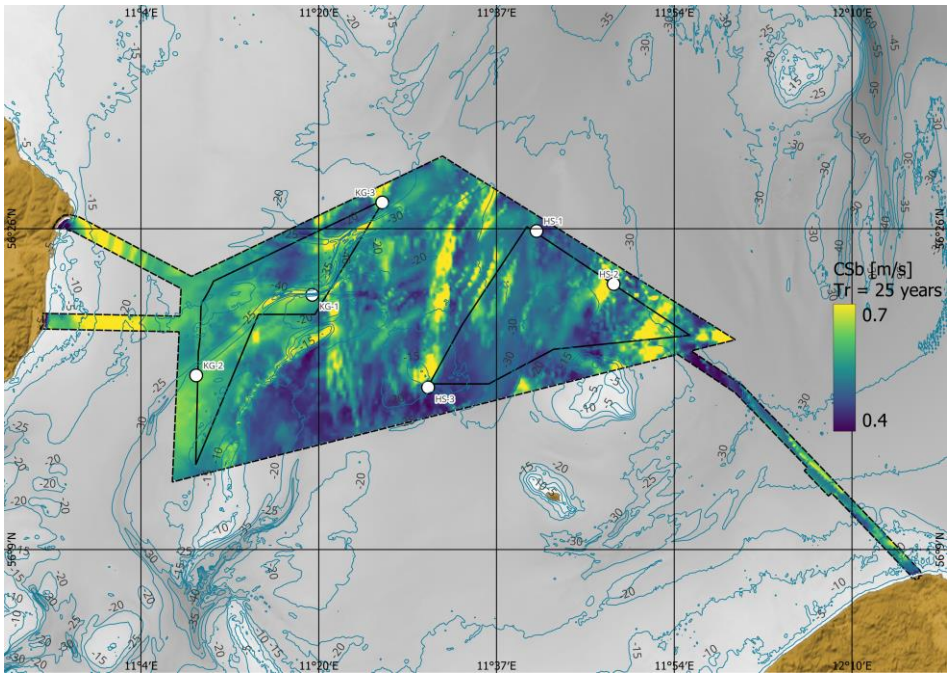

Figure 6-52 Spatial variation across the data delivery area of KG of CS_{btot} for return periods of 25 years. The colour map shows the current speed, and the contours show water depths.

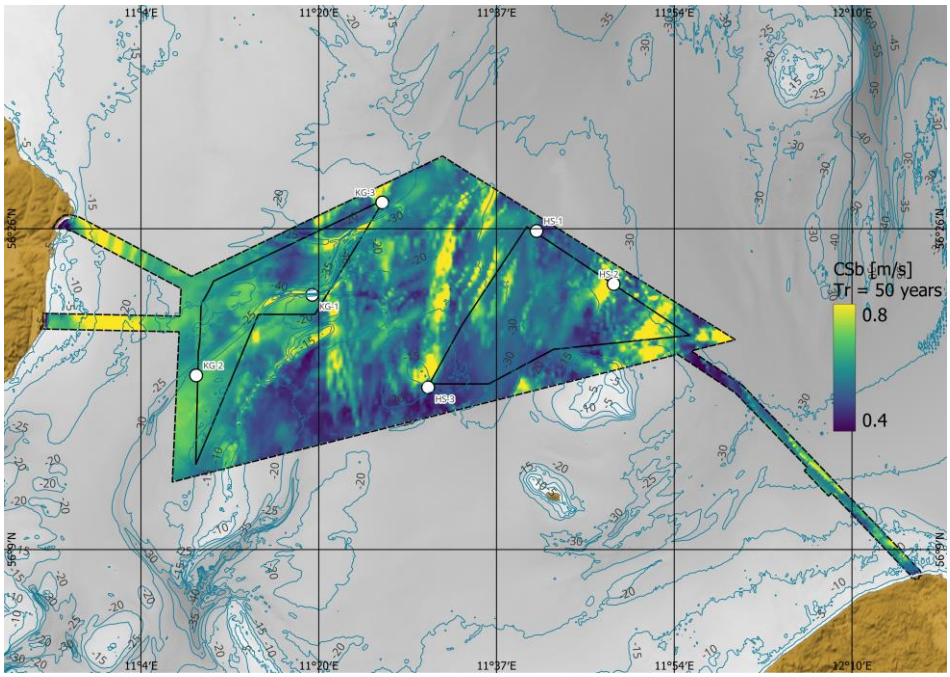

Figure 6-53 Spatial variation across the data delivery area of KG of CS_{btot} for return periods of 50 years. The colour map shows the current speed, and the contours show water depths.

6.3 Extreme current conditions scaled

Section 6.2 presents the results of the EVA analysis of the extreme current conditions. DNV-RP-C205 section 3.6.5.6 presents a method for scaling the

results of the EVA analysis. The applicability of the scaling method will not be discussed further here, but due care is advised when applying the results of the scaling.

Scaling according to DNV-RP-C205 section 3.6.5.6 has been performed for the extreme current conditions and is available in the Appendices.

7 Wave conditions

This section presents a summary of the wave data basis established in [1]**, followed by a presentation of normal and extreme wave conditions at the KG area.**

The wave dataset includes only the total wave component [1]**,** without distinguishing between windsea and swell components. Table 7-1 summarises the metadata of the dataset.

Table 7-1 Metadata of the wave dataset.

Name	Value
Start Date [UTC]:	1979-01-01 00:00:00
End Date [UTC]:	2023-12-31 23:00:00
Time Step [s]	3600

The wave data is considered representative of 3-hour average sea state, assuming stationarity of the sea surface elevation for 3 hours as is standard practice, and is given at 1-hour interval. The wave analyses are presented in height bins of 0.5 m, period bins of 0.5 s, and directional bins of 22.5°.

Table 7-2 presents the variables of the wave dataset, incl. the bin sizes applied in analyses throughout this report.

Table 7-2 Wave variables of the wave dataset

Variable name	Abbrev.	Unit	Bin size
Significant wave height	H_{m0}	m	0.5
Maximum wave height	H_{max}	m	0.5
Peak wave period	T_p	s	0.5
Mean wave period	T_{m01}	s	0.5
Zero-crossing wave period	T_{m02}	s	0.5
Mean energy period	T_{mm10}	s	0.5
Peak wave direction	PWD	°N (coming from)	22.5
Mean wave direction	MWD	°N (coming from)	22.5
Direction standard deviation	DSD	°	22.5
Maximum wave crest height	C_{max}	m	0.5

The wave analyses cover the data period 1979-01-01 to 2023-12-31 (45 years).

7.1 Normal wave conditions

The normal wave conditions are presented in terms of:

- Time series
- Wave roses
- Histograms
- Monthly statistics
- Directional statistics
- Scatter diagrams for correlation
- Wind-wave misalignment
- Wave spectra
- Wave maps

7.1.1 Timeseries

Figure 7-1 and Figure 7-2 shows timeseries of H_{m0}, T_p, and T_{m02}, T_{mm10} and T_{m01} at KG-1 during the 45-year hindcast period. An overview of simple statistics for the wave variables are given in Table 7-3.

Table 7-3 Overview of simple statistics for wave variables data period 1979-01-01 to 2023-12-31 at KG-1.

Variable	MIN	MEAN	MAX
H_{m0} [m]	0.0	0.9	4.7
T_p [s]	1.1	4.1	7.9
T_{m02} [s]	0.7	2.9	6.3
T_{mm10} [s]	1.1	3.6	7.1
T_{m01} [s]	0.9	3.2	6.6

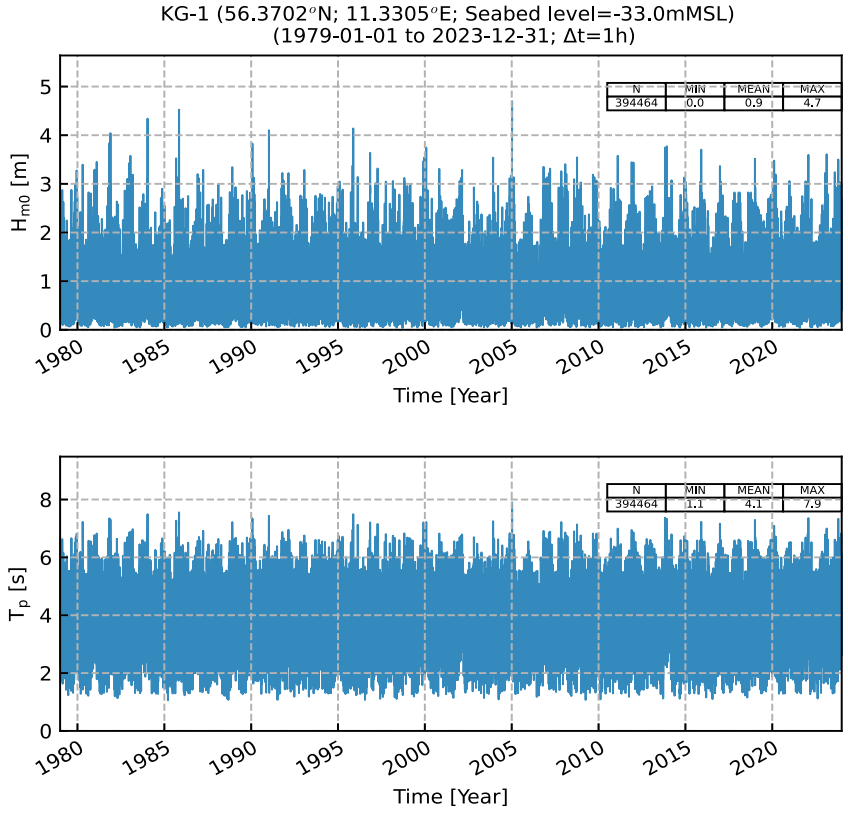

Figure 7-1 Timeseries of H_{m0} and T_p at KG-1.

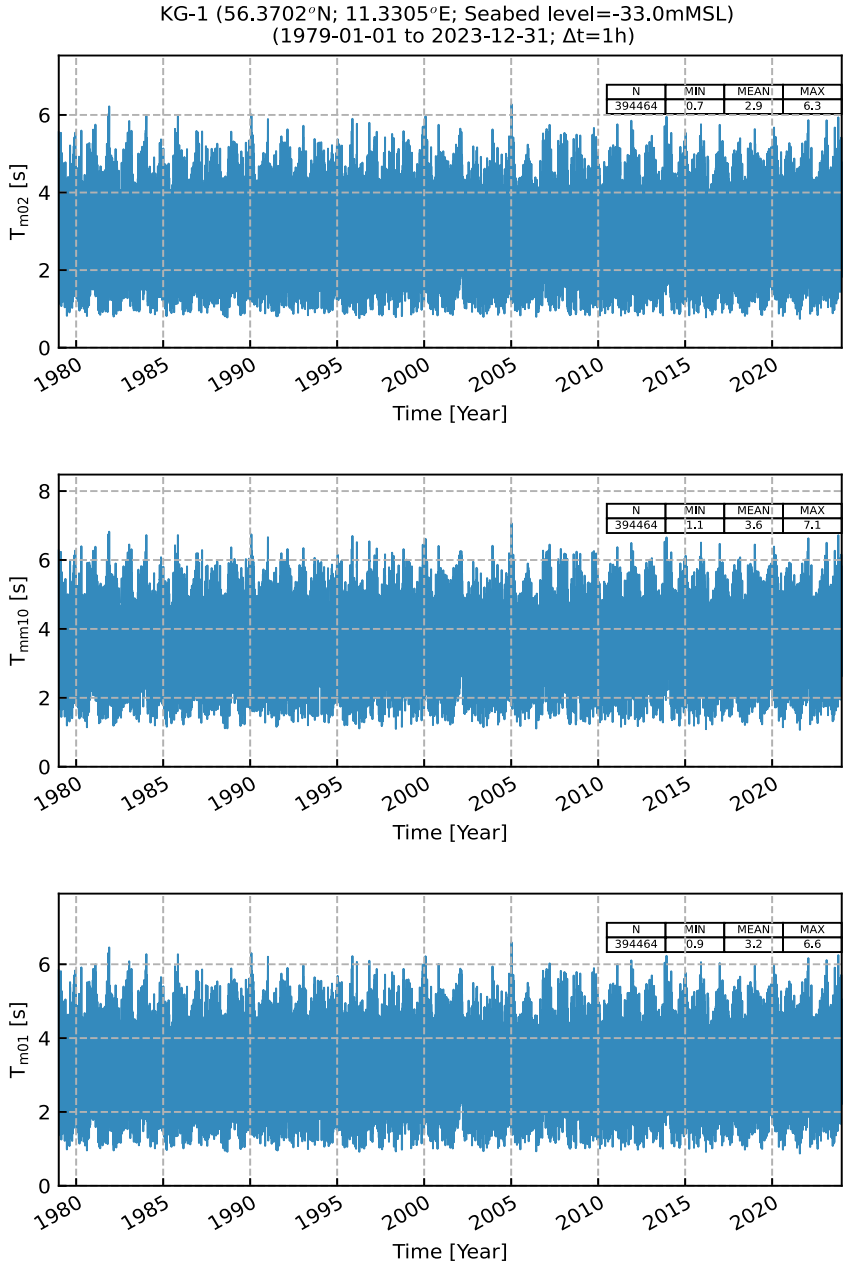

Figure 7-2 Timeseries of T_{m02}, T_{m10}, T_{m01} at KG-1.

7.1.2 Wave roses

Figure 7-3 and Figure 7-4 show wave roses at KG-1 based on H_{m0}, T_p and MWD for the total wave component. The wave rose indicate the predominance of waves coming from westerly sectors: SSW and WSW.

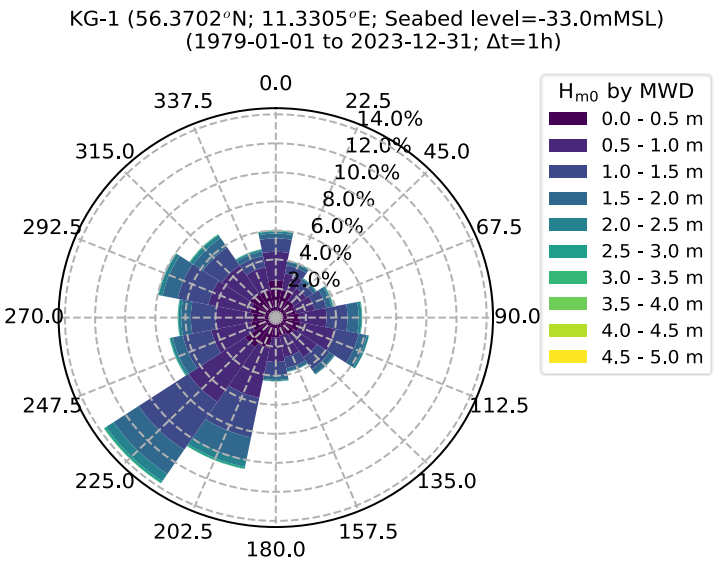

Figure 7-3 Rose plot of H_{m0}, sorted by MWD, at KG-1.

Table 7-4 Table of H_{m0} and MWD in percentage, at KG-1.

	MWD [°N-from]																
H_{m0} [m]	0.0	22.5	45.0	67.5	90.0	112.5	135.0	157.5	180.0	202.5	225.0	247.5	270.0	292.5	315.0	337.5	Omni
0.0 - 0.5	2.55	1.93	1.45	1.35	1.56	1.68	1.43	1.27	1.36	2.13	2.44	1.66	1.56	1.74	2.05	1.91	28.1
0.5 - 1.0	1.98	1.19	1.00	1.29	1.81	2.37	1.86	1.51	1.70	3.51	4.53	2.71	2.43	2.82	2.26	1.62	34.6
1.0 - 1.5	0.93	0.57	0.52	0.78	1.40	1.56	1.00	0.76	0.91	2.77	3.98	1.92	1.65	2.08	1.50	0.79	23.1
1.5 - 2.0	0.33	0.25	0.22	0.36	0.74	0.54	0.36	0.23	0.32	1.59	2.01	0.68	0.64	1.03	0.77	0.32	10.4
2.0 - 2.5	0.16	0.07	0.07	0.10	0.18	0.14	0.06	0.05	0.08	0.49	0.59	0.17	0.19	0.26	0.25	0.12	3.0
2.5 - 3.0	0.05	0.01	0.01	0.03	0.05	0.01	0.00	0.00	0.02	0.13	0.15	0.05	0.04	0.05	0.05	0.04	0.7
3.0 - 3.5	0.01	0.00	0.00	0.01	0.01	0.00	0.00	0.00	0.00	0.02	0.02	0.01	0.01	0.01	0.02	0.01	0.1
3.5 - 4.0	0.00	0.00	0.00	0.00	0.00	0.00	0.00	0.00	0.00	0.00	0.01	0.00	0.00	0.00	0.00	0.00	0.0
4.0 - 4.5	0.00	0.00	0.00	0.00	0.00	0.00	0.00	0.00	0.00	0.00	0.00	0.00	0.00	0.00	0.00	0.00	0.0
4.5 - 5.0	0.00	0.00	0.00	0.00	0.00	0.00	0.00	0.00	0.00	0.00	0.00	0.00	0.00	0.00	0.00	0.00	0.0
All	6.0	4.0	3.3	3.9	5.7	6.3	4.7	3.8	4.4	10.6	13.7	7.2	6.5	8.0	6.9	4.8	100.0

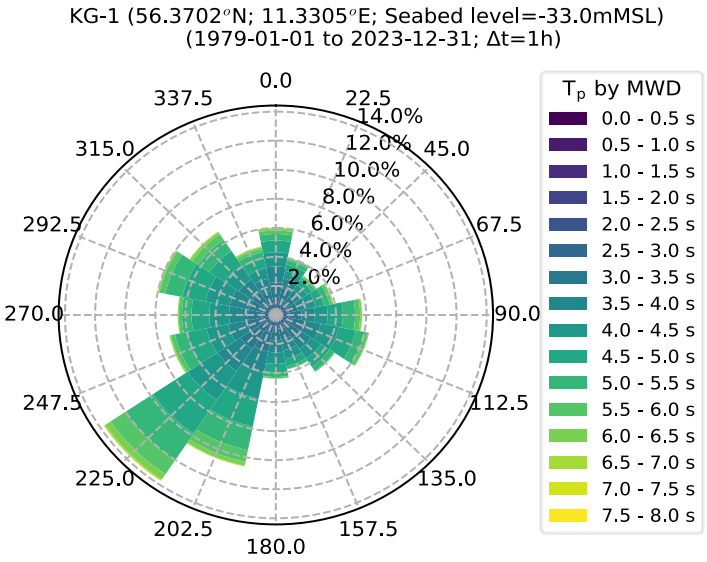

Figure 7-4 Rose plot of T_P, sorted by MWD, at KG-1.

Table 7-5 Table of T_p and MWD in percentage, at KG-1.

	MWD [°N-from]																
T_p [s]	0.0	22.5	45.0	67.5	90.0	112.5	135.0	157.5	180.0	202.5	225.0	247.5	270.0	292.5	315.0	337.5	Omni
0.0 - 0.5	0.00	0.00	0.00	0.00	0.00	0.00	0.00	0.00	0.00	0.00	0.00	0.00	0.00	0.00	0.00	0.00	0.0
0.5 - 1.0	0.00	0.00	0.00	0.00	0.00	0.00	0.00	0.00	0.00	0.00	0.00	0.00	0.00	0.00	0.00	0.00	0.0
1.0 - 1.5	0.01	0.01	0.01	0.01	0.01	0.01	0.01	0.01	0.01	0.01	0.00	0.01	0.01	0.01	0.01	0.01	0.2
1.5 - 2.0	0.08	0.10	0.12	0.10	0.11	0.13	0.11	0.11	0.09	0.11	0.12	0.09	0.10	0.06	0.06	0.07	1.6
2.0 - 2.5	0.30	0.32	0.29	0.26	0.28	0.33	0.34	0.30	0.31	0.37	0.43	0.33	0.28	0.25	0.26	0.22	4.9
2.5 - 3.0	0.72	0.63	0.47	0.48	0.52	0.60	0.55	0.54	0.55	0.77	0.85	0.60	0.57	0.51	0.55	0.53	9.5
3.0 - 3.5	1.13	0.80	0.62	0.62	0.78	0.91	0.89	0.77	0.78	1.31	1.43	0.98	0.90	0.98	0.95	0.86	14.7
3.5 - 4.0	1.10	0.69	0.56	0.61	0.84	1.05	0.90	0.75	0.83	1.51	1.83	1.21	1.25	1.31	1.10	0.86	16.4
4.0 - 4.5	0.98	0.54	0.43	0.61	0.89	1.21	0.80	0.63	0.79	1.78	2.38	1.47	1.32	1.63	1.16	0.75	17.4
4.5 - 5.0	0.81	0.44	0.39	0.56	1.01	1.17	0.68	0.48	0.61	1.97	2.78	1.37	1.17	1.59	1.20	0.68	16.9
5.0 - 5.5	0.45	0.29	0.22	0.38	0.81	0.64	0.35	0.19	0.30	1.65	2.23	0.76	0.63	1.14	0.93	0.45	11.4
5.5 - 6.0	0.24	0.14	0.11	0.18	0.33	0.20	0.07	0.05	0.10	0.82	1.14	0.27	0.23	0.40	0.45	0.22	5.0
6.0 - 6.5	0.15	0.05	0.04	0.07	0.12	0.06	0.00	0.00	0.02	0.27	0.43	0.09	0.05	0.09	0.18	0.12	1.7
6.5 - 7.0	0.05	0.00	0.00	0.02	0.02	0.00	0.00	0.00	0.00	0.05	0.10	0.02	0.01	0.02	0.04	0.04	0.4
7.0 - 7.5	0.01	0.00	0.00	0.00	0.00	0.00	0.00	0.00	0.00	0.00	0.01	0.00	0.00	0.00	0.01	0.01	0.1
7.5 - 8.0	0.00	0.00	0.00	0.00	0.00	0.00	0.00	0.00	0.00	0.00	0.00	0.00	0.00	0.00	0.00	0.00	0.0
All	6.0	4.0	3.3	3.9	5.7	6.3	4.7	3.8	4.4	10.6	13.7	7.2	6.5	8.0	6.9	4.8	100.0

7.1.3 Histogram

The histogram on Figure 7-5 shows the significant wave height distribution with bins of 0.5 m. Additionally the cumulative probability distribution is also shown with the 30%, 50% and 70% quantile. The histogram for T_p is presented on Figure 7-6.

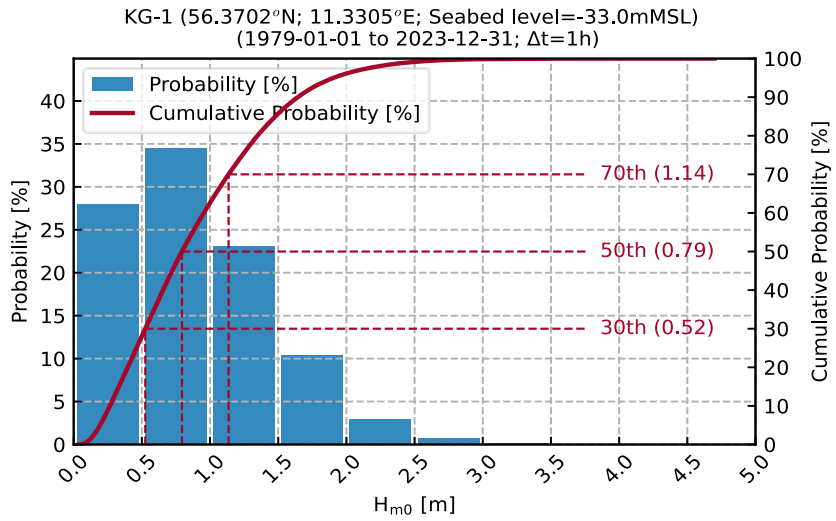

Figure 7-5 Probability plot of H_{m0} at KG-1.

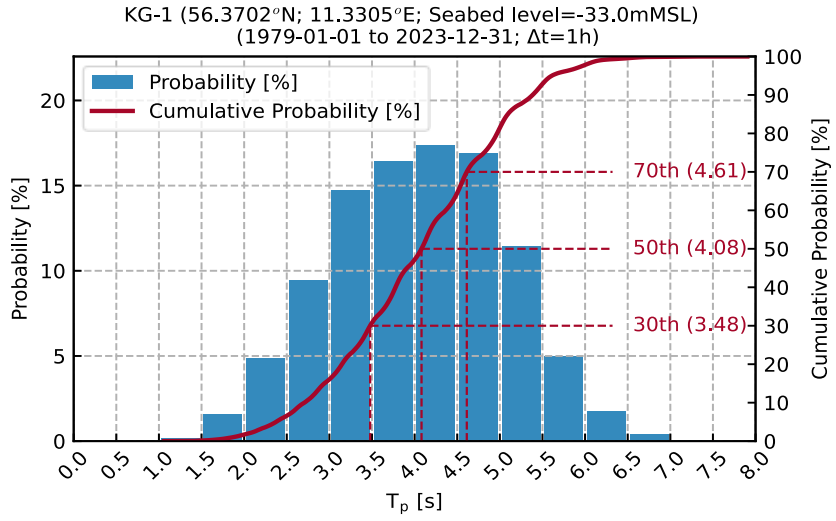

Figure 7-6 Probability plot of T_p at KG-1.

7.1.4 Monthly statistics

Figure 7-7 shows monthly statistics for the significant wave height, H_{m0}, at KG-1. The mean varies from 0.7m during summer to 1.2m during winter and the highest waves occurring in January. T_p is shown on Figure 7-8.

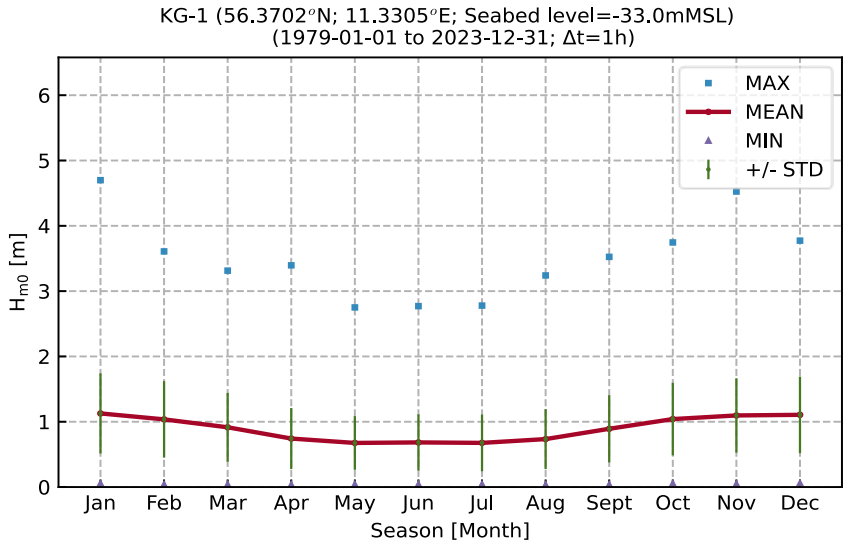

Figure 7-7 Monthly statistics of H_{m0} at KG-1.

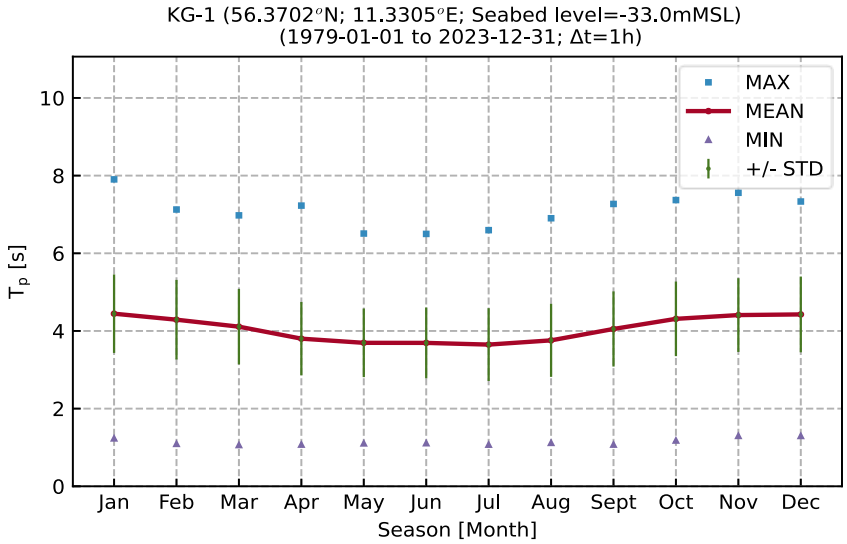

Figure 7-8 Monthly statistics of T_p at KG-1.

7.1.5 Directional statistics

Figure 7-9 shows directional statistics for the significant wave height, H_{m0}, at KG-1. The mean and maximum significant wave height is from southwest. T_p is shown on Figure 7-10.

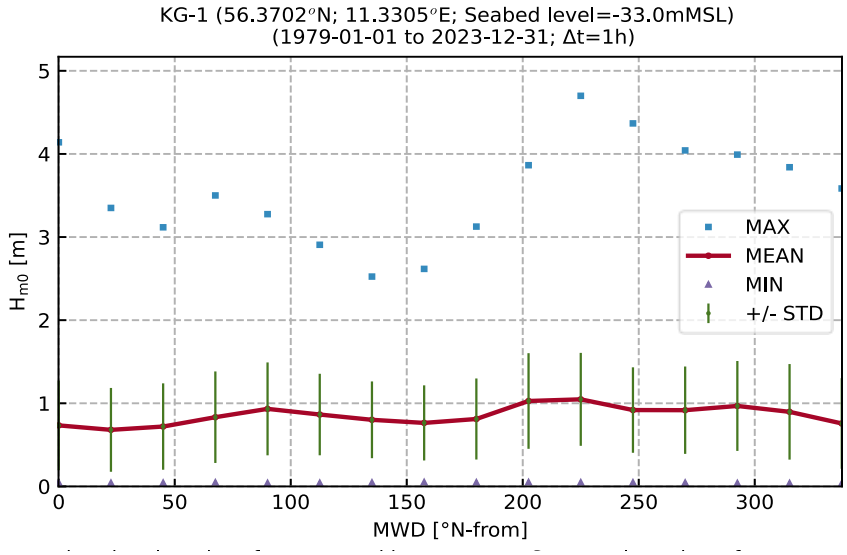

Figure 7-9 Directional statistics of H_{m0} sorted by MWD at KG-1.

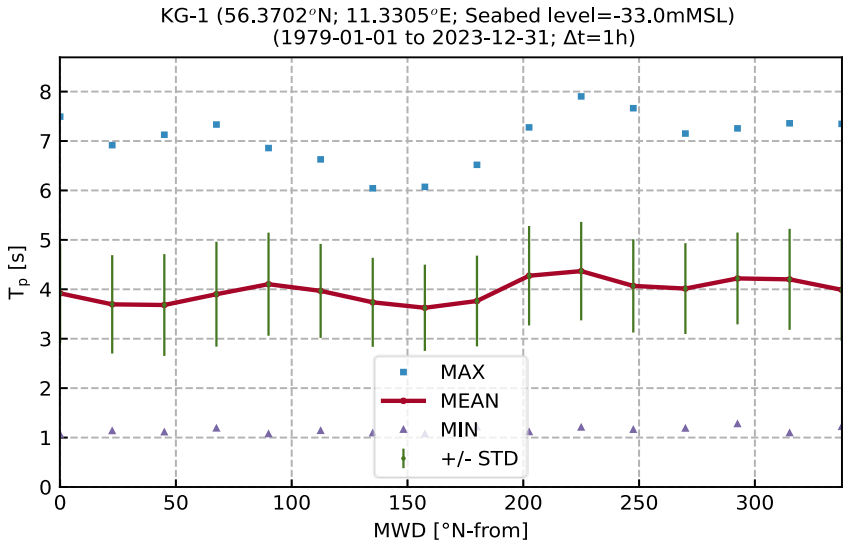

Figure 7-10 Directional statistics of T_p sorted by MWD at KG-1.

7.1.6 Correlation between wave height and period

On Figure 7-11 the correlation between H_{m0} and T_p at KG-1 is presented for omni, similar plots are presented in the Appendices for all directions. The scatter shows the 2.5%, mean and 97.5% quantile. A power fit curve is fitted to the mean of H_{m0}.

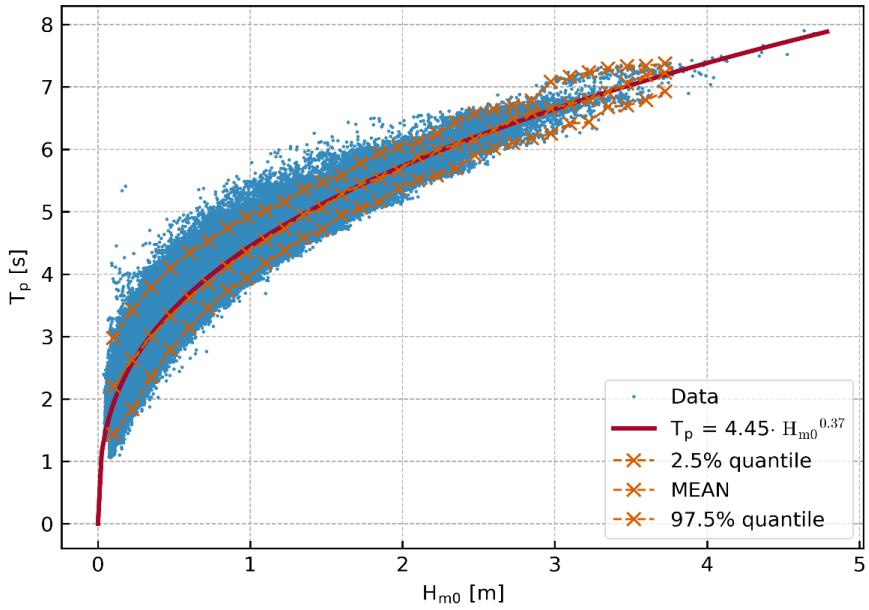

Figure 7-11 T_p based on the mean of H_{m0} at KG-1 for omni.

7.1.7 Maps of H_{m0}

Figure 7-12, Figure 7-13, Figure 7-14 and Figure 7-15 present maps across the data delivery area of the normalised moment of significant wave height, H_{m0}, calculated as follows.

$$\overline{H_{m0}} = \left[\frac{1}{N}\sum_{i=1}^{N} {H_{m0_i}}^m\right]^{\frac{1}{m}}$$

where m = (1,2,4,5) is the power coefficient, and N is the total number of hindcast data points. m = 1 is the mean H_{m0} and m = 2 is the root-mean-square wave energy.

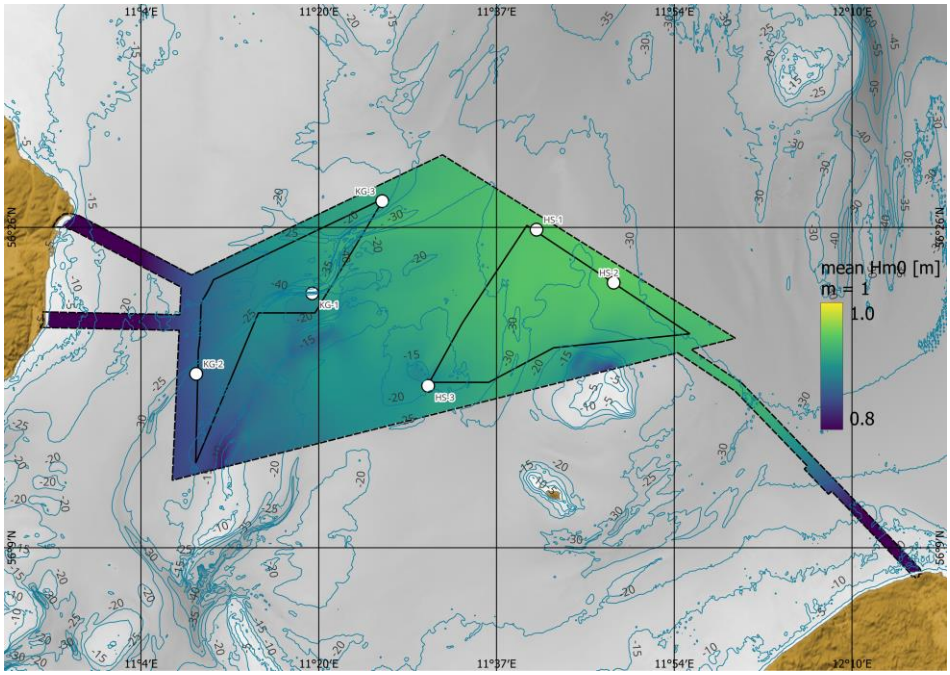

Figure 7-12 Spatial variation of moments of H_{m0} across the data delivery area, m=1.

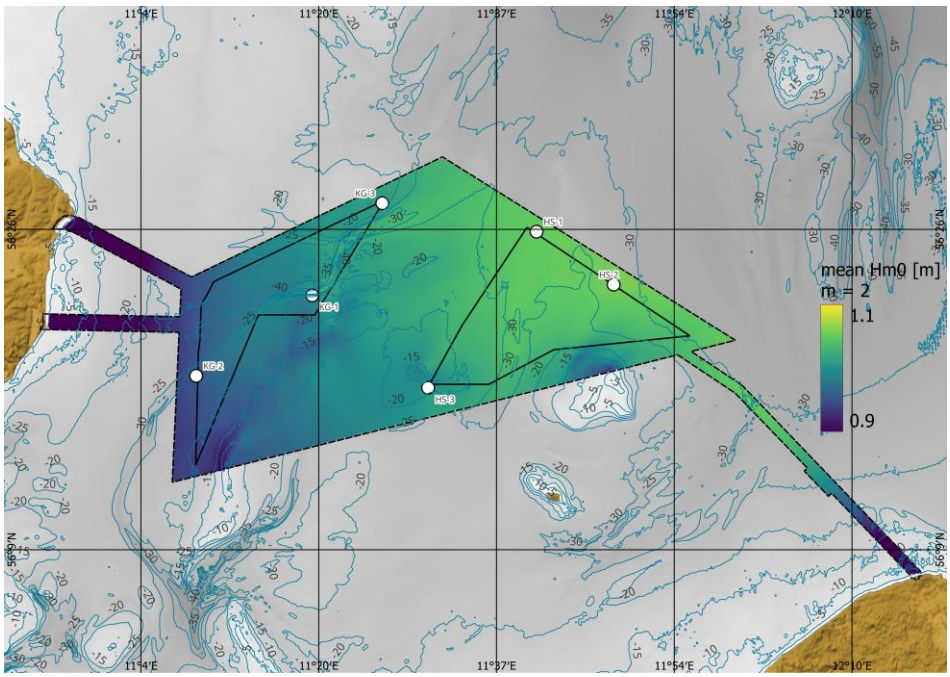

Figure 7-13 Spatial variation of moments of H_{m0} across the data delivery area, m=2.

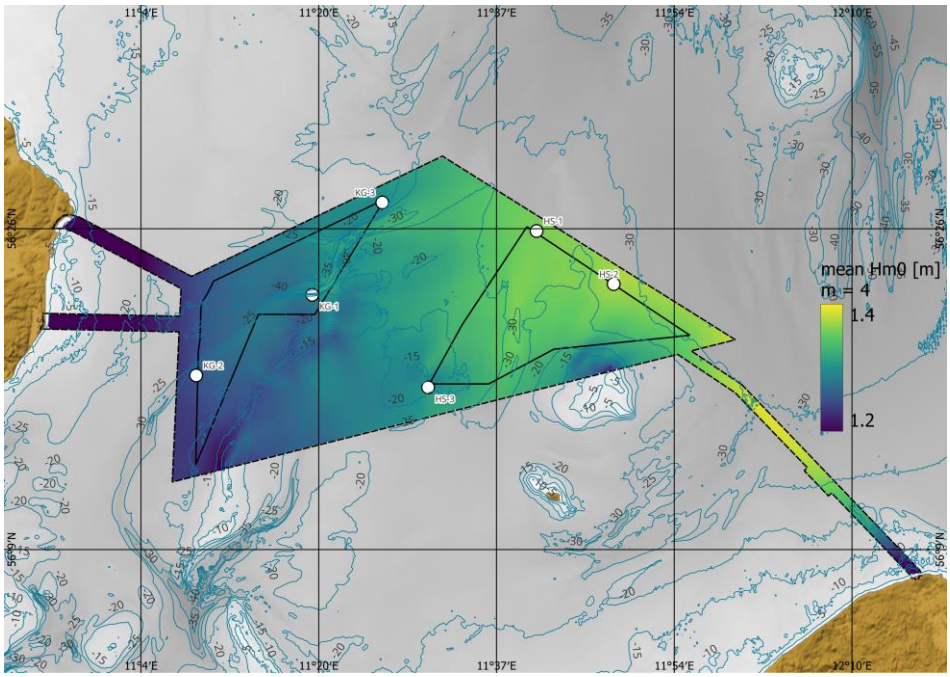

Figure 7-14 Spatial variation of moments of H_{m0} across the data delivery area, m=4.

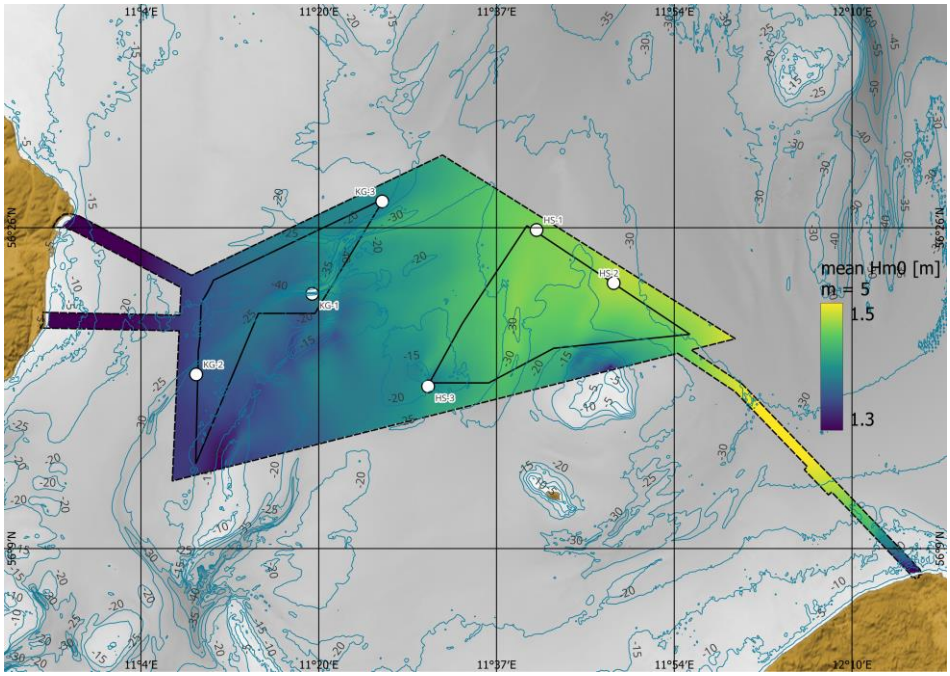

Figure 7-15 Spatial variation of moments of H_{m0} across the data delivery area, m=5.

7.2 Extreme wave conditions unscaled

It is noted that all Extreme Value Analysis results presented in this section are unscaled, in other words raw results from the EVA without scaling with regards to directionality. Scaled results according to DNV-RPC205 where consistency between directional extremes and Omni for all return periods are ensured can be found in the appendices, see section 7.3 for details on the scaling.

7.2.1 Extreme H_{m0}

Extreme wave conditions are established using Extreme Value Analysis. The analysis is based on its performance and sensitivity to selection of distribution, threshold selection method, λ-value evaluation and fitting estimator. A description of the methodology and the selection of settings is available in Appendix B.

For waves, the 3-parameter Weibull distribution was fitted by the least square method to 45 peak events (λ=1) separated by at least 72 hours.

The omnidirectional extreme wave fit is shown on Figure 7-16. The Weibull distribution fitted with the least squares method in shown along the upper 97.5% and lower 2.5% confidence interval.

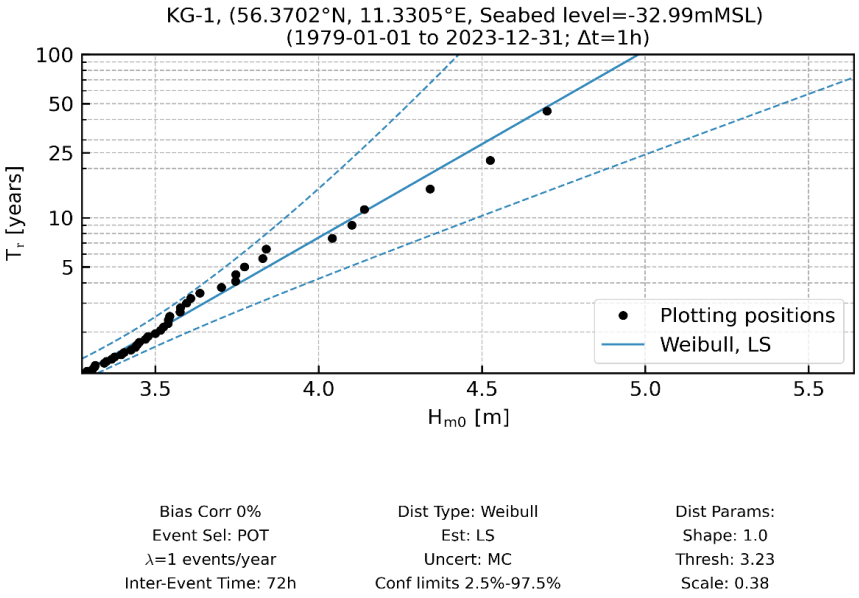

Figure 7-16 Extreme H_{m0} for omni at KG-1

The extreme wave fit for each direction is included in Table 7-6 as well as shown for each directional sector on Figure 7-17 and Figure 7-18.

Table 7-6 Marginal directional EVA estimates of H_{m0}, at KG-1

Sector	H_{m0} [m]					
MWD [°N-from]	Quantile	T_r 1	T_r 5	T_r 10	T_r 25	T_r 50
0.0	Central estimate	2.4	3	3.3	3.7	4
22.5		2	2.6	2.9	3.1	3.3
45.0		1.8	2.5	2.7	3	3.1
67.5		2	2.7	2.9	3.2	3.4
90.0		2.1	2.8	2.9	3.2	3.3
112.5		2.2	2.5	2.6	2.8	2.9
135.0		1.9	2.4	2.4	2.5	2.6
157.5		2	2.3	2.4	2.6	2.7
180.0		2.3	2.8	2.9	3.1	3.2
202.5		2.9	3.3	3.5	3.7	3.9
225.0		2.8	3.6	4	4.4	4.7
247.5		2.6	3.3	3.6	3.8	4
270.0		2.7	3.3	3.5	3.8	4.1
292.5		2.7	3.3	3.6	3.9	4.2
315.0		2.7	3.3	3.5	3.8	4
337.5		2.5	3.1	3.3	3.6	3.9
Omni		3.2	3.8	4.1	4.4	4.7

Table 7-7 Peak wave period associated with the extreme H_{m0} at KG-1 based on mean correlation between H_{m0} and T_p.

Sector	T_p [s]					
MWD [°N-from]	Quantile	T_r 1	T_r 5	T_r 10	T_r 25	T_r 50
0.0	Mean estimate	6.2	6.8	7	7.2	7.4
22.5		5.7	6.3	6.5	6.7	6.8
45.0		5.5	6.2	6.4	6.6	6.8
67.5		5.8	6.4	6.6	6.9	7.1
90.0		5.8	6.5	6.6	6.8	6.9
112.5		5.8	6.1	6.2	6.4	6.5
135.0		5.4	5.8	5.9	6	6
157.5		5.4	5.7	5.8	5.9	6
180.0		5.8	6.2	6.3	6.5	6.6
202.5		6.5	6.8	7	7.2	7.3
225.0		6.6	7.2	7.4	7.7	8
247.5		6.3	6.8	7	7.2	7.3
270.0		6.1	6.6	6.8	7	7.1
292.5		6.3	6.8	6.9	7.2	7.3
315.0		6.5	6.9	7.1	7.3	7.4
337.5		6.4	6.9	7.1	7.3	7.5
Omni		6.8	7.3	7.5	7.7	7.8

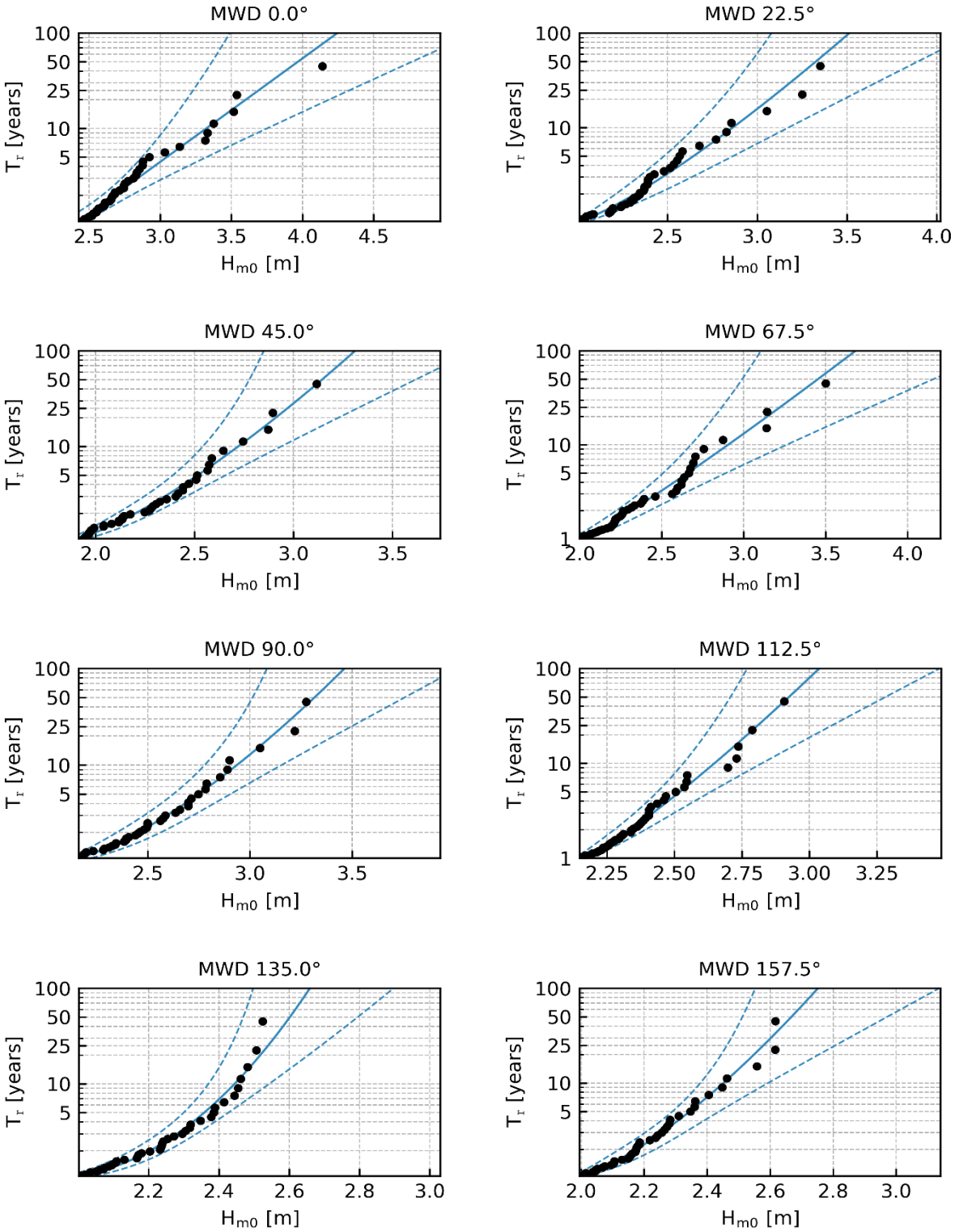

Figure 7-17 Extreme H_{m0} for MWD directional sectors at KG-1 (56.4251°E, 11.6797°N, Seabed level=-27.61mMSL, 1979-01-01 to 2023-12-31; Δt=1h). Weibull LS, λ = 1. Confidence limits 2.5% - 97.5%.

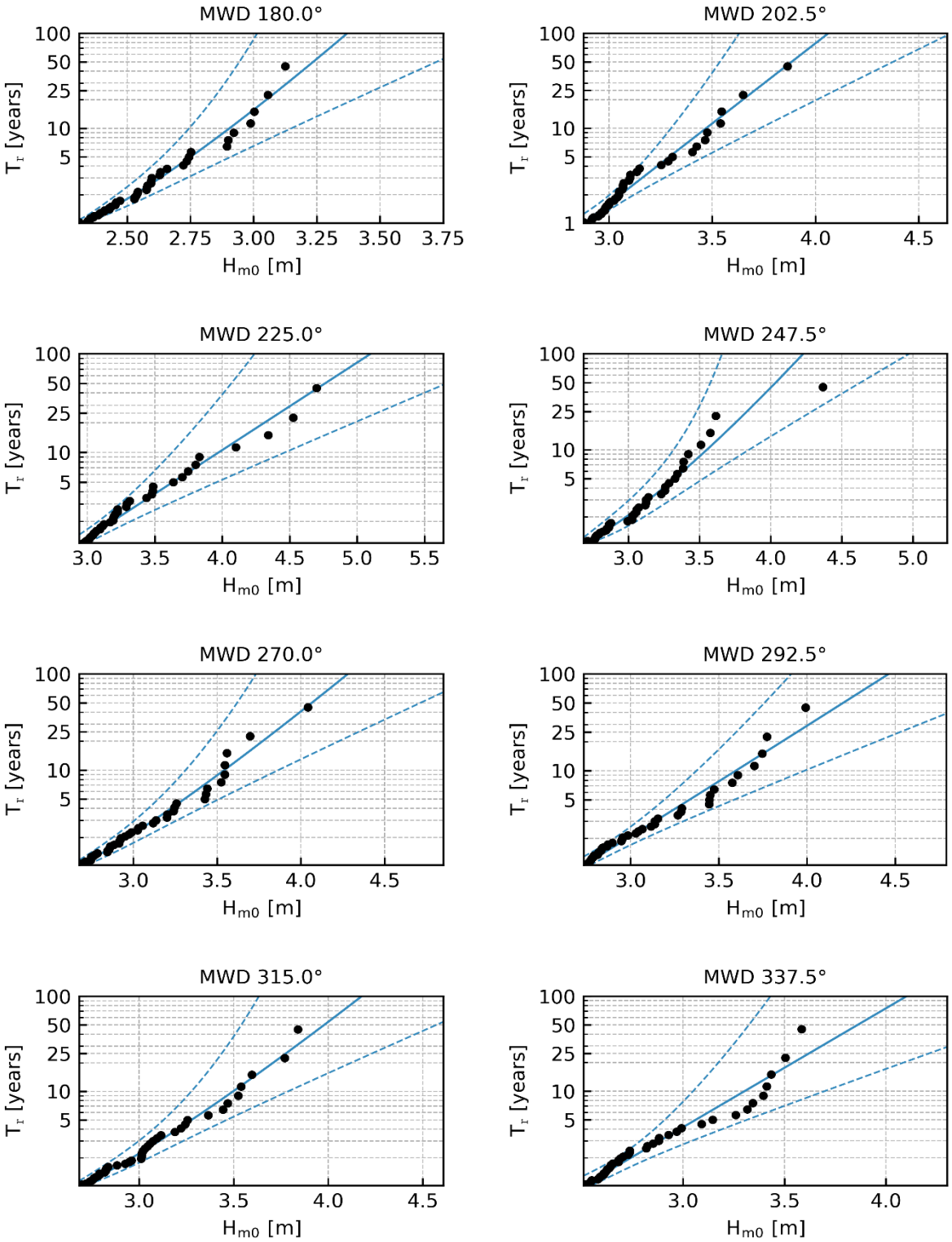

Figure 7-18 Extreme H_{m0} for MWD directional sectors at KG-1 (56.4251°E, 11.6797°N, Seabed level=-27.61mMSL, 1979-01-01 to 2023-12-31; Δt=1h). Weibull LS, λ = 1. Confidence limits 2.5% - 97.5%.

7.2.1.1 *Maps of extreme H_{m0}*

Figure 7-19 present the spatial variation of H_{m0} across the data delivery area for return periods of 50-years. The wave height is based on extreme value analysis at each grid point in the data delivery area. The figures for return periods of 1, 5, 10 and 25 years return period can be found in Figure 7-20, Figure 7-21, Figure 7-22 and Figure 7-23.

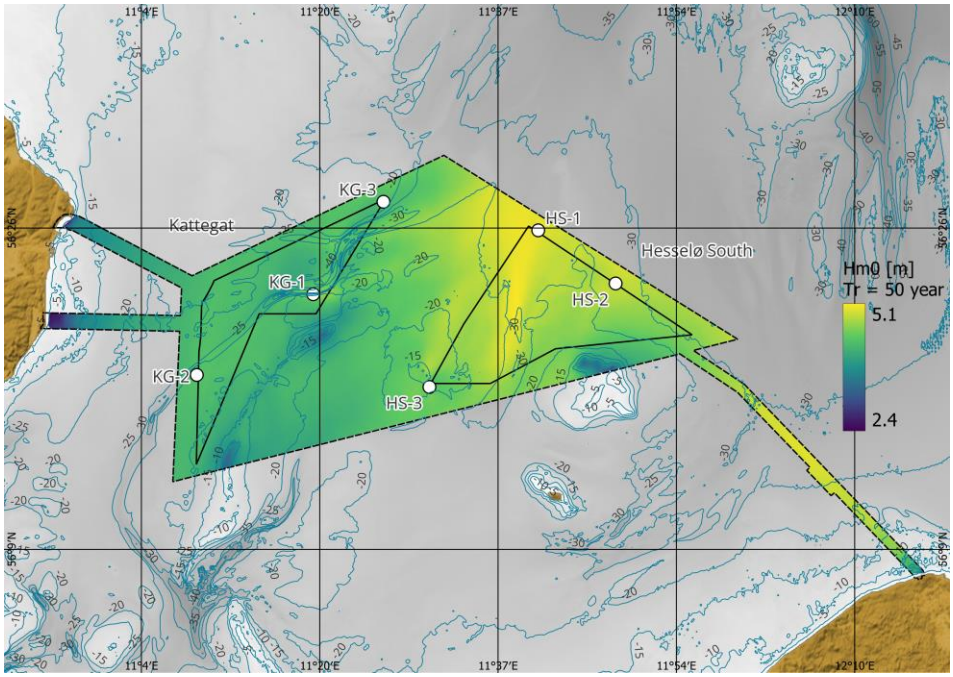

Figure 7-19 Spatial variation across the data delivery area of KG of H_{m0} for return periods of 50 years. The colour map shows the wave height, and the contours shows water depth.

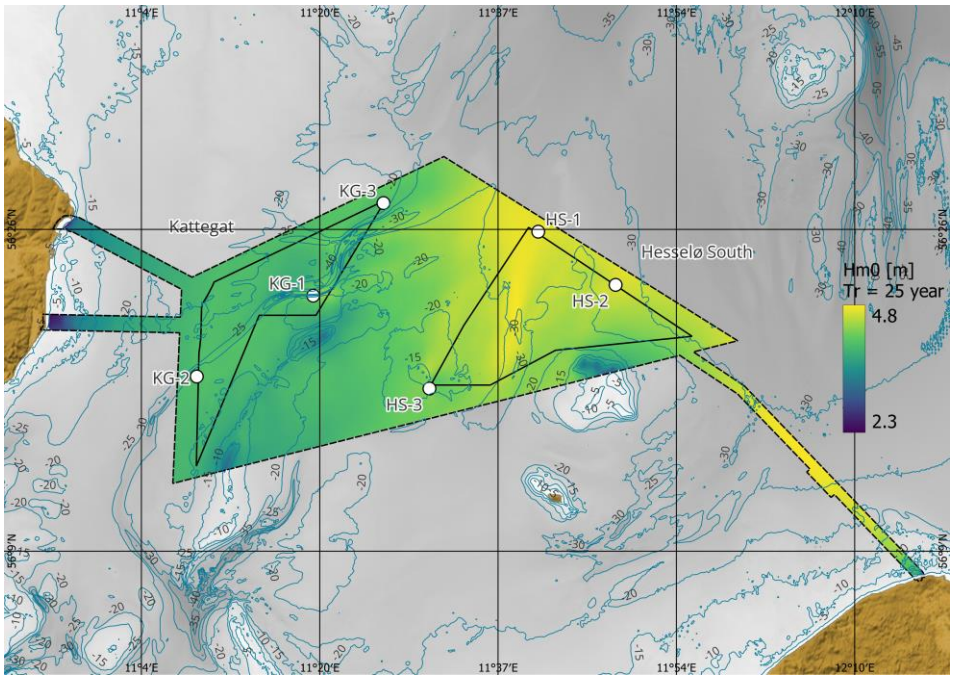

Figure 7-20 Spatial variation across the data delivery area of KG of H_{m0} for return periods of 25 years. The colour map shows the wave height, and the contours shows water depth.

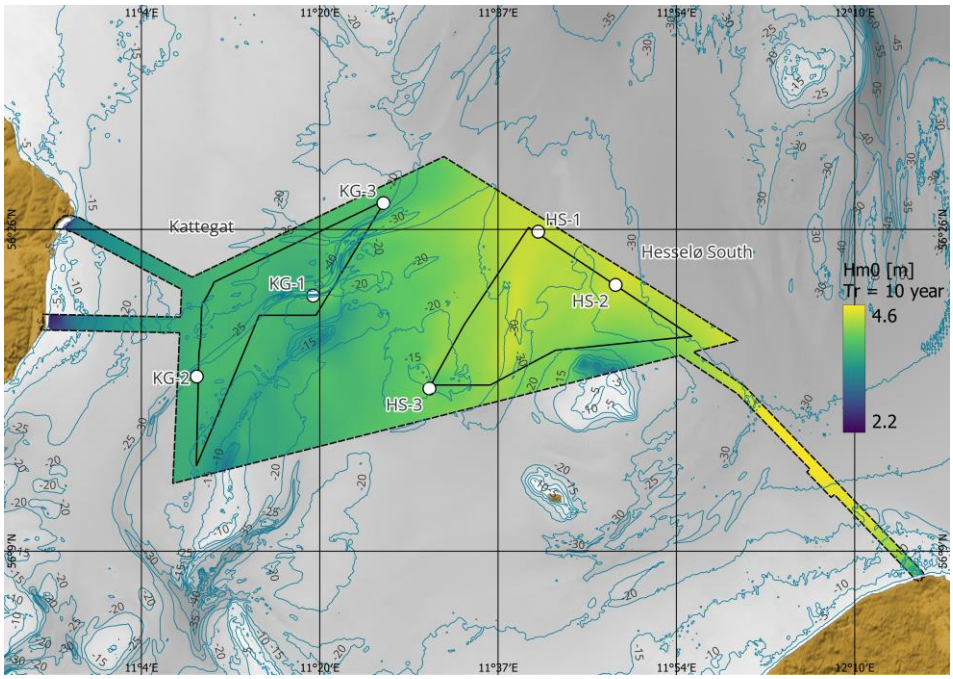

Figure 7-21 Spatial variation across the data delivery area of KG of H_{m0} for return periods of 10 years. The colour map shows the wave height, and the contours shows water depth.

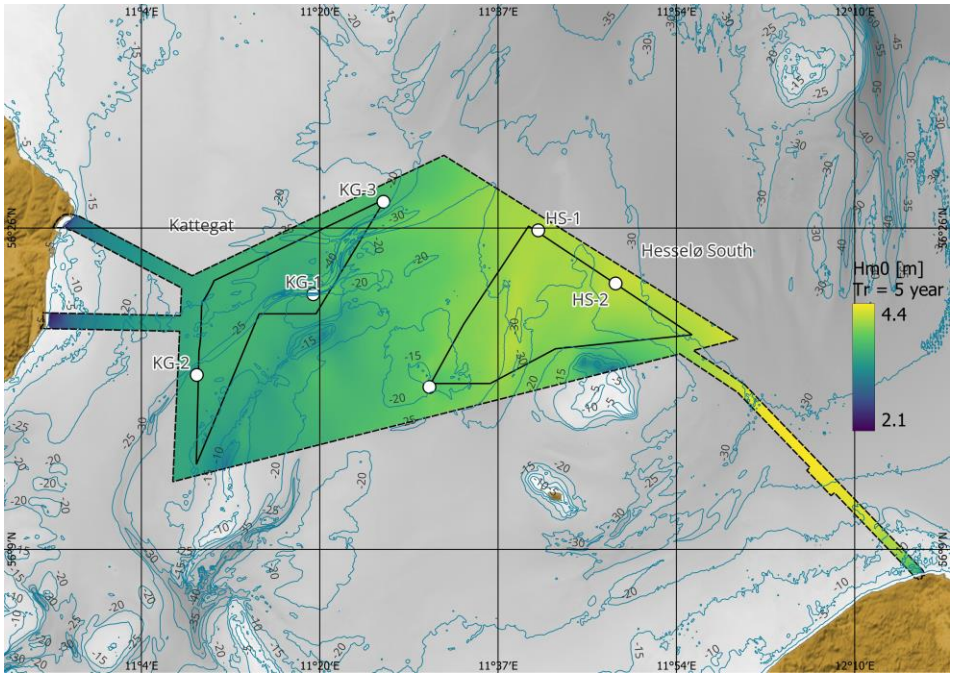

Figure 7-22 Spatial variation across the data delivery area of KG of H_{m0} for return periods of 5 years. The colour map shows the wave height, and the contours shows water depth.

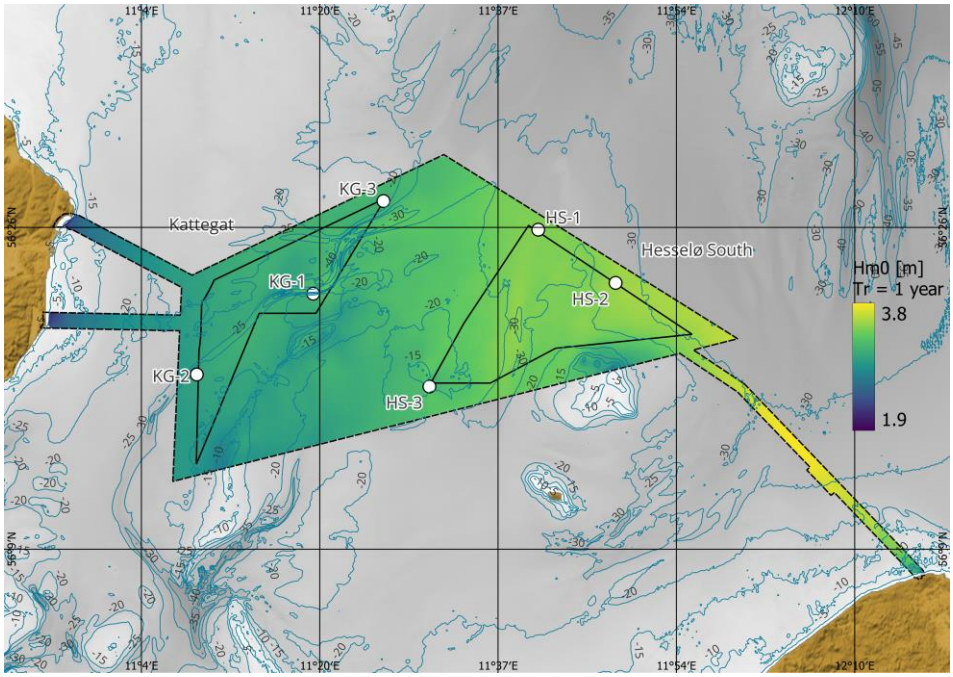

Figure 7-23 Spatial variation across the data delivery area of KG of H_{m0} for return periods of 1 year. The colour map shows the wave height, and the contours shows water depth.

7.2.1.2 *Depth-limited significant wave height*

A common approach to access the validity of the extreme wave conditions is to consider the relationship between the wave height and the water depth. Waves are considered depth-limited when their height is constrained by the water depth. This usually occurs in shallow waters as waves approach the shore. Waves start to break when their height reaches a certain fraction of the water depth. For significant wave heights this fraction is typically around 0.5-0.6 for mildly sloping seabed, for steep sloping seabed this fraction can be higher.

When inspecting the area plot of the relationship between 50 year return period H_{m0} and waterdepth at MSL on Figure 7-24, the largest values are in the order of ≈ 0.57, indicating that the extreme H_{m0} is realistic for the entire area.

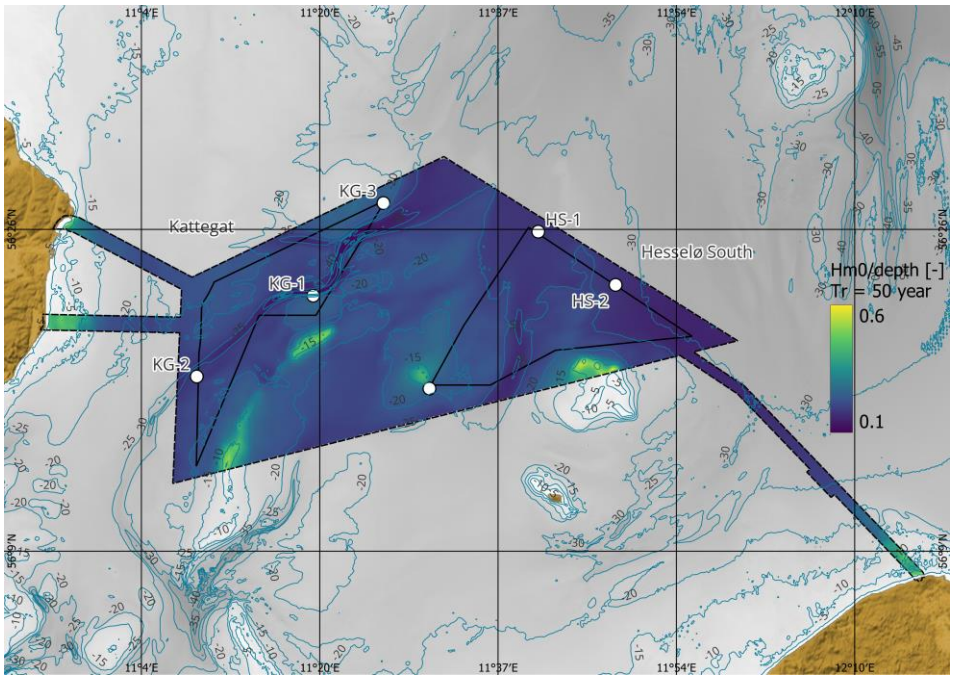

Figure 7-24 Relationship between the extreme wave height with a return period of 50 years and the depth at MSL at each model grid point in KG.

7.2.2 Extreme H_{max}

The derivation of H_{max} for long return periods (long-term distribution) is based on a constant factor of H_{max}/H_{m0} = 1.95. This factor is higher than for example the short term Rayleigh or Forristall distribution H_{max}/H_{m0}, which by themselves only accounts for H_{max} of the individual seastate and therefor underestimates H_{max} for long return periods. H_{max}/H_{m0} = 1.95 is a common factor to assume to account for the long-term uncertainty and short-term uncertainty combined, and is slightly higher than the factor of 1.9 described in DNV-RP-C205.

The maximum wave height, H_{max}, for each direction is included in Table 7-8 and the mode wave period associated with the maximum wave height, T_{Hmax} is presented in Table 7-9. T_{Hmax} is based on $T_{Hmax} = 0.9 \times T_p$ as suggested in DNV-RP-C205:2021-09. The range of the wave period associated with H_{max} ($T_{Hmax,ass}$)

is based on equation (11) in IEC 61400-3-1:2019. The wave periods are presented in Table 7-10 and Table 7-11.

It is noted that the 50 year omni H_{max} = 9.2m is far below the shallow water breaking limit (H/d=0.78, where H is the wave height and d is the water depth), indicating that the extreme maximum wave heights are realistic and the approach is reasonable as the waves are not exposed to water depth induced wave breaking. Furthermore the associated crest maximum of H_{max} is calculated by Stream Function theory in section 7.2.3 based on the range of $T_{Hmax,ass}$, which verifies the wave steepness criteria for breaking waves have not been exceeded.

Current induced wave breaking has not been accounted for in the model and is also not relevant in the area given the low current speeds.

Table 7-8 Marginal directional estimates of H_{max}, at KG-1

Sector	H_{max} [m]					
MWD [°N-from]	Quantile	T_r 1	T_r 5	T_r 10	T_r 25	T_r 50
0.0	Mean estimate	4.7	6	6.5	7.2	7.7
22.5		3.9	5.2	5.6	6.1	6.5
45.0		3.6	4.9	5.3	5.8	6.1
67.5		3.9	5.2	5.7	6.3	6.7
90.0		4	5.4	5.7	6.2	6.5
112.5		4.2	4.9	5.2	5.5	5.7
135.0		3.7	4.6	4.8	5	5.1
157.5		3.8	4.6	4.8	5	5.2
180.0		4.5	5.4	5.6	6	6.3
202.5		5.6	6.4	6.8	7.2	7.6
225.0		5.6	7.1	7.7	8.6	9.2
247.5		5.1	6.5	6.9	7.5	7.9
270.0		5.2	6.4	6.9	7.5	7.9
292.5		5.3	6.5	7	7.7	8.2
315.0		5.2	6.4	6.8	7.4	7.8
337.5		4.9	6	6.4	7.1	7.5
Omni		6.3	7.5	8	8.7	9.2

Table 7-9 Mode wave period associated with the maximum wave height at KG-1.

Sector		T_{hmax}				
MWD [°N-from]	Quantile	T_r 1	T_r 5	T_r 10	T_r 25	T_r 50
0.0	Mean estimate	5.6	6.1	6.3	6.5	6.7
22.5		5.1	5.7	5.8	6	6.2
45.0		5	5.6	5.8	6	6.1
67.5		5.2	5.8	6	6.2	6.4
90.0		5.2	5.8	6	6.1	6.2
112.5		5.2	5.5	5.6	5.8	5.8
135.0		4.8	5.2	5.3	5.4	5.4
157.5		4.8	5.1	5.2	5.3	5.4
180.0		5.2	5.6	5.7	5.8	5.9
202.5		5.9	6.2	6.3	6.4	6.5
225.0		5.9	6.5	6.7	7	7.2
247.5		5.6	6.1	6.3	6.5	6.6
270.0		5.5	6	6.1	6.3	6.4
292.5		5.7	6.1	6.2	6.4	6.6
315.0		5.8	6.2	6.4	6.6	6.7
337.5		5.8	6.2	6.4	6.6	6.7
Omni		6.2	6.6	6.7	6.9	7.1

Table 7-10 Wave period (low) associated with the maximum wave height at KG-1.

Sector		$T_{Hmax,ass,low}$ [s]				
MWD [°N-from]	Quantile	T_r 1	T_r 5	T_r 10	T_r 25	T_r 50
0.0	Mean estimate	5.5	6.2	6.5	6.8	7.1
22.5		5	5.8	6	6.3	6.5
45.0		4.8	5.6	5.8	6.1	6.3
67.5		5	5.8	6	6.4	6.6
90.0		5.1	5.9	6.1	6.3	6.5
112.5		5.2	5.6	5.8	5.9	6.1
135.0		4.9	5.4	5.5	5.6	5.7
157.5		5	5.4	5.5	5.7	5.8
180.0		5.4	5.9	6	6.2	6.4
202.5		6	6.4	6.6	6.8	7
225.0		6	6.8	7.1	7.5	7.7
247.5		5.7	6.5	6.7	6.9	7.1
270.0		5.8	6.4	6.7	6.9	7.1
292.5		5.8	6.5	6.7	7	7.3
315.0		5.8	6.4	6.6	6.9	7.1
337.5		5.6	6.2	6.4	6.7	7
Omni		6.4	6.9	7.2	7.5	7.7

Table 7-11 Wave period (high) associated with the maximum wave height at KG-1.

Sector		$T_{Hmax,ass,high}$ [s]				
MWD [°N-from]	Quantile	T_r 1	T_r 5	T_r 10	T_r 25	T_r 50
0.0	Mean estimate	7.1	8	8.3	8.8	9.1
22.5		6.4	7.4	7.7	8.1	8.3
45.0		6.2	7.2	7.5	7.9	8.1
67.5		6.5	7.4	7.8	8.2	8.5
90.0		6.6	7.6	7.8	8.1	8.3
112.5		6.7	7.2	7.4	7.7	7.8
135.0		6.3	7	7.1	7.3	7.4
157.5		6.4	7	7.1	7.3	7.5
180.0		6.9	7.6	7.8	8	8.2
202.5		7.7	8.3	8.5	8.8	9
225.0		7.7	8.7	9.1	9.6	10
247.5		7.4	8.3	8.6	8.9	9.2
270.0		7.4	8.3	8.6	8.9	9.2
292.5		7.5	8.3	8.7	9.1	9.4
315.0		7.5	8.3	8.5	8.9	9.1
337.5		7.2	8	8.3	8.7	9
Omni		8.2	8.9	9.3	9.6	9.9

7.2.3 Extreme C_{max}

For C_{max}, the Stream Function theory is used based on the derived H_{max} and $T_{Hmax,ass}$ in section 7.2.2 and the water depth at MSL. This is a slightly conservative approach. C_{max} is based on MSL and does not include contribution from high/low water level.

The maximum wave crest height, C_{max}, for each direction is included in Table 7-12.

Table 7-12 Marginal directional extreme estimates of C_{max}, at KG-1.

Sector	C_{max} [m AMSL]					
MWD [°N-from]	Quantile	T_r 1	T_r 5	T_r 10	T_r 25	T_r 50
0.0	Mean estimate	2.6	3.4	3.7	4.2	4.5
22.5		2.2	3	3.2	3.5	3.8
45.0		2	2.8	3	3.3	3.5
67.5		2.2	3	3.2	3.6	3.9
90.0		2.3	3.1	3.3	3.6	3.8
112.5		2.4	2.8	3	3.2	3.3
135.0		2.1	2.7	2.8	2.9	2.9
157.5		2.2	2.6	2.8	2.9	3
180.0		2.6	3.1	3.3	3.5	3.7
202.5		3.2	3.7	3.9	4.2	4.4
225.0		3.2	4.1	4.5	5.1	5.5
247.5		2.9	3.8	4	4.4	4.6
270.0		3	3.8	4.1	4.4	4.7
292.5		3	3.8	4.1	4.6	4.9
315.0		3	3.7	4	4.3	4.6
337.5		2.8	3.4	3.7	4.1	4.4
Omni		3.6	4.4	4.7	5.2	5.5

7.3 Extreme wave conditions scaled

Section 7.2 presents the results of the EVA analysis of the extreme wave conditions. DNV-RP-C205 section 3.6.5.6 presents a method for scaling the results of the EVA analysis. The applicability of the scaling method will not be discussed further here, but due care is advised when applying the results of the scaling.

Scaling according to DNV-RP-C205 section 3.6.5.6 has been performed for the extreme wave conditions and is available in the Appendices.

7.4 Wave Spectrum

Full directional spectra are available in hindcast format, and a comparison with measured wave spectra has been performed in [1].

A comparison between hindcast wave spectra and JONSWAP spectra (as defined in DNV-RP-C205:2021-09) has been performed for a number of H_{m0} ranges. The comparison for several H_{m0} bins is presented in the appendices, and in Figure 7-25 an example is presented.

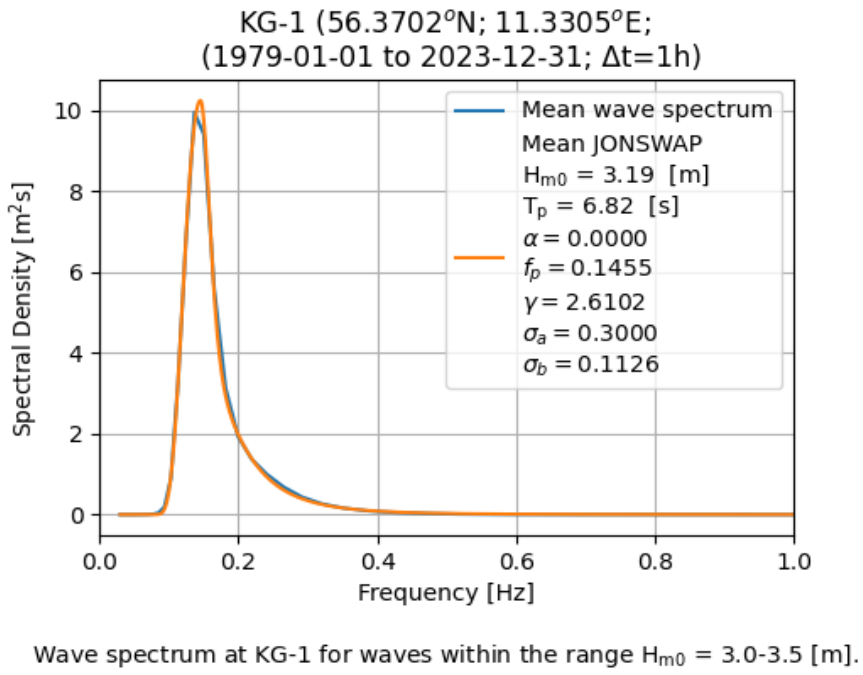

Figure 7-25 Comparison of hindcast (mean wave spectrum) and JONSWAP spectra for H_{m0} = 3.5-4.0 m at KG-1.

The analysis shows that the hindcast spectra cannot be represented precisely by the JONSWAP spectrum at the peak by the recommendations in DNV-RP-C205:2021-09, but that the overall fit is good. It is noted that in [1] the comparison between the hindcast spectrum and the measured spectrum is good, but the hindcast spectrum tends to undershoot the measured peak, thus the JONSWAP fit is closer to the measured spectrum. Therefor the JONSWAP wave spectrum is recommended for all stochastic wave series based on the recommendations in DNV-RP-C205:2021-09. The peak enhancement factor (γ) can be determined using the following relationship:

$$\gamma = \begin{cases} 5 & for \quad \frac{T_p}{\sqrt{H_s}} \le 3.6 \\ \exp\left(5.75 - 1.15\frac{T_p}{\sqrt{H_s}}\right) & for \quad 3.6 < \frac{T_p}{\sqrt{H_s}} \le 5 \\ 1 & for \quad 5 < \frac{T_p}{\sqrt{H_s}} \end{cases}$$

7.4.1 Directional Spreading

The directional spreading factor is used to modify uni-directional regular wave theories. The directional spreading factor can be applied if no significant refraction is present.

Figure 7-26 shows the wave directional standard deviation as a function of the significant wave height.

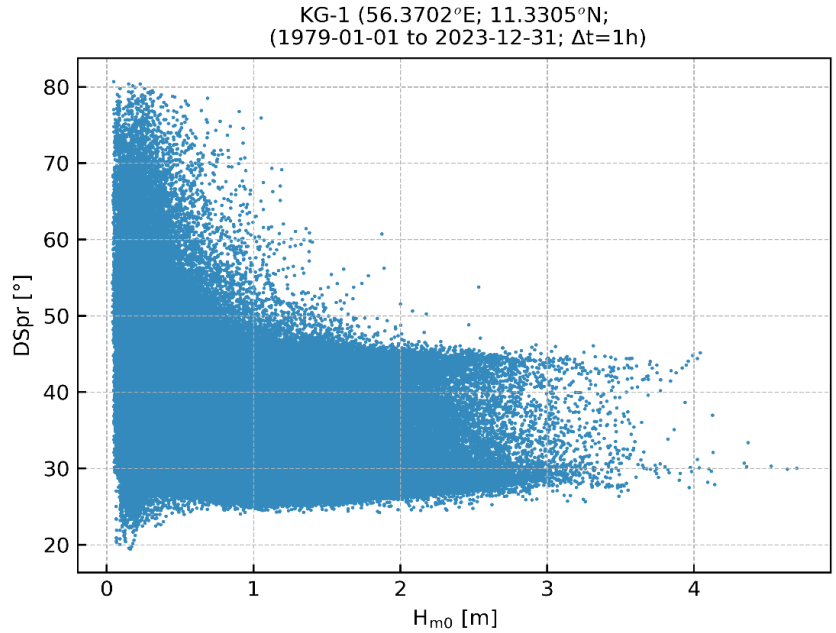

Figure 7-26 Wave directional standard deviation as a function H_{m0}.

Based on Figure 7-26 a conservative estimate of the wave directional standard deviation for extreme conditions is found to be 24°.

In Figure 7-27 the spreading factor as a function of the directional standard deviation can be seen.

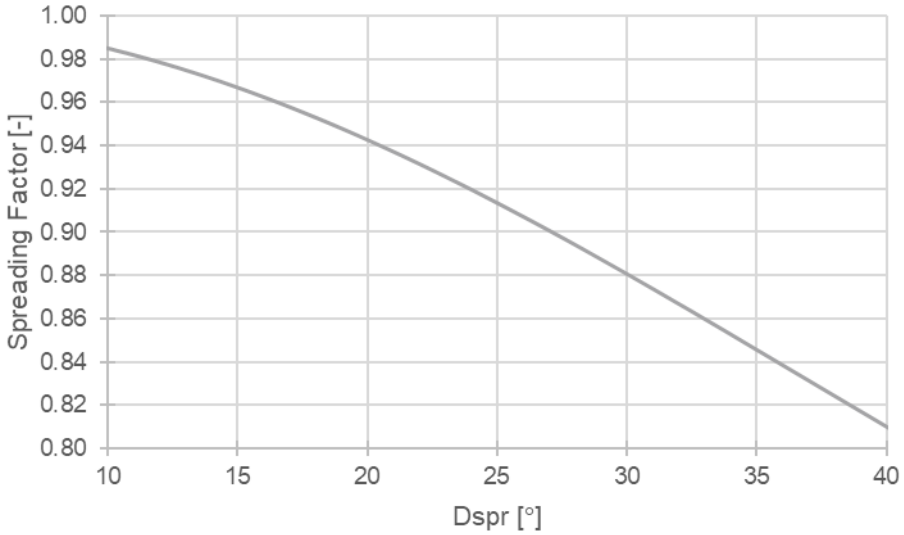

Figure 7-27 Relationship between directional standard deviation and Spreading factor applied in ISO 19901-1:2015.

In Figure 7-27 it is seen that the conservative estimate of a wave directional standard deviation of 24° yields a spreading factor of 0.92.

8 Scatter Distributions

This section presents a scatter diagrams and figures between various parameters.

8.1.1 Wind-wave misalignment

The scatter of MWD and U_{150dir} is presented on Figure 8-1 and in Table 8-1. The scatter shows a clear trend along the 1:1 line with some scatter evenly spread across the range. The higher density areas opposite to the 1:1 line is due to the wrap around.

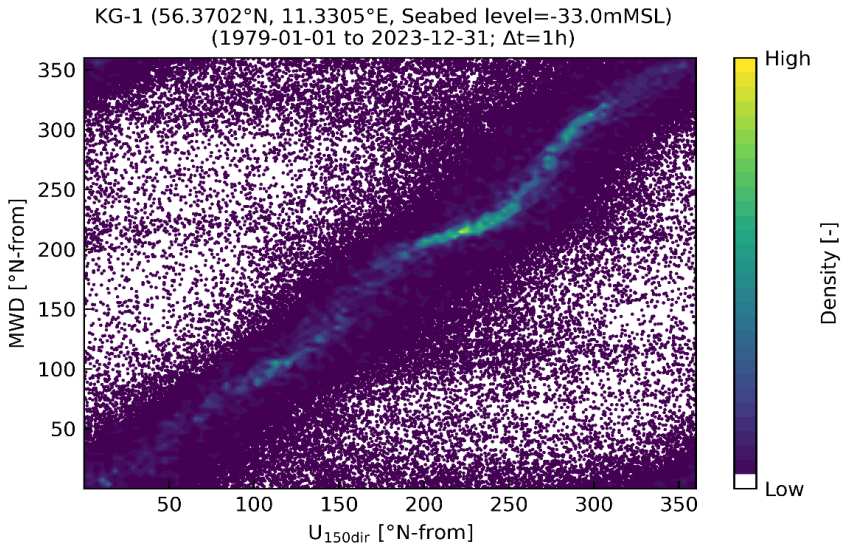

Figure 8-1 Scatter of MWD and U_{150dir} at KG-1

Table 8-1 Table of U_{150dir} and MWD in percentage, at KG-1.

U_{150dir} [°N-from]	MWD [°N-from]																
	0.0	22.5	45.0	67.5	90.0	112.5	135.0	157.5	180.0	202.5	225.0	247.5	270.0	292.5	315.0	337.5	Omni
0.0	2.48	1.23	0.28	0.11	0.06	0.05	0.06	0.05	0.05	0.06	0.07	0.07	0.08	0.12	0.24	1.00	6.0
22.5	0.41	1.53	1.09	0.30	0.14	0.08	0.06	0.05	0.04	0.03	0.03	0.04	0.04	0.03	0.06	0.10	4.0
45.0	0.08	0.31	1.31	0.92	0.26	0.11	0.06	0.03	0.02	0.03	0.02	0.02	0.02	0.02	0.02	0.03	3.3
67.5	0.03	0.07	0.33	1.77	1.19	0.24	0.10	0.05	0.03	0.02	0.02	0.02	0.01	0.01	0.01	0.02	3.9
90.0	0.02	0.03	0.07	0.35	2.43	2.22	0.31	0.10	0.06	0.03	0.02	0.03	0.02	0.02	0.01	0.01	5.7
112.5	0.02	0.01	0.02	0.04	0.26	2.48	2.61	0.41	0.15	0.08	0.07	0.05	0.04	0.02	0.02	0.02	6.3
135.0	0.01	0.01	0.01	0.02	0.04	0.28	2.11	1.55	0.37	0.13	0.07	0.04	0.03	0.02	0.01	0.01	4.7
157.5	0.01	0.01	0.01	0.01	0.02	0.07	0.49	1.88	0.84	0.26	0.12	0.06	0.03	0.02	0.01	0.01	3.8
180.0	0.01	0.01	0.01	0.01	0.01	0.03	0.11	0.86	2.17	0.74	0.24	0.10	0.05	0.02	0.02	0.01	4.4
202.5	0.02	0.01	0.01	0.01	0.01	0.03	0.04	0.15	1.61	5.24	2.85	0.44	0.11	0.05	0.03	0.02	10.6
225.0	0.02	0.02	0.02	0.01	0.02	0.02	0.02	0.05	0.11	0.74	5.72	5.99	0.79	0.15	0.05	0.02	13.7
247.5	0.02	0.01	0.01	0.01	0.01	0.01	0.02	0.03	0.05	0.14	0.44	2.97	3.05	0.33	0.07	0.03	7.2
270.0	0.02	0.01	0.01	0.01	0.01	0.01	0.02	0.02	0.04	0.08	0.17	0.73	4.32	0.90	0.13	0.05	6.5
292.5	0.03	0.02	0.01	0.01	0.01	0.01	0.02	0.02	0.04	0.07	0.12	0.29	2.56	4.28	0.40	0.09	8.0
315.0	0.10	0.04	0.03	0.03	0.03	0.03	0.03	0.04	0.04	0.05	0.09	0.14	0.33	3.19	2.28	0.44	6.9
337.5	0.64	0.15	0.06	0.04	0.04	0.03	0.03	0.03	0.04	0.04	0.05	0.08	0.13	0.35	1.39	1.72	4.8
Omni	3.9	3.5	3.3	3.7	4.6	5.7	6.1	5.3	5.7	7.7	10.1	11.1	11.6	9.5	4.7	3.6	100

The wind-wave misalignment is calculated as U_{10mag} minus MWD. Figure 8-2 and Table 8-2 presents the misalignment vs. U_{150mag} at KG-1. The misalignment shows a high scatter for wind speeds less than ~5 m/s, while the scatter (misalignment) is relatively low for higher wind speeds.

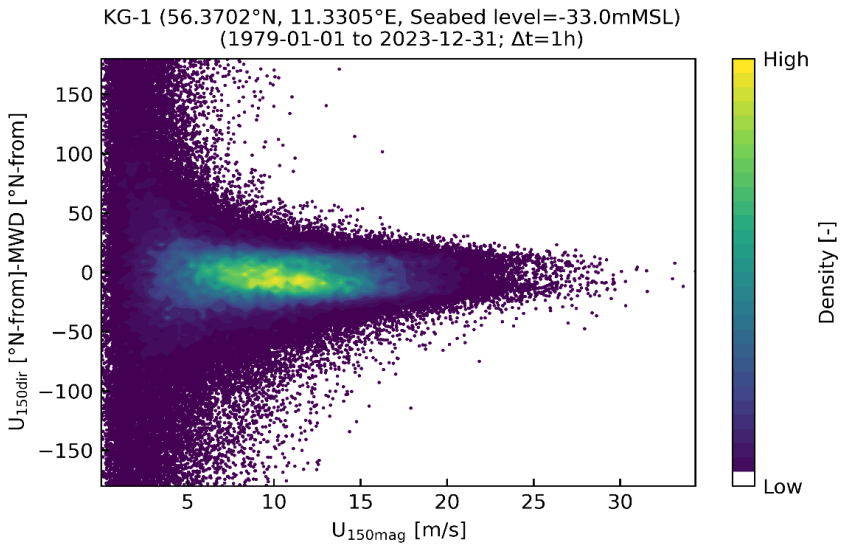

Figure 8-2 Scatter of U_{150mag} and U_{150dir} – MWD

Table 8-2 Table of U_{150mag} and U_{150dir}–MWD in percentage, at KG-1.

	U_{150dir} - MWD [°N-from]																
U_{150mag} [m/s]	-180.0 - -157.5	-157.5 - -135.0	-135.0 - -112.5	-112.5 - -90.0	-90.0 - -67.5	-67.5 - -45.0	-45.0 - -22.5	-22.5 - 0.0	0.0 - 22.5	22.5 - 45.0	45.0 - 67.5	67.5 - 90.0	90.0 - 112.5	112.5 - 135.0	135.0 - 157.5	157.5 - 180.0	Sum
0.0 - 2.0	0.12	0.14	0.14	0.16	0.19	0.23	0.28	0.31	0.32	0.30	0.26	0.21	0.18	0.16	0.14	0.15	3.3
2.0 - 4.0	0.14	0.16	0.17	0.22	0.34	0.60	1.16	1.81	1.75	1.11	0.63	0.35	0.21	0.16	0.15	0.14	9.1
4.0 - 6.0	0.04	0.07	0.08	0.13	0.25	0.62	1.80	4.23	4.01	1.26	0.32	0.12	0.06	0.04	0.03	0.04	13.1
6.0 - 8.0	0.02	0.03	0.03	0.06	0.13	0.41	1.84	6.61	5.55	0.78	0.10	0.02	0.01	0.01	0.01	0.01	15.6
8.0 - 10.0	0.01	0.01	0.02	0.03	0.07	0.23	1.65	8.60	5.93	0.47	0.03	0.01	0.00	0.00	0.00	0.00	17.1
10.0 - 12.0	0.00	0.00	0.00	0.01	0.03	0.15	1.24	8.68	5.26	0.25	0.01	0.00	0.00	0.00	0.00	0.00	15.6
12.0 - 14.0	0.00	0.00	0.00	0.00	0.01	0.06	0.80	7.20	4.00	0.12	0.00	0.00	0.00	0.00	0.00	0.00	12.2
14.0 - 16.0	0.00	0.00	0.00	0.00	0.01	0.03	0.42	4.58	2.42	0.05	0.00	0.00	0.00	0.00	0.00	0.00	7.5
16.0 - 18.0	0.00	0.00	0.00	0.00	0.00	0.01	0.20	2.26	1.33	0.03	0.00	0.00	0.00	0.00	0.00	0.00	3.8
18.0 - 20.0	0.00	0.00	0.00	0.00	0.00	0.00	0.08	0.96	0.62	0.01	0.00	0.00	0.00	0.00	0.00	0.00	1.7
20.0 - 22.0	0.00	0.00	0.00	0.00	0.00	0.00	0.02	0.36	0.28	0.00	0.00	0.00	0.00	0.00	0.00	0.00	0.7
22.0 - 24.0	0.00	0.00	0.00	0.00	0.00	0.00	0.01	0.11	0.09	0.00	0.00	0.00	0.00	0.00	0.00	0.00	0.2
24.0 - 26.0	0.00	0.00	0.00	0.00	0.00	0.00	0.00	0.04	0.03	0.00	0.00	0.00	0.00	0.00	0.00	0.00	0.1
26.0 - 28.0	0.00	0.00	0.00	0.00	0.00	0.00	0.00	0.01	0.01	0.00	0.00	0.00	0.00	0.00	0.00	0.00	0.0
28.0 - 30.0	0.00	0.00	0.00	0.00	0.00	0.00	0.00	0.01	0.00	0.00	0.00	0.00	0.00	0.00	0.00	0.00	0.0
30.0 - 32.0	0.00	0.00	0.00	0.00	0.00	0.00	0.00	0.00	0.00	0.00	0.00	0.00	0.00	0.00	0.00	0.00	0.0
32.0 - 34.0	0.00	0.00	0.00	0.00	0.00	0.00	0.00	0.00	0.00	0.00	0.00	0.00	0.00	0.00	0.00	0.00	0.0
34.0 - 36.0	0.00	0.00	0.00	0.00	0.00	0.00	0.00	0.00	0.00	0.00	0.00	0.00	0.00	0.00	0.00	0.00	0.0
Sum	0.3	0.4	0.4	0.6	1.0	2.3	9.5	45.8	31.6	4.4	1.4	0.7	0.5	0.4	0.3	0.3	100

8.1.2 Scatter distribution of wave height and water level

The scatter of H_{m0} and WL is presented on Figure 8-3 and in Table 8-3. The scatter distribution shows a weak correlation between high water and high wave height. In the appendices figures for all directions of MWD can be found.

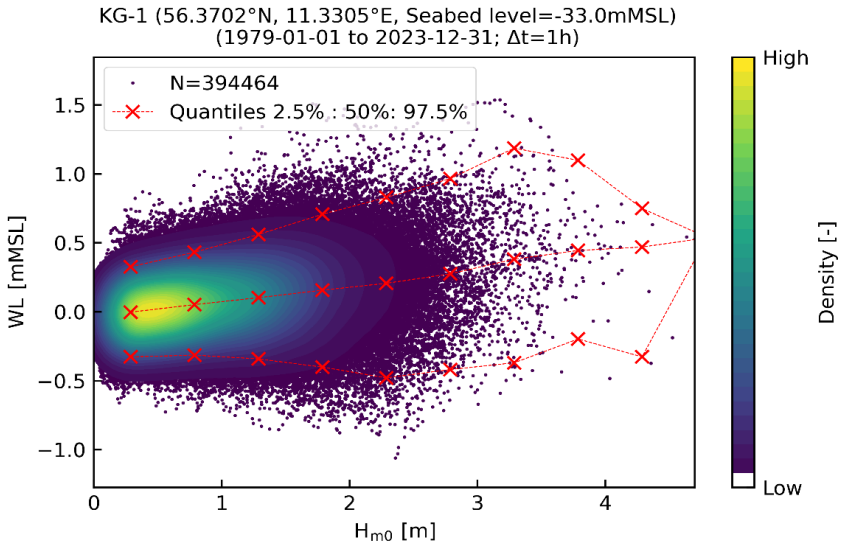

Figure 8-3 Scatter of H_{m0} and WL at KG-1. Plots for all directions of MWD are in the appendices.

Table 8-3 Table of H_{m0} and WL in percentage, at KG-1.

	H_{m0} [m]										
WL [mMSL]	0.0 - 0.5	0.5 - 1.0	1.0 - 1.5	1.5 - 2.0	2.0 - 2.5	2.5 - 3.0	3.0 - 3.5	3.5 - 4.0	4.0 - 4.5	4.5 - 5.0	Sum
-1.1 - -1.0	0.00	0.00	0.00	0.00	0.00	0.00	0.00	0.00	0.00	0.00	0.0
-1.0 - -0.9	0.00	0.00	0.00	0.00	0.00	0.00	0.00	0.00	0.00	0.00	0.0
-0.9 - -0.8	0.00	0.00	0.00	0.00	0.00	0.00	0.00	0.00	0.00	0.00	0.0
-0.8 - -0.7	0.00	0.00	0.00	0.01	0.01	0.00	0.00	0.00	0.00	0.00	0.0
-0.7 - -0.6	0.00	0.00	0.01	0.02	0.01	0.00	0.00	0.00	0.00	0.00	0.0
-0.6 - -0.5	0.01	0.02	0.04	0.05	0.03	0.01	0.00	0.00	0.00	0.00	0.1
-0.5 - -0.4	0.11	0.15	0.15	0.12	0.05	0.01	0.00	0.00	0.00	0.00	0.6
-0.4 - -0.3	0.57	0.55	0.45	0.28	0.08	0.02	0.00	0.00	0.00	0.00	2.0
-0.3 - -0.2	1.89	1.66	1.04	0.49	0.14	0.03	0.00	0.00	0.00	0.00	5.3
-0.2 - -0.1	4.24	3.81	2.02	0.75	0.17	0.03	0.01	0.00	0.00	0.00	11.0
-0.1 - 0.0	6.27	6.33	3.13	1.11	0.24	0.06	0.01	0.00	0.00	0.00	17.1
0.0 - 0.1	6.35	7.35	4.08	1.36	0.31	0.06	0.01	0.00	0.00	0.00	19.5
0.1 - 0.2	4.95	6.68	4.26	1.56	0.37	0.08	0.01	0.00	0.00	0.00	17.9
0.2 - 0.3	2.57	4.58	3.54	1.54	0.38	0.08	0.01	0.00	0.00	0.00	12.7
0.3 - 0.4	0.83	2.23	2.26	1.27	0.34	0.08	0.01	0.00	0.00	0.00	7.0
0.4 - 0.5	0.21	0.82	1.21	0.86	0.31	0.07	0.01	0.00	0.00	0.00	3.5
0.5 - 0.6	0.05	0.28	0.55	0.48	0.22	0.06	0.01	0.00	0.00	0.00	1.6
0.6 - 0.7	0.01	0.08	0.24	0.24	0.15	0.05	0.01	0.00	0.00	0.00	0.8
0.7 - 0.8	0.00	0.02	0.09	0.14	0.08	0.04	0.01	0.00	0.00	0.00	0.4
0.8 - 0.9	0.00	0.00	0.04	0.07	0.04	0.02	0.01	0.00	0.00	0.00	0.2
0.9 - 1.0	0.00	0.00	0.01	0.03	0.02	0.01	0.00	0.00	0.00	0.00	0.1
1.0 - 1.1	0.00	0.00	0.00	0.01	0.01	0.00	0.00	0.00	0.00	0.00	0.0
1.1 - 1.2	0.00	0.00	0.00	0.00	0.01	0.00	0.00	0.00	0.00	0.00	0.0
1.2 - 1.3	0.00	0.00	0.00	0.00	0.00	0.00	0.00	0.00	0.00	0.00	0.0
1.3 - 1.4	0.00	0.00	0.00	0.00	0.00	0.00	0.00	0.00	0.00	0.00	0.0
1.4 - 1.5	0.00	0.00	0.00	0.00	0.00	0.00	0.00	0.00	0.00	0.00	0.0
1.5 - 1.6	0.00	0.00	0.00	0.00	0.00	0.00	0.00	0.00	0.00	0.00	0.0
Sum	28.1	34.6	23.1	10.4	3.0	0.7	0.1	0.0	0.0	0.0	100.0

9 Reference Sea States

This section presents the reference sea states; Normal Sea State, Severe Sea State and Extreme Sea State in line with IEC 61400-3-1:2019.

The NSS and SSS are conditioned on the 10-minute average wind speed at hub height as required by the client. The conversion from 1 hour averaging to 10-minute averaging has been obtained by the conversion factor in IEC 61400-3-1:2019 of 1/0.95.

The wave hindcast data has a resolution of 1 hour but is considered representative of a 3-hour reference period as is standard practice.

9.1 Normal Sea State

NSS, characterized by a significant wave height and peak wave period, is defined as the expected significant wave height conditioned on the average wind speed at hub height.

NSS is given as a table with significant wave height and peak wave periods for different ranges of wind speeds and different directional sectors of MWD in the Appendices, Figure 9-1 presents an example for the omnidirectional description. Note that H_{m0} is capped with the 50-year return period value of H_{m0} from section 7.2.1 and the peak period is derived from the analysis in 7.1.6.

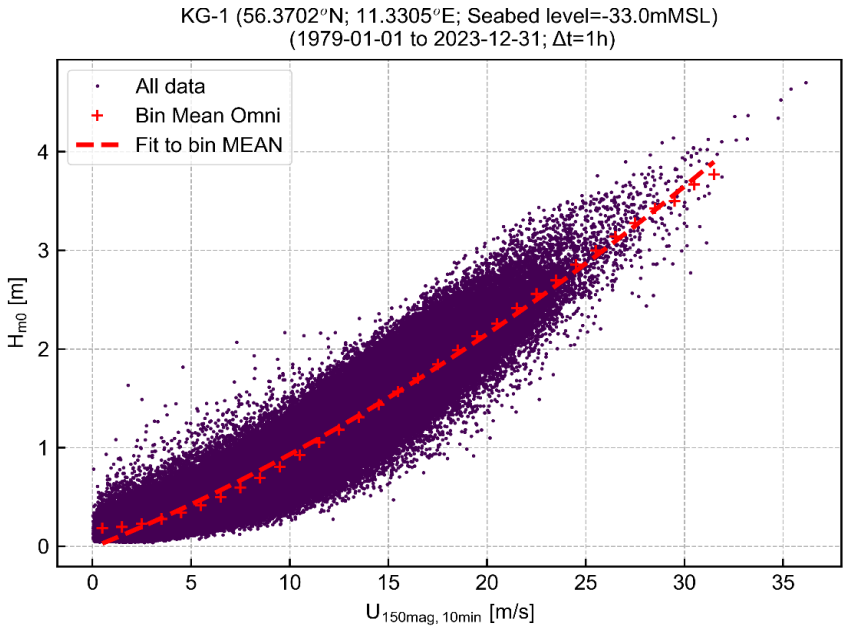

Figure 9-1 NSS for omni with fit. Fits and coefficients for all directional sectors are presented in the appendices.

9.2 Severe Sea State

SSS is a modelled as a sea state described by a combination of normal wind conditions and the significant wave height used for calculation of the ultimate loading of an offshore wind turbine during power production. SSS associates a severe sea state with each mean wind speed in the range corresponding to power production from cut-in to cut-out. The combination of wind speed and height is used to determine the 50-year return period contour to derive the individual significant wave height for each wind speed. The IFORM (IEC 61400-3-1:2019) and joint distribution is described by a global hierarchical model. In this model, one variable is taken as independent, and the other variables are modelled to be conditional on this variable using dependence functions. The wind speed is here taken as the independent variable and the wave height is used the dependent variable. The method revolves around the description of the two variables in their joint distribution. Both variables are described by and fitted to the Exponentiated Weibull Distribution (EWD). The EWD is a generalization of the Weibull distribution. The fitted and observed data in the separate bins are shown on Figure 9-3 and Figure 9-4 and show a good approximation of the Weibull distribution to the data.

The result is shown on Figure 9-2. On the figure is both the scatter data coloured by the density and the IFORM contour with a 50-year return period. The contour follows along the density of the data.

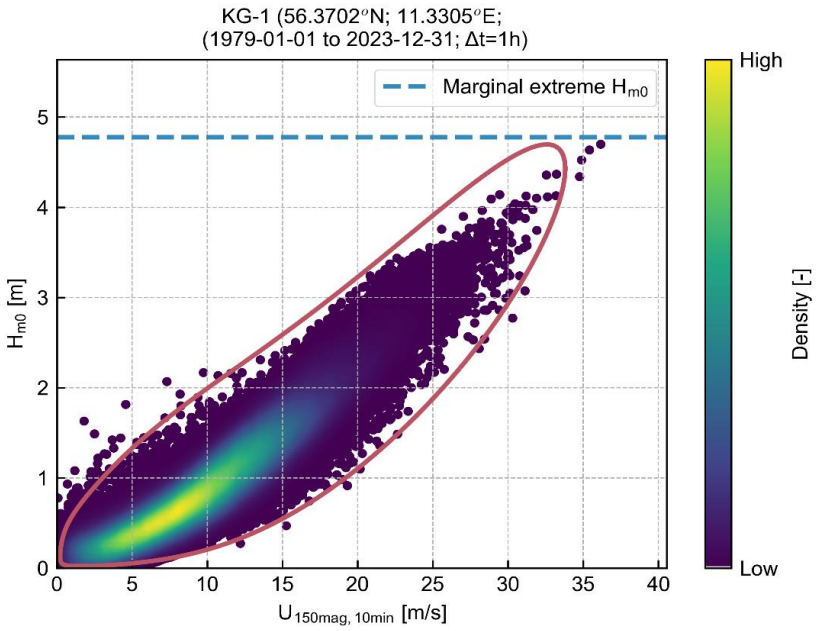

Figure 9-2 IFORM contour for SSS with a 50-year return period for H_{m0} and $U_{150mag,10min}$ at KG-1. The blue line shows the marginal 50-year return period H_{m0}.

Associated parameters for SSS are presented in Table 9-1. T_p is based on section 7.1.6, H_{max} is derived corresponding to section 7.2.2, T_{Hmax} is 0.9xT_p and $T_{Hmax,ass}$ is based on equation (11) in IEC 61400-3-1:2019.

Table 9-1 SSS from the 50-year return period environmental contour for H_{m0} and $U_{150mag,10min}$.

U_{150mag} [m/s]	H_{m0} [m]	T_p [s]	H_{max} [m]	$T_{Hmax,ass,low}$ [s]	$T_{Hmax,ass,high}$ [s]	T_{Hmax} [s]
0-2.5	0.6	3.8	1.2	3.6	3.4	0-2.5
2.5-3.5	1.0	4.5	1.9	4.6	4.0	2.5-3.5
3.5-4.5	1.2	4.7	2.3	4.9	4.3	3.5-4.5
4.5-5.5	1.3	5.0	2.6	5.3	4.5	4.5-5.5
5.5-6.5	1.5	5.2	2.9	5.6	4.6	5.5-6.5
6.5-7.5	1.6	5.3	3.2	5.8	4.8	6.5-7.5
7.5-8.5	1.8	5.5	3.4	6.0	4.9	7.5-8.5
8.5-9.5	1.9	5.6	3.7	6.2	5.1	8.5-9.5
9.5-10.5	2.0	5.8	3.9	6.4	5.2	9.5-10.5
10.5-11.5	2.1	5.9	4.1	6.6	5.3	10.5-11.5
11.5-12.5	2.2	6.0	4.4	6.8	5.4	11.5-12.5
12.5-13.5	2.4	6.1	4.6	7.0	5.5	12.5-13.5
13.5-14.5	2.5	6.2	4.8	7.2	5.6	13.5-14.5
14.5-15.5	2.6	6.3	5.1	7.3	5.7	14.5-15.5
15.5-16.5	2.7	6.5	5.3	7.5	5.8	15.5-16.5
16.5-17.5	2.8	6.6	5.5	7.7	5.9	16.5-17.5
17.5-18.5	3.0	6.7	5.8	7.9	6.0	17.5-18.5
18.5-19.5	3.1	6.8	6.0	8.0	6.1	18.5-19.5
19.5-20.5	3.2	6.9	6.3	8.2	6.2	19.5-20.5
20.5-21.5	3.4	7.0	6.6	8.4	6.3	20.5-21.5
21.5-22.5	3.5	7.1	6.8	8.5	6.4	21.5-22.5
22.5-23.5	3.6	7.2	7.1	8.7	6.5	22.5-23.5
23.5-24.5	3.8	7.3	7.4	8.9	6.6	23.5-24.5
24.5-25.5	3.9	7.4	7.6	9.0	6.6	24.5-25.5
25.5-26.5	4.0	7.5	7.9	9.2	6.7	25.5-26.5
26.5-27.5	4.2	7.6	8.1	9.3	6.8	26.5-27.5
27.5-28.5	4.3	7.6	8.4	9.5	6.9	27.5-28.5
28.5-29.5	4.4	7.7	8.6	9.6	7.0	28.5-29.5
29.5-30.5	4.5	7.8	8.8	9.7	7.0	29.5-30.5
30.5-31.5	4.6	7.9	9.0	9.8	7.1	30.5-31.5
31.5-32.5	4.7	7.9	9.1	9.9	7.1	31.5-32.5
32.5-33.5	4.7	7.9	9.1	9.9	7.1	32.5-33.5

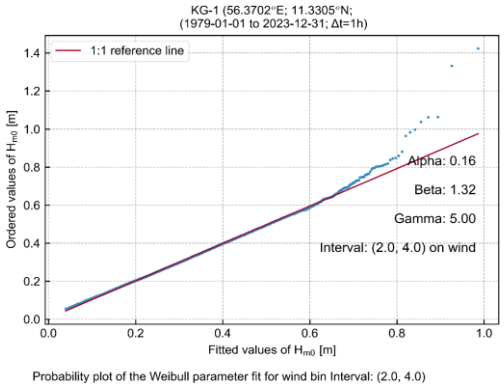

Probability plot of the Weibull parameter fit for wind bin Interval: (2.0, 4.0)

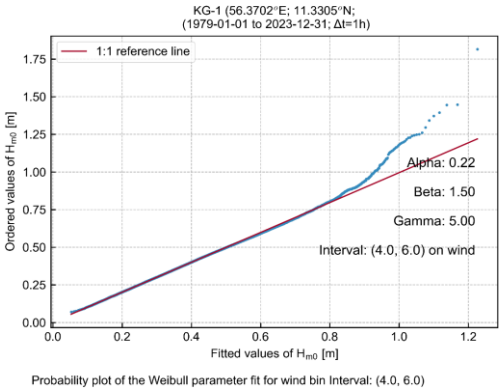

Probability plot of the Weibull parameter fit for wind bin Interval: (4.0, 6.0)

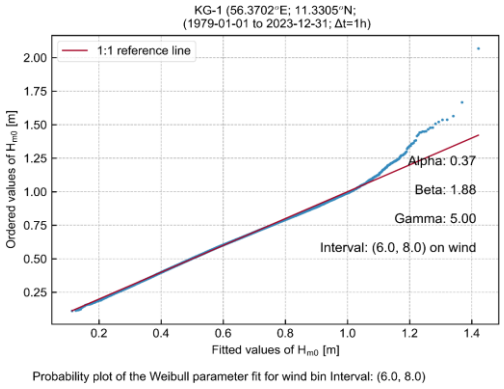

Probability plot of the Weibull parameter fit for wind bin Interval: (6.0, 8.0)

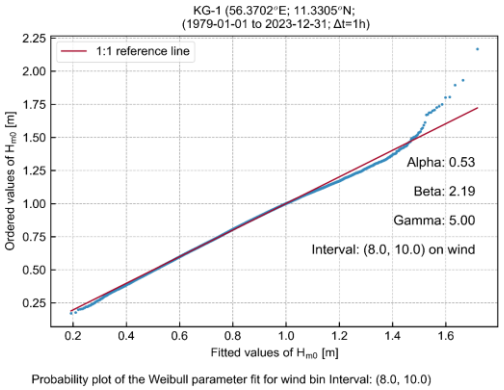

Probability plot of the Weibull parameter fit for wind bin Interval: (8.0, 10.0)

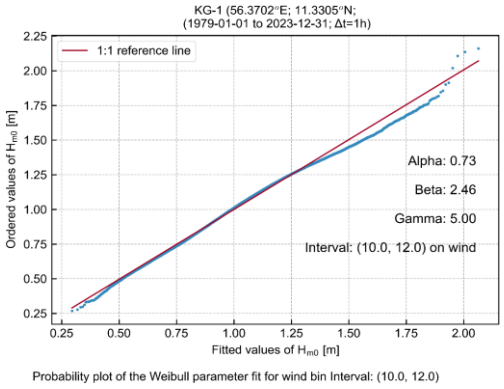

Probability plot of the Weibull parameter fit for wind bin Interval: (10.0, 12.0)

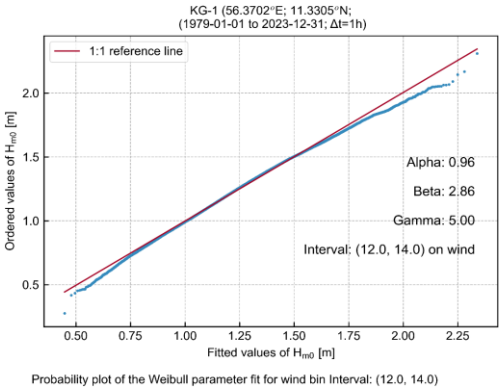

Probability plot of the Weibull parameter fit for wind bin Interval: (12.0, 14.0)

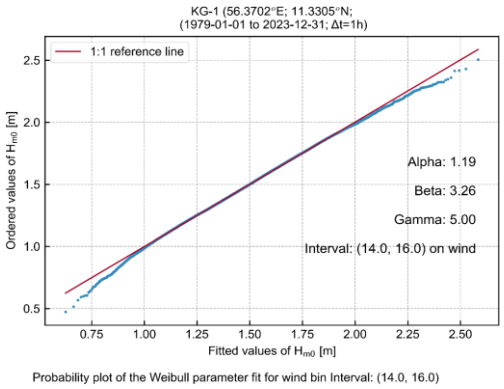

Probability plot of the Weibull parameter fit for wind bin Interval: (14.0, 16.0)

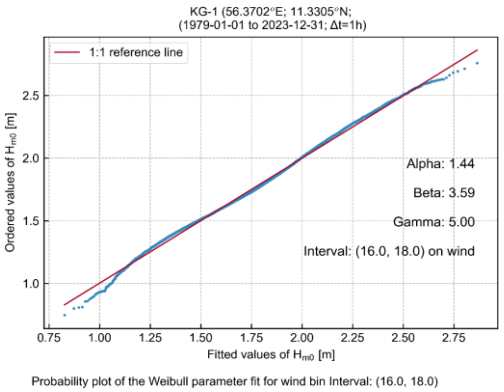

Probability plot of the Weibull parameter fit for wind bin Interval: (16.0, 18.0)

Figure 9-3 Exponentiated Weibull fit for sections of H_{m0} data binned by 2 m/s intervals of $U_{150mag,10min}$.

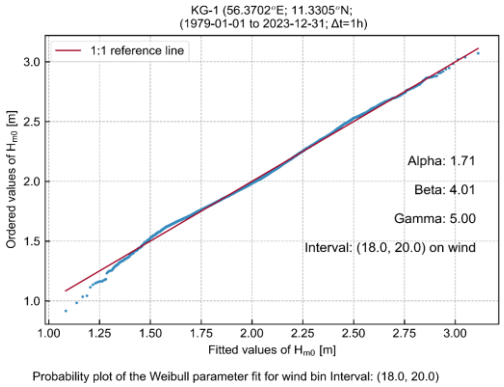

Probability plot of the Weibull parameter fit for wind bin Interval: (18.0, 20.0)

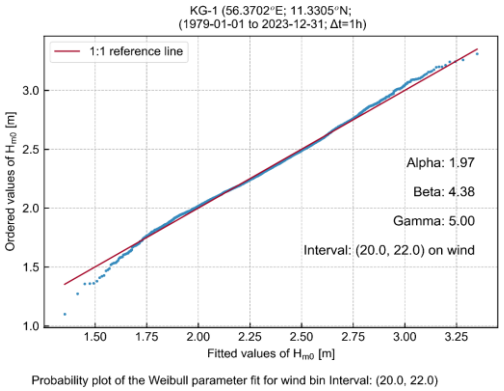

Probability plot of the Weibull parameter fit for wind bin Interval: (20.0, 22.0)

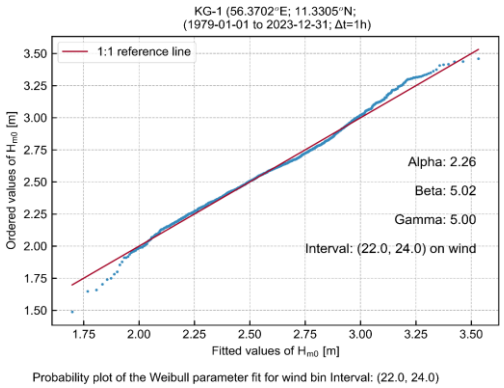

Probability plot of the Weibull parameter fit for wind bin Interval: (22.0, 24.0)

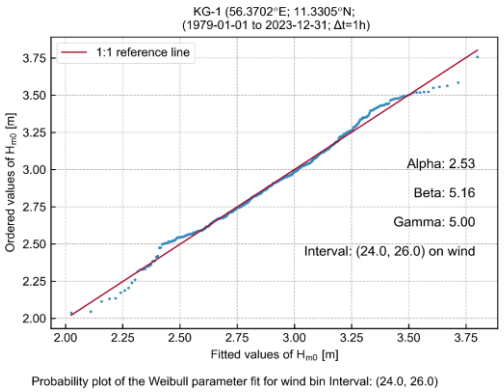

Probability plot of the Weibull parameter fit for wind bin Interval: (24.0, 26.0)

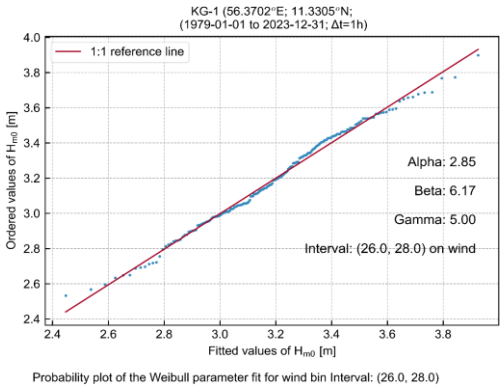

Probability plot of the Weibull parameter fit for wind bin Interval: (26.0, 28.0)

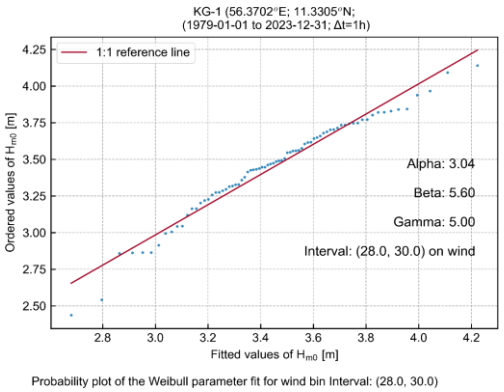

Probability plot of the Weibull parameter fit for wind bin Interval: (28.0, 30.0)

Figure 9-4 Exponentiated Weibull fit for sections of H_{m0} data binned by 2 m/s intervals of $U_{150mag,10min}$.

9.3 Extreme Sea State

ESS characterised by a significant wave height, a peak wave period and a wave direction, is given by the unconditional significant wave height with estimated average recurrence periods of 1 year and 50 years.

ESS, based on section 7.2, is given as tables with significant wave height for different directional sectors of MWD in Table 9-2 and Table 9-3. Associated parameters for the sea state are also presented. Results presented below are unscaled. Results scaled according to DNV-RPC205 can be found in the appendices, i.e. section 7.3.

Table 9-2 ESS for 50-year return period at KG-1 (unscaled).

	MWD [°N-from]																
Parameter	0.0	22.5	45.0	67.5	90.0	112.5	135.0	157.5	180.0	202.5	225.0	247.5	270.0	292.5	315.0	337.5	Omni
H_{m0} [m]	4.0	3.3	3.1	3.5	3.3	2.9	2.6	2.7	3.2	3.9	4.7	4.0	4.1	4.2	4.0	3.9	4.7
T_p [s]	7.4	6.8	6.8	7.1	6.9	6.5	6.0	6.0	6.6	7.3	7.8	7.3	7.1	7.3	7.4	7.5	7.8
H_{max} [m]	7.7	6.5	6.1	6.7	6.5	5.7	5.1	5.2	6.3	7.6	9.2	7.9	7.9	8.2	7.8	7.5	9.2
$T_{Hmax,ass,low}$ [s]	7.1	6.5	6.3	6.6	6.5	6.1	5.7	5.8	6.4	7.0	7.7	7.1	7.2	7.3	7.1	7.0	7.7
$T_{Hmax,ass,high}$ [s]	9.1	8.3	8.1	8.5	8.3	7.8	7.4	7.5	8.2	9.0	9.9	9.2	9.2	9.4	9.1	9.0	9.9
C_{max} [m]	4.5	3.8	3.5	3.9	3.8	3.3	2.9	3	3.7	4.4	5.5	4.6	4.7	4.9	4.6	4.4	5.5

Table 9-3 ESS for 1-year return period at KG-1 (unscaled).

	MWD [°N-from]																
Parameter	0.0	22.5	45.0	67.5	90.0	112.5	135.0	157.5	180.0	202.5	225.0	247.5	270.0	292.5	315.0	337.5	Omni
H_{m0} [m]	2.4	2.0	1.8	2.0	2.1	2.2	1.9	2.0	2.3	2.9	2.9	2.6	2.7	2.7	2.7	2.5	3.2
T_p [s]	6.3	5.7	5.5	5.8	5.8	5.8	5.4	5.4	5.8	6.5	6.6	6.3	6.1	6.3	6.5	6.4	6.8
H_{max} [m]	4.7	3.9	3.6	3.9	4.0	4.2	3.7	3.8	4.5	5.6	5.6	5.1	5.2	5.3	5.2	4.9	6.3
$T_{Hmax,ass,low}$ [s]	5.5	5.0	4.8	5.0	5.1	5.2	4.9	5.0	5.4	6.0	6.0	5.8	5.8	5.8	5.8	5.6	6.4
$T_{Hmax,ass,high}$ [s]	7.1	6.4	6.2	6.5	6.6	6.7	6.3	6.4	6.9	7.8	7.7	7.4	7.5	7.5	7.5	7.2	8.2
C_{max} [m]	2.6	2.2	2	2.2	2.3	2.4	2.1	2.2	2.6	3.2	3.2	2.9	3	3	3	2.8	3.6

10 Other atmospheric and oceanographic conditions

This section presents analyses of other atmospheric- and oceanographic conditions. The atmospheric conditions are air temperature, humidity, solar radiation and lightning and the oceanographic conditions are seawater temperature and salinity as well as the marine growth.

10.1 Air temperature, pressure, humidity, and solar radiation

Modelled air temperature at 2 m above sea level, air pressure at 2 m above sea level, relative humidity and solar radiation are based on ERA5 (1979-01-15 to 2023-12-31), The results are presented in Figure 10-1, Figure 10-2, Figure 10-3, and Figure 10-4, and summarised on Table 10-1, Table 10-2, Table 10-3 and Table 10-4.

There is a clear seasonal variation for all four variables. Air temperature, relative humidity and solar radiation are larger during the summer months and lower during the winter months.

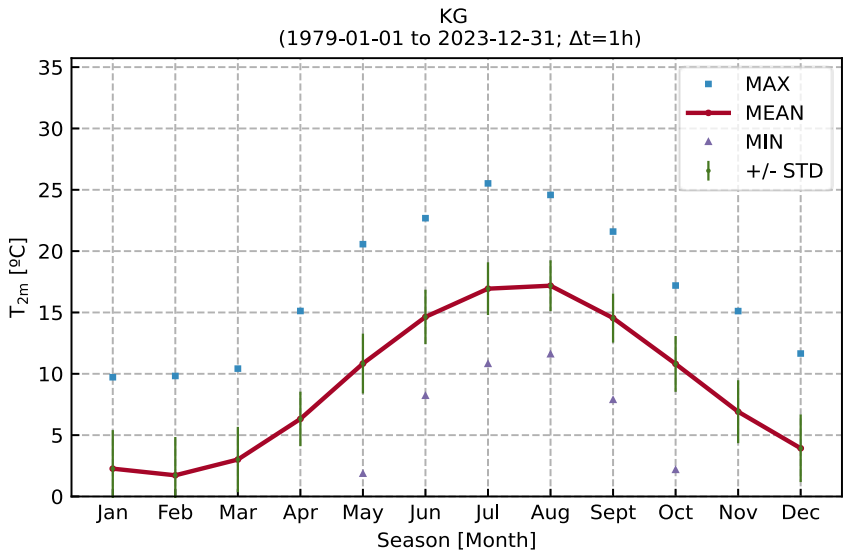

Figure 10-1 Monthly statistics of air temperature at 2 m above sea level

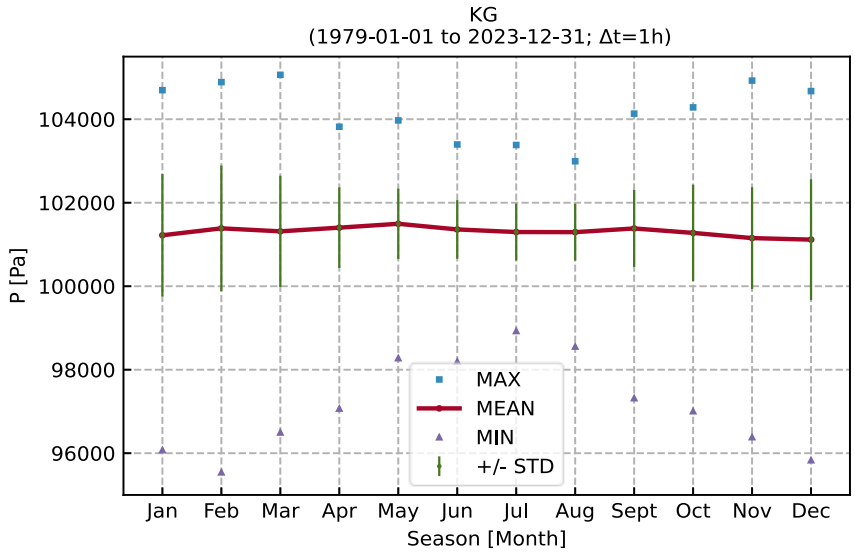

Figure 10-2 Monthly statistics of pressure at 2 m above sea level

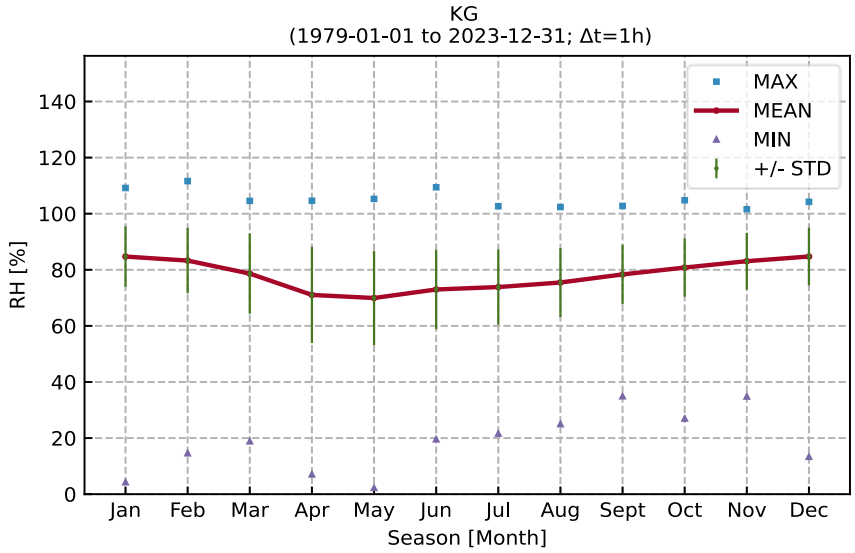

Figure 10-3 Monthly statistics of relative humidity at 2 m above sea level

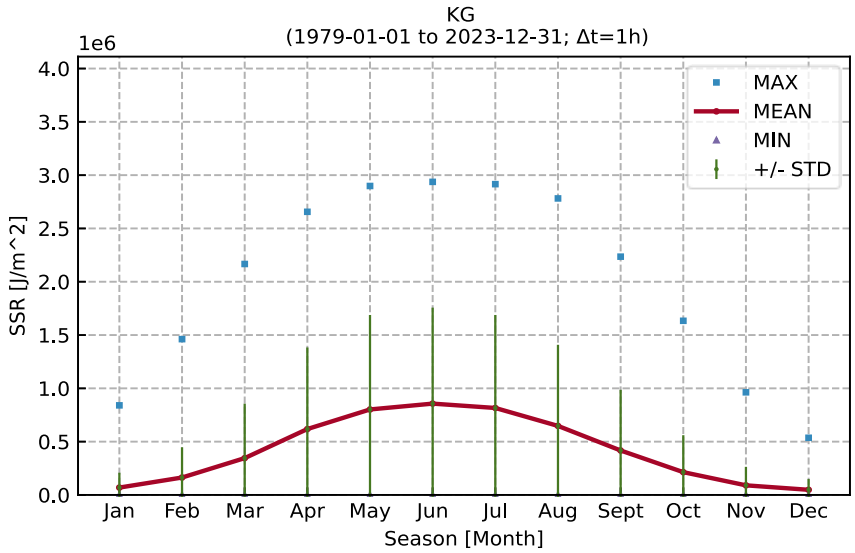

Figure 10-4 Monthly statistics of downward solar radiation

Table 10-1 Monthly statistics for air temperature at 2 m above sea level at KG-1

Season	T_{2m} [ºC]							
Month	N [-]	MEAN	STD	MIN	P05	P50	P95	MAX
Jan	33,480.0	2.3	3.1	-12.0	-3.2	2.6	6.7	9.7
Feb	30,504.0	1.7	3.1	-12.3	-3.7	2.0	6.1	9.8
Mar	33,480.0	3.0	2.7	-13.3	-1.5	3.4	6.6	10.4
Apr	32,400.0	6.3	2.2	-1.2	2.7	6.3	10.2	15.1
May	33,480.0	10.8	2.4	1.9	6.9	10.9	14.9	20.6
Jun	32,400.0	14.6	2.2	8.2	11.1	14.6	18.4	22.7
Jul	33,480.0	16.9	2.2	10.8	13.6	16.8	20.6	25.5
Aug	33,480.0	17.2	2.1	11.6	14.0	17.1	21.0	24.6
Sept	32,400.0	14.5	2.0	7.9	11.3	14.5	17.9	21.6
Oct	33,480.0	10.8	2.3	2.2	6.7	11.0	14.2	17.2
Nov	32,400.0	6.9	2.6	-3.6	2.4	7.1	10.8	15.1
Dec	33,480.0	3.9	2.8	-7.1	-0.9	4.2	8.0	11.7

Table 10-2 Monthly statistics for pressure at KG-1 at 2 m above sea level at KG-1

Season	P [Pa]							
Month	N [-]	MEAN	STD	MIN	P05	P50	P95	MAX
Jan	33,480	101,220	1,467	96,074	98,719	101,303	103,456	104,696
Feb	30,504	101,387	1,505	95,540	98,816	101,512	103,668	104,889
Mar	33,480	101,315	1,333	96,495	99,061	101,364	103,337	105,063
Apr	32,400	101,403	966	97,067	99,744	101,460	102,878	103,820
May	33,480	101,495	842	98,276	100,092	101,496	102,841	103,972
Jun	32,400	101,360	702	98,196	100,180	101,390	102,460	103,396
Jul	33,480	101,298	684	98,926	100,081	101,346	102,314	103,383
Aug	33,480	101,296	684	98,554	100,074	101,347	102,305	102,994
Sept	32,400	101,384	922	97,318	99,707	101,472	102,753	104,134
Oct	33,480	101,277	1,154	97,005	99,258	101,357	103,060	104,284
Nov	32,400	101,153	1,217	96,383	99,113	101,195	103,071	104,925
Dec	33,480	101,116	1,445	95,831	98,637	101,175	103,489	104,674

Table 10-3 Monthly statistics for relative humidity at KG-1

Season	RH [%]							
Month	N [-]	MEAN	STD	MIN	P05	P50	P95	MAX
Jan	33,480	85	11	4	65	86	99	109
Feb	30,504	83	12	15	61	85	99	112
Mar	33,480	79	14	19	51	82	97	105
Apr	32,400	71	17	7	39	74	94	105
May	33,480	70	17	2	38	73	93	105
Jun	32,400	73	14	20	46	76	92	109
Jul	33,480	74	13	22	48	77	92	103
Aug	33,480	75	12	25	52	78	92	102
Sept	32,400	78	11	35	59	80	93	103
Oct	33,480	81	10	27	61	82	95	105
Nov	32,400	83	10	35	64	85	97	102
Dec	33,480	85	10	13	65	86	99	104

Table 10-4 Annual and monthly statistics for downward solar radiation at KG-1

Season	SSR [J/m^2]							
Month	N [-]	MEAN	STD	MIN	P05	P50	P95	MAX
Jan	33,480	69,139	139,434	0	0	0	403,855	840,446
Feb	30,504	163,412	283,663	0	0	0	827,224	1,461,595
Mar	33,480	345,432	510,757	0	0	6,320	1,490,779	2,166,616
Apr	32,400	618,140	765,412	0	0	187,924	2,158,856	2,656,042
May	33,480	802,020	886,095	0	0	422,796	2,497,775	2,898,362
Jun	32,400	856,685	900,306	0	0	515,878	2,551,778	2,937,003
Jul	33,480	815,875	872,390	0	0	479,494	2,445,072	2,915,515
Aug	33,480	647,580	760,979	0	0	268,051	2,127,163	2,781,625
Sept	32,400	417,102	569,049	0	0	45,954	1,610,652	2,235,412
Oct	33,480	213,768	346,704	0	0	0	1,003,340	1,633,584
Nov	32,400	90,175	173,485	0	0	0	508,114	962,780
Dec	33,480	48,295	100,901	0	0	0	303,713	536,282

10.2 Lightning

This section presents the occurrence and frequency of lightning in the KG area (data delivery area). By using measurement data from the Danish Meteorological Institute (DMI) [6], a comprehensive time series for lightning strikes is established. The frequency and the intensity of lightning strikes over time is analysed by aggregating the data into hourly values. The timeseries consist of both cloud to ground (positive and negative) and cloud to cloud lightning. Lightning strikes are registered with an accuracy of 500-2000 meters.

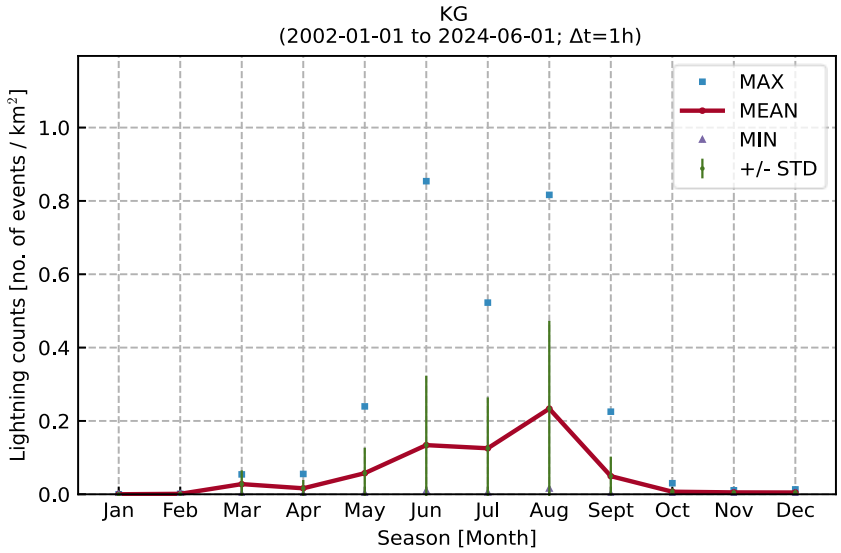

Figure 10-5 Monthly statistics of lightning counts at the data delivery area.

During the full 22-year period a total amount of 10,977 lightning strikes was observed within the data delivery area. This amounts to an average during that full period of 0.51 LTG/km^2/year. This average provides a baseline understanding of lightning activity in the KG, illustrating that while intense thunderstorms can occur, the overall frequency of lightning strikes is relatively low.

The values correspond well with the general rule that in Denmark with a value of 1 LTG/km^2/year across landmasses and less across water bodies. The expected seasonal variation expects ~75% of lightning strikes observed from June to August. and this area agrees with those findings.

Table 10-5 Seasonal variation of lightning strike across the data delivery area.

Season	Lightning counts [no. of events / year / km^2]							
Month	N [-]	MEAN	STD	MIN	P05	P50	P95	MAX
Jan	0.0	0.0	0.0	0.0	0.0	0.0	0.0	0.0
Feb	2.0	0.0	0.0	0.0	0.0	0.0	0.0	0.0
Mar	46.0	0.0	0.0	0.0	0.0	0.0	0.1	0.1
Apr	81.0	0.0	0.0	0.0	0.0	0.0	0.1	0.1
May	1,003.0	0.1	0.1	0.0	0.0	0.0	0.2	0.2
Jun	2,337.0	0.1	0.2	0.0	0.0	0.1	0.4	0.9
Jul	2,291.0	0.1	0.1	0.0	0.0	0.1	0.4	0.5
Aug	4,264.0	0.2	0.2	0.0	0.0	0.1	0.7	0.8
Sept	862.0	0.1	0.1	0.0	0.0	0.0	0.1	0.2
Oct	58.0	0.0	0.0	0.0	0.0	0.0	0.0	0.0
Nov	17.0	0.0	0.0	0.0	0.0	0.0	0.0	0.0
Dec	16.0	0.0	0.0	0.0	0.0	0.0	0.0	0.0

10.3 Salinity, seawater temperature and density

The oceanographic properties were derived from the hydrodynamic dataset. Time series data for density, seawater temperature and salinity were extracted at three depth levels: near-surface, mid-depth, and near-seabed. This part of the dataset spans a 10-year period (2014 to 2023) with a temporal resolution of one hour. The analysis presents the monthly variations in seawater temperature, density, and salinity across the three levels. Oceanographic variables of the hydrodynamic dataset presented in this section is listed in Table 10-6. The following sections are split into variables name and level.

Table 10-6 Oceanographic variables of the hydrodynamic dataset

Variable name	Abbrev.	Unit	Bin size
Seawater temperature	T_{sw}	ºC	1
Salinity	Sal	PSU	2
Water density	D_{sw}	kg/m³	2

10.3.1 Salinity

Figure 10-6, Figure 10-7, Figure 10-8, Table 10-7, Table 10-8 and Table 10-9 show the monthly salinity at KG-1, at near-surface, mid-depth, and near-seabed, respectively.

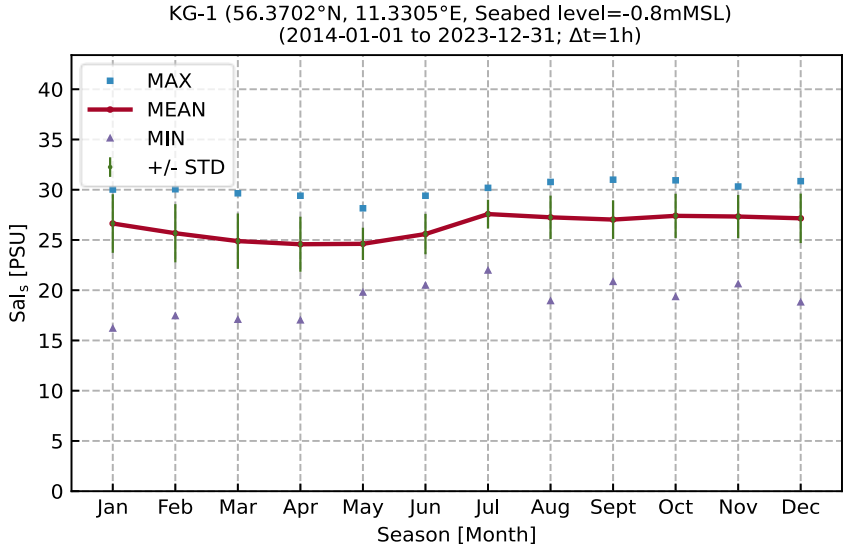

Figure 10-6 Plot of monthly statistics of Sal_s, at KG-1.

Table 10-7 Table with monthly statistics of Sal_s, at KG-1.

Season	Sal_s [PSU]							
Month	N [-]	MEAN	STD	MIN	P05	P50	P95	MAX
Jan	7,430.0	26.6	2.9	16.2	20.2	27.7	29.6	30.0
Feb	6,759.0	25.7	2.9	17.4	20.4	25.6	29.6	30.1
Mar	7,436.0	24.9	2.8	17.1	19.3	25.5	28.4	29.7
Apr	7,194.0	24.6	2.7	17.0	19.3	24.7	28.8	29.4
May	7,439.0	24.6	1.6	19.8	21.7	24.8	27.2	28.2
Jun	7,199.0	25.6	2.0	20.5	21.9	25.7	28.7	29.4
Jul	7,432.0	27.6	1.4	22.0	24.9	28.0	29.3	30.2
Aug	7,437.0	27.3	2.2	18.9	23.5	27.6	29.9	30.8
Sept	7,188.0	27.0	1.9	20.8	23.4	27.1	29.8	31.0
Oct	7,430.0	27.4	2.2	19.3	23.2	27.7	30.6	30.9
Nov	7,190.0	27.3	2.1	20.6	22.7	28.0	29.8	30.3
Dec	7,417.0	27.2	2.5	18.8	22.6	27.7	30.4	30.9

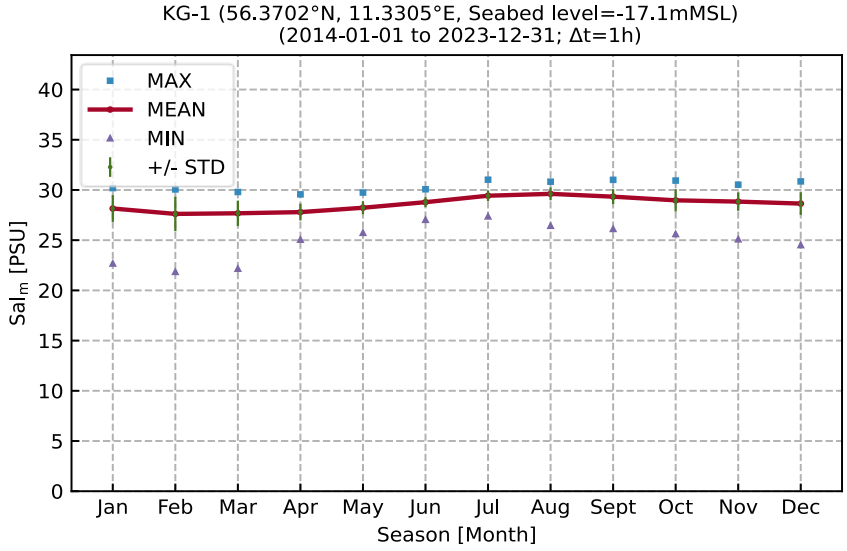

Figure 10-7 Plot of monthly statistics of Sal_m, at KG-1.

Table 10-8 Table with monthly statistics of Sal_m, at KG-1.

Season	Sal_m [PSU]							
Month	N [-]	MEAN	STD	MIN	P05	P50	P95	MAX
Jan	7,437.0	28.2	1.3	22.7	25.5	28.6	29.8	30.2
Feb	6,763.0	27.6	1.7	21.8	24.3	28.1	29.7	30.1
Mar	7,440.0	27.7	1.3	22.2	25.2	27.9	29.2	29.8
Apr	7,198.0	27.8	0.8	25.1	26.4	27.8	29.1	29.6
May	7,439.0	28.2	0.7	25.7	27.1	28.3	29.2	29.7
Jun	7,200.0	28.8	0.5	27.0	27.9	28.8	29.6	30.1
Jul	7,437.0	29.4	0.5	27.4	28.5	29.5	30.3	31.0
Aug	7,437.0	29.6	0.6	26.4	28.5	29.7	30.5	30.8
Sept	7,195.0	29.3	0.7	26.1	27.8	29.4	30.4	31.0
Oct	7,438.0	29.0	1.1	25.6	26.9	29.0	30.7	30.9
Nov	7,196.0	28.8	0.9	25.1	27.0	29.0	30.1	30.5
Dec	7,426.0	28.6	1.1	24.5	26.7	28.7	30.5	30.9

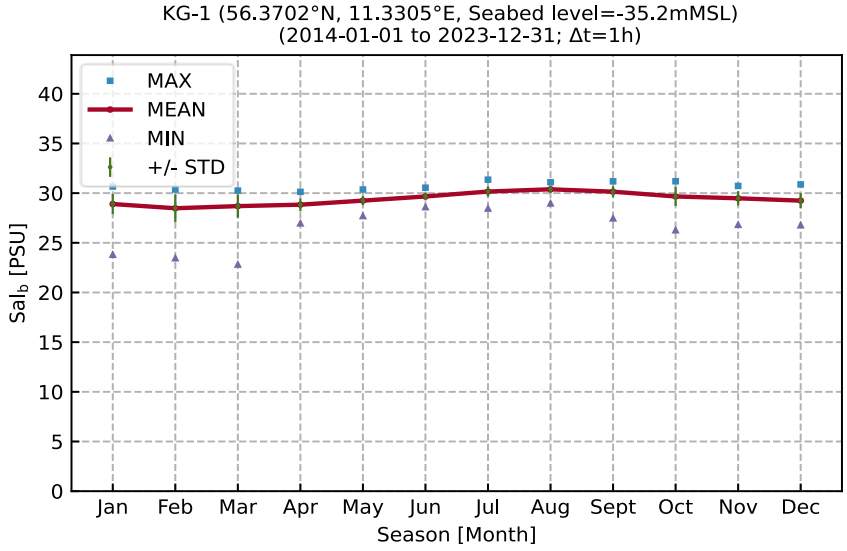

Figure 10-8 Plot of monthly statistics of Sal_b, at KG-1.

Table 10-9 Table with monthly statistics of Sal_b, at KG-1.

Season	Sal_b [PSU]							
Month	N [-]	MEAN	STD	MIN	P05	P50	P95	MAX
Jan	7,437.0	28.9	1.0	23.8	27.0	29.2	30.0	30.7
Feb	6,763.0	28.5	1.4	23.5	25.6	29.0	30.0	30.4
Mar	7,440.0	28.7	1.2	22.8	26.8	29.0	30.0	30.3
Apr	7,198.0	28.8	0.6	27.0	27.5	28.9	29.8	30.1
May	7,439.0	29.3	0.5	27.7	28.5	29.3	30.0	30.4
Jun	7,200.0	29.7	0.4	28.6	29.1	29.7	30.4	30.6
Jul	7,437.0	30.2	0.5	28.4	29.3	30.2	31.0	31.4
Aug	7,434.0	30.4	0.3	29.0	29.8	30.4	30.8	31.1
Sept	7,193.0	30.2	0.6	27.5	29.2	30.3	30.9	31.2
Oct	7,437.0	29.7	1.0	26.3	27.9	29.8	30.9	31.2
Nov	7,196.0	29.5	0.7	26.8	28.0	29.6	30.5	30.7
Dec	7,426.0	29.2	0.8	26.8	27.9	29.3	30.7	30.9

10.3.2 Seawater temperature

Figure 10-9, Figure 10-10, Figure 10-11, Table 10-10, Table 10-11 and Table 10-12 show the monthly seawater temperature at KG-1, at near-surface, mid-depth, and near-seabed, respectively.

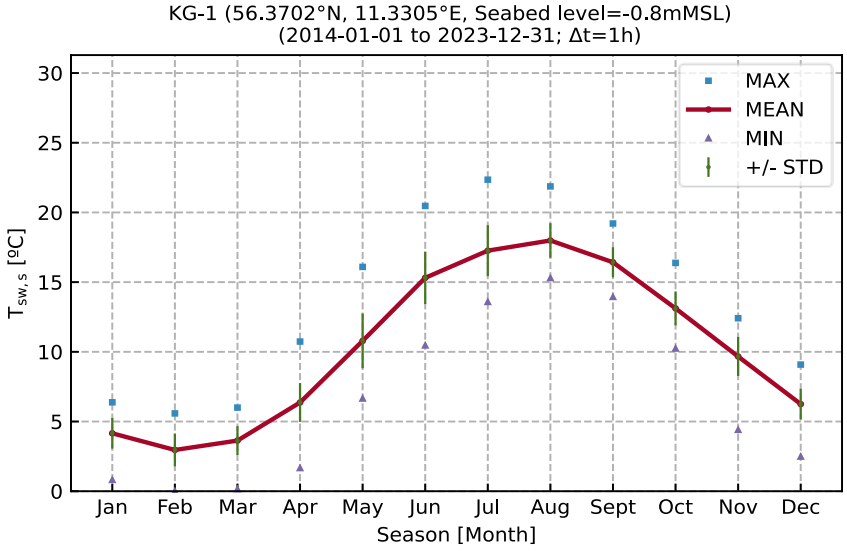

Figure 10-9 Plot of monthly statistics of $T_{sw,s}$, at KG-1.

Table 10-10 Table with monthly statistics of $T_{sw,s}$, at KG-1.

Season	$T_{sw,s}$ [ºC]							
Month	N [-]	MEAN	STD	MIN	P05	P50	P95	MAX
Jan	7,430.0	4.2	1.1	0.8	2.2	4.2	5.8	6.4
Feb	6,759.0	3.0	1.2	0.0	0.9	3.0	5.1	5.6
Mar	7,436.0	3.6	1.0	0.2	1.6	3.8	5.0	6.0
Apr	7,194.0	6.4	1.4	1.7	4.5	6.3	8.9	10.7
May	7,439.0	10.8	2.0	6.7	8.0	10.6	14.6	16.1
Jun	7,199.0	15.3	1.9	10.5	12.3	15.3	18.3	20.5
Jul	7,432.0	17.3	1.8	13.6	14.7	16.9	20.9	22.4
Aug	7,437.0	18.0	1.2	15.3	16.1	17.8	20.4	21.9
Sept	7,188.0	16.4	1.1	13.9	14.8	16.4	18.2	19.2
Oct	7,430.0	13.1	1.2	10.2	11.0	13.0	15.4	16.4
Nov	7,190.0	9.7	1.4	4.4	7.2	9.9	11.8	12.4
Dec	7,417.0	6.3	1.1	2.5	4.6	6.2	8.0	9.1

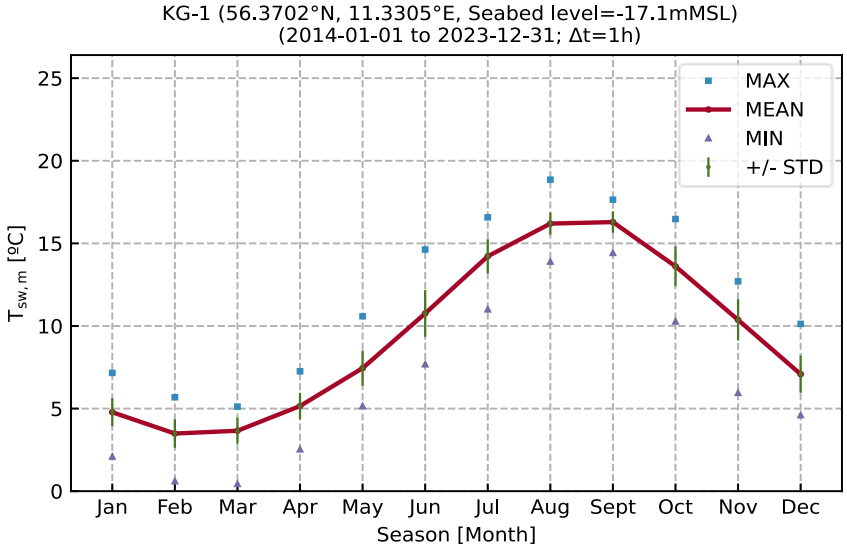

Figure 10-10 Plot of monthly statistics of $T_{sw,m}$, at KG-1.

Table 10-11 Table with monthly statistics of $T_{sw,m}$, at KG-1.

Season	$T_{sw,m}$ [ºC]							
Month	N [-]	MEAN	STD	MIN	P05	P50	P95	MAX
Jan	7,437.0	4.8	0.9	2.1	3.4	4.8	5.9	7.2
Feb	6,763.0	3.5	0.9	0.6	2.2	3.5	5.1	5.7
Mar	7,440.0	3.7	0.8	0.4	2.2	3.7	4.9	5.1
Apr	7,198.0	5.2	0.8	2.5	3.8	5.1	6.3	7.3
May	7,439.0	7.5	1.1	5.2	5.9	7.4	9.2	10.6
Jun	7,200.0	10.8	1.4	7.7	8.6	10.6	13.2	14.6
Jul	7,437.0	14.2	1.0	11.0	12.4	14.3	15.7	16.6
Aug	7,437.0	16.2	0.7	13.9	15.1	16.2	17.3	18.9
Sept	7,195.0	16.3	0.6	14.4	15.1	16.4	17.2	17.7
Oct	7,438.0	13.6	1.2	10.3	11.8	13.5	15.8	16.5
Nov	7,196.0	10.4	1.3	6.0	8.0	10.6	12.0	12.7
Dec	7,426.0	7.1	1.1	4.6	5.4	7.1	9.2	10.1

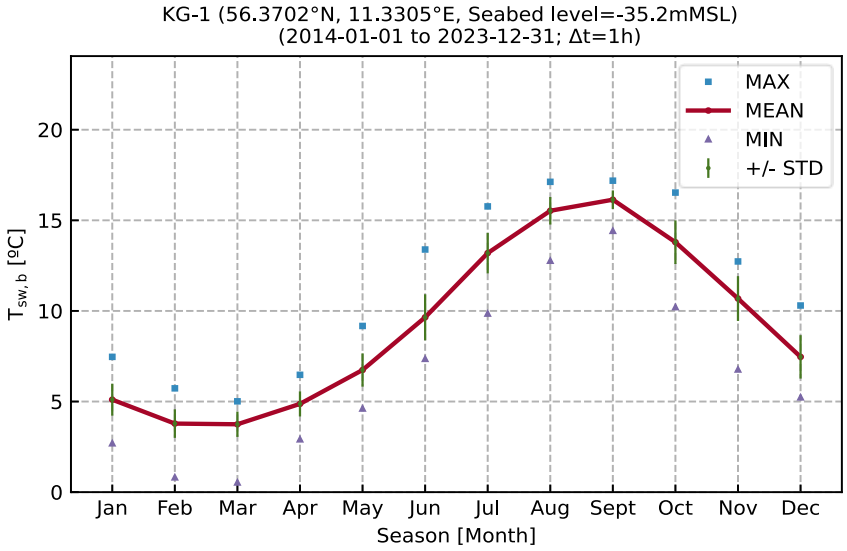

Figure 10-11 Plot of monthly statistics of $T_{sw,b}$, at KG-1.

Table 10-12 Table with monthly statistics of $T_{sw,b}$, at KG-1.

Season	$T_{sw,b}$ [ºC]							
Month	N [-]	MEAN	STD	MIN	P05	P50	P95	MAX
Jan	7,437.0	5.1	0.9	2.7	3.6	5.1	6.4	7.5
Feb	6,763.0	3.8	0.8	0.8	2.6	3.8	5.2	5.7
Mar	7,440.0	3.8	0.7	0.5	2.8	3.8	4.9	5.0
Apr	7,198.0	4.9	0.7	2.9	3.7	4.9	6.0	6.5
May	7,439.0	6.7	0.9	4.6	5.5	6.6	8.4	9.2
Jun	7,200.0	9.7	1.3	7.4	7.7	9.5	12.0	13.4
Jul	7,437.0	13.2	1.1	9.9	11.4	13.2	14.8	15.8
Aug	7,434.0	15.5	0.8	12.8	14.2	15.6	16.5	17.1
Sept	7,193.0	16.1	0.5	14.4	15.1	16.2	16.8	17.2
Oct	7,437.0	13.8	1.2	10.2	11.9	13.6	15.8	16.5
Nov	7,196.0	10.7	1.2	6.8	8.3	10.9	12.3	12.7
Dec	7,426.0	7.5	1.2	5.2	5.7	7.4	9.7	10.3

10.3.3 Density

Figure 10-12, Figure 10-13, Figure 10-14, Table 10-13, Table 10-14 and Table 10-15 show the monthly seawater density at KG-1, at near-surface, mid-depth, and near-seabed, respectively.

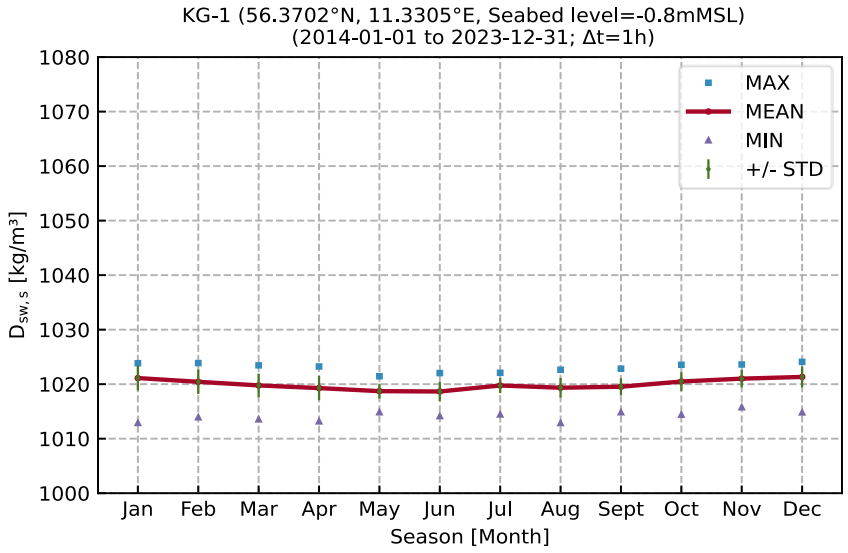

Figure 10-12 Plot of monthly statistics of $D_{sw,s}$, at KG-1.

Table 10-13 Table with monthly statistics of $D_{sw,s}$, at KG-1.

Season	$D_{sw,s}$ [kg/m³]							
Month	N [-]	MEAN	STD	MIN	P05	P50	P95	MAX
Jan	7,430.0	1,021.1	2.3	1,012.9	1,016.1	1,022.0	1,023.5	1,023.9
Feb	6,759.0	1,020.4	2.3	1,013.9	1,016.3	1,020.4	1,023.4	1,023.9
Mar	7,436.0	1,019.8	2.2	1,013.6	1,015.4	1,020.3	1,022.6	1,023.5
Apr	7,194.0	1,019.3	2.2	1,013.2	1,015.1	1,019.4	1,022.6	1,023.2
May	7,439.0	1,018.7	1.4	1,014.9	1,016.4	1,018.8	1,020.9	1,021.5
Jun	7,199.0	1,018.7	1.8	1,014.1	1,015.6	1,018.7	1,021.4	1,022.0
Jul	7,432.0	1,019.8	1.4	1,014.4	1,017.2	1,020.1	1,021.5	1,022.1
Aug	7,437.0	1,019.4	1.8	1,012.9	1,016.0	1,019.6	1,021.8	1,022.6
Sept	7,188.0	1,019.5	1.6	1,014.8	1,016.8	1,019.6	1,021.6	1,022.9
Oct	7,430.0	1,020.5	1.7	1,014.4	1,017.3	1,020.7	1,022.9	1,023.6
Nov	7,190.0	1,021.0	1.6	1,015.8	1,017.5	1,021.5	1,023.0	1,023.6
Dec	7,417.0	1,021.3	1.9	1,014.8	1,017.7	1,021.8	1,023.8	1,024.1

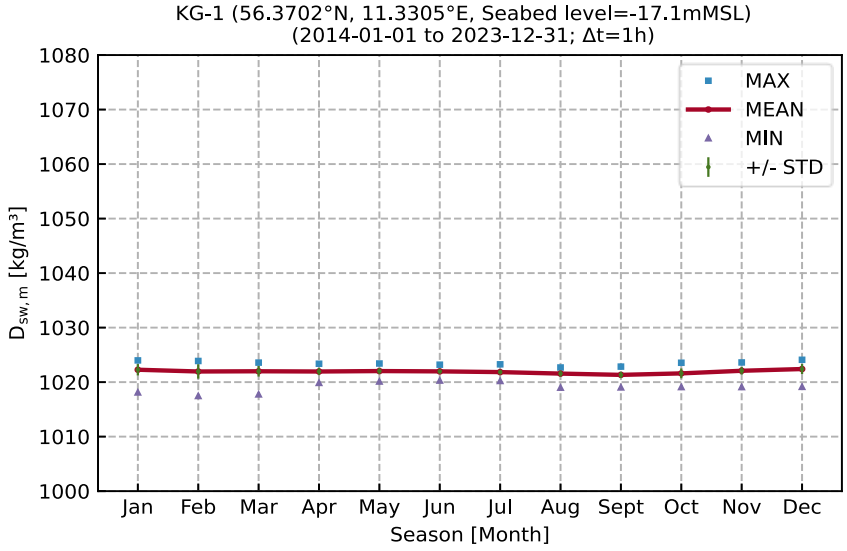

Figure 10-13 Plot of monthly statistics of $D_{sw,m}$, at KG-1.

Table 10-14 Table with monthly statistics of $D_{sw,m}$, at KG-1.

Season	$D_{sw,m}$ [kg/m³]							
Month	N [-]	MEAN	STD	MIN	P05	P50	P95	MAX
Jan	7,437.0	1,022.3	1.0	1,018.1	1,020.2	1,022.6	1,023.6	1,024.0
Feb	6,763.0	1,022.0	1.3	1,017.5	1,019.4	1,022.3	1,023.6	1,023.9
Mar	7,440.0	1,022.0	1.0	1,017.7	1,020.1	1,022.2	1,023.2	1,023.6
Apr	7,198.0	1,022.0	0.7	1,019.9	1,020.8	1,022.0	1,023.0	1,023.4
May	7,439.0	1,022.0	0.6	1,020.1	1,021.1	1,022.1	1,022.9	1,023.4
Jun	7,200.0	1,022.0	0.5	1,020.3	1,021.2	1,022.0	1,022.7	1,023.2
Jul	7,437.0	1,021.8	0.5	1,020.2	1,021.1	1,021.8	1,022.7	1,023.3
Aug	7,437.0	1,021.6	0.6	1,019.0	1,020.5	1,021.6	1,022.3	1,022.7
Sept	7,195.0	1,021.3	0.6	1,019.0	1,020.1	1,021.4	1,022.1	1,022.8
Oct	7,438.0	1,021.6	0.9	1,019.1	1,019.8	1,021.6	1,023.0	1,023.6
Nov	7,196.0	1,022.1	0.7	1,019.1	1,020.7	1,022.2	1,023.1	1,023.6
Dec	7,426.0	1,022.4	0.9	1,019.1	1,020.8	1,022.5	1,023.9	1,024.1

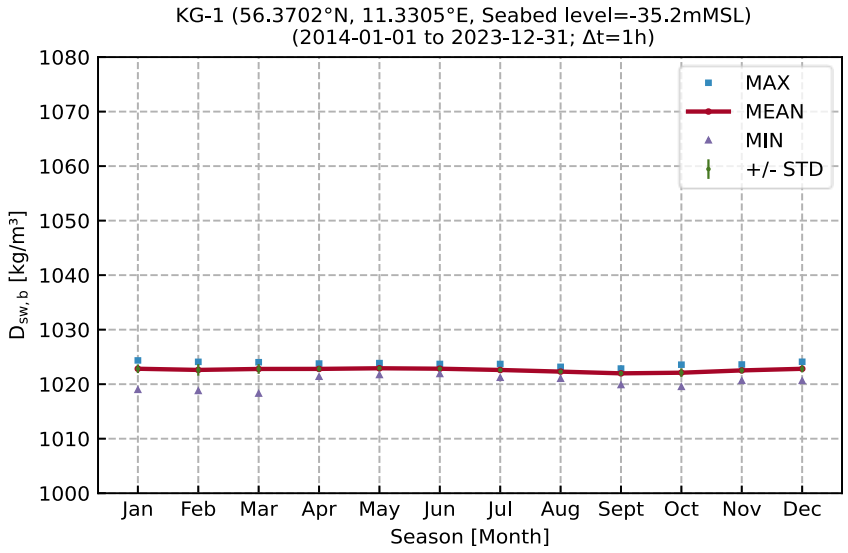

Figure 10-14 Plot of monthly statistics of $D_{sw,b}$, at KG-1.

Table 10-15 Table with monthly statistics of $D_{sw,b}$, at KG-1.

Season	$D_{sw,b}$ [kg/m³]							
Month	N [-]	MEAN	STD	MIN	P05	P50	P95	MAX
Jan	7,437.0	1,022.8	0.8	1,019.0	1,021.3	1,023.0	1,023.8	1,024.4
Feb	6,763.0	1,022.6	1.1	1,018.8	1,020.4	1,023.0	1,023.8	1,024.1
Mar	7,440.0	1,022.8	0.9	1,018.3	1,021.3	1,023.0	1,023.8	1,024.0
Apr	7,198.0	1,022.8	0.5	1,021.4	1,021.8	1,022.8	1,023.6	1,023.8
May	7,439.0	1,022.9	0.4	1,021.7	1,022.2	1,023.0	1,023.6	1,023.9
Jun	7,200.0	1,022.8	0.4	1,021.9	1,022.2	1,022.8	1,023.5	1,023.7
Jul	7,437.0	1,022.6	0.4	1,021.2	1,022.0	1,022.6	1,023.4	1,023.7
Aug	7,434.0	1,022.3	0.4	1,021.0	1,021.7	1,022.4	1,022.9	1,023.2
Sept	7,193.0	1,022.0	0.4	1,019.8	1,021.3	1,022.1	1,022.6	1,022.9
Oct	7,437.0	1,022.1	0.8	1,019.5	1,020.6	1,022.2	1,023.1	1,023.6
Nov	7,196.0	1,022.5	0.6	1,020.6	1,021.5	1,022.6	1,023.3	1,023.6
Dec	7,426.0	1,022.8	0.7	1,020.6	1,021.7	1,022.9	1,023.9	1,024.1

10.4 Marine growth

Marine growth or biofouling refers to the growth or establishment of marine organisms, such as algae, marine animals, and bacteria, on submerged surfaces like piers, buoys, ship hulls, and offshore structures. For offshore structures, like wind farms, it is important to consider marine growth to minimize its effects, as it can affect the hydrodynamic efficiency and structural integrity of the structures [7].

The structure and composition of marine growth depend on various physical and environmental factors, including temperature, salinity, currents, wave

exposure and food availability [8]. The community and abundance of species inhabiting such structures therefore varies depending on geographical areas. For example, seaweed and kelp are often more prevalent on structures that are protected from waves and currents, while mussels are more successful in turbid environments. The colonization of marine structures generally occurs over a period of 2 to 3 years [9], during which there is a succession of species, with those abundant during the early colonization phase changing over time [10].

Limited data is available regarding the composition and density of marine growth in the southern part of Kattegat, including KG. However, investigations in nearby areas in the Baltic Sea and the North Sea have shown that mussels, barnacles, other crustacean species, large seaweed, and kelp are the dominant groups colonizing these structures [11, 12]. For example, after the establishment of a wind park in Fehmarn Belt (Nysted, Denmark), mussels and barnacles dominated the structures, with a few other crustacean species (including barnacles) and algae documented at depths of 1 to 5 meters on the vertical structures [11]. *Mytilus edulis* and *Balanus spp.,* in which case the latter mainly covered the upper layer of the structure, were the dominant species in terms of abundance and biomass on the vertical structures. The composition of marine growth also showed vertical differentiation in biomass, with a decline in these parameters observed in deeper layers.

Similar results have been documented at Darss Sill, where mussels (mainly *Mytilus edulis*) and crustaceans (mainly *Balanus spp.)* dominated the established test structures in terms of abundance and biomass at depths between 4 and 20 meters [12]. It was documented that 143 days after exposure *Mytilus edulis* and *Balanus spp.* had obtained biomass of 1,7-22,3 and 8,8-146 g afdw/m², respectively, with biomass further increasing by day 246 and 470, especially higher in the water column. The results also indicated vertical differentiation, with a decrease in abundance and biomass of marine growth in deeper layers. Colonization of these structures was characterized by a succession, where barnacles, which originally dominated the structures, were subsequently taken over by mussels.

The data and results from the investigations from the Baltic and North Sea cannot be directly applied to KG in Kattegat. However, considering the salinity, temperature regime, and the direction and intensity of prevalent currents in this area, a similar composition of species as documented in the North and Baltic Sea would be expected, with mussels, barnacles, other species of crustaceans and algae being the dominant species inhabiting the OFW structures and making up most of the biomass. Particularly, *Mytilus edulis* and *Balanus spp.* are prevalent in this area. Given their life-history patterns and colonization ability [13, 14], especially in high current velocity areas, they are expected to be the main colonizers on new structures established in KG, making up the majority of the biomass.

The thickness of marine growth also depends on project specific conditions such as the position of the structural component relative to the sea level, the orientation of the component relative to the sea level and relative to the dominant current, the age of the component, and the maintenance strategy for the component, apart from salinity, oxygen content, pH value, current and temperature (DNV-ST-0437:2024-05).

A marine growth density of 1325 kg/m^3 and a marine growth thickness of 100 mm from the seafloor to -2 mMSL is recommended in DNV-ST-0437:2024-05 for the central North Sea and the Baltic Sea.

Since project specific conditions, and composition and biomass data for the KG area, are not available, and since data from the North Sea and Baltic Sea does not indicate otherwise, it is recommended to use an standard (DNV-ST-0437:2024-05) density of 1325 kg/m^3 and a marine growth thickness of 100 mm from the seafloor to -2 mMSL.

11 Bibliography

[1] Sweco/Deltares, “41011328A_KG-HS_PartA_Measurements_and_Hindcast_Data_Basis,” 2024.

[2] DMI, Storms in Denmark since 1981, March 4th, 2024.

[3] DMI, Stormens ABC, January 28th, 2022.

[4] Kystdirektoratet, Højvandsstatistikker 2024, Kystdirektoratet, Miljøminisateriet, 2024.

[5] ECMWF, “ERA5,” [Online]. Available: https://cds.climate.copernicus.eu/cdsapp#!/dataset/reanalysis-era5-single-levels?tab=form.

[6] DMI, “Frie Data,” [Online]. Available: https://www.dmi.dk/frie-data/.

[7] W. P. H. C. B. J. H. K. C. W. K. Y. C. &. S. H. K. (. Shi, “Study on the marine growth effect on the dynamic response of offshore wind turbines,” *International Journal of Precision Engineering and Manufacturing,* vol. 13, pp. 1167-1176, 2012.

[8] C. O. R. Energy, “Marine growth mapping and monitoring,” 2016.

[9] J. K. Petersen, E. Stenalt and W. B. Hansen, “Invertebrate re-colonisation in Mariager Fjord (Denmar) after severe hypoxia. II. Blue mussels (Mytilus edulis L.),” *Ophelia,* vol. 56, pp. 215-225, 2002.

[10] A. Dziubinska and A. Szaniawska, “Short-term study on the early succesion stages of fouling communities in the coastal zone of Puck Bay (Southern Baltic Sea),” *Oceanological and Hydrobilogical studies,* vol. 39, pp. 3-16, 2010.

[11] E. E. A/S, “Development of the fouling community of trubine foundations and scour protections in Nysted offshore wind farm, 2003,” 2003.

[12] M. L. Zettler and F. Pollehne, “The impact of wind engine constructions on benthic growth patterns in the western Baltic,” in *Offshore wind energy: Research on environmental impacts*, 2006, pp. 201-222.

[13] A.-L. Wrange, C. André, T. Lundh, U. Lind, A. Blomberg and P. J. Jonsson, “Importance of plasticity and local adaptation for coping with changing salinity in coastal areas: a test case with barnacles in the Baltic Sea,” *BMC Evolutionary Biology,* vol. 14, pp. 1-15, 2014.

[14] P. Strelkov, M. Katolikova and R. Väinolä, “Temporal change of the Baltic Sea-North Sea blue mussel hybrid zon over two decades,” *Marine Biology,* vol. 164, p. 214, 2017.

Appendix A

A number of excel workbooks (and PDF versions of the workbooks) accompany this report. A list of these Data Reports and a brief description of their content is provided below. X in the list below denotes the reference location number 1-3.

- **Normal_KG-X**
  - Contains presentation of data for individual parameters of wind, waves, current and water level in the form figures and tables of timeseries, roses, statistics (monthly and directional) and probabilities for operational conditions.

- **Wave spectra_KG-X**
  - Contains a comparison between hindcast wave spectra and JONSWAP spectra (as defined in DNV-RP-C205:2021-09) a number of H_{m0} ranges.

- **Sensitivity_KG-X**
  - Contains presentation of sensitivity analyses of marginal EVA to determine the suitable distribution, threshold (POT), and fitting methods for individual parameters of waves, current and water level.

- **EVA_KG-X**
  - Contains presentation of marginal EVA results for individual parameters of waves, current and water level.

- **EVA_Scaled_KG-X**
  - Contains presentation of marginal EVA results for individual parameters of waves and current scaled according to DNV-RP-C205.

- **Scatter_KG-X**
  - Contains presentation of scatter diagrams and figures between various parameters such as: wind-waves (incl. misalignment and water level-waves.

- **Sea_State_KG-X**
  - Contains a presentation of NSS, SSS, ESS and ESS_Scaled (scaled according to DNV-RPC205).

- **Atmospheric _KG**
  - Contains a presentation of air temperature, humidity, solar radiation, and lightning.

- **Oceanographic_KG-X**
  - Contains a presentation of seawater temperature, salinity and density.

- **Oceanographic_profile_HS-X**

- Contains a presentation of current speed, seawater temperature, and salinity profiles across the water depth.

Appendix B

This section presents a sensitivity analysis of marginal EVA to determine the suitable distribution, threshold (POT), and fitting methods for the setup of EVA. Statistical independence is ensured by the inter-event time, and identical distribution is ensured as only windsea components are present for waves, for water level and current these are completely dominated by the residual component thereby ensuring identical distribution.

The figures below show the sensitivity of the 50-year return period for the respective parameters against different events per year. On each figure, different common fitting methods (Maximum likelihood (MLE), Least-Squares (LS) and Method of Moments (MM)) have been used to fit different common long-term extreme value distributions (Weibull, Gumbel, Generalized Pareto and Frechet). More details on average relative error and the actual fits are presented in the appendices. The data and fits have been evaluated considering the visual fit, the average relative error and stability for the various distributions, thresholds (POT), and fitting methods.

Based on the approach outlined above, the selected EVA settings are as follows:

- Waves: 3-parameter Weibull distribution fitted with Least-Squares to the 44 peak events with an inter-event time of 72 hours.
- Water level (high): 3-parameter Weibull distribution fitted with Least-Squares to the 180 peak events with an inter-event time of 72 hours.
- Current speed: 3-parameter Weibull distribution fitted with Least-Squares to the 45 peak events with an inter-event time of 72 hours.

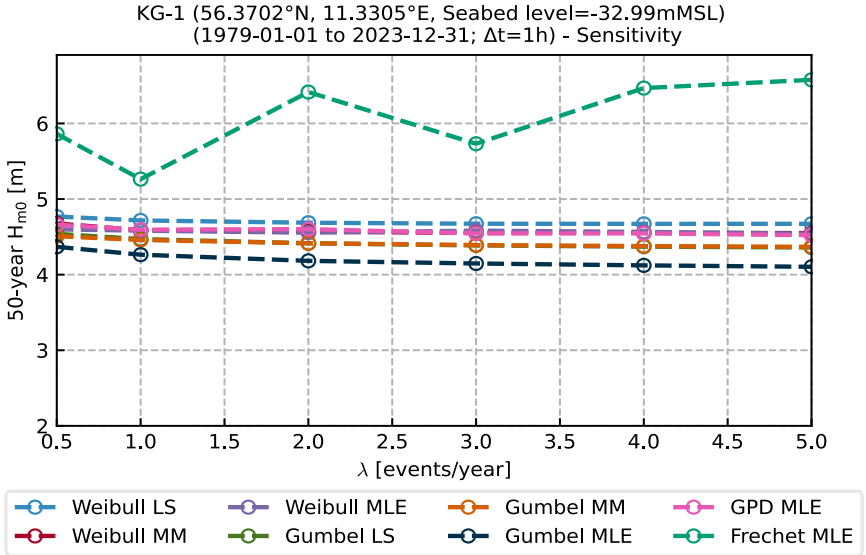

Figure 11-1 Sensitivity of 50 year marginal H_{m0} EVA to distribution, threshold, and fitting. Inter-event time 72h.

Together with our clients and the collective knowledge of our 22,000 architects, engineers and other specialists, we co-create solutions that address urbanisation, capture the power of digitalisation, and make our societies more sustainable.

Sweco – Transforming society together

SWECO